UNIVERSITY OF CALIFORNIA, SAN DIEGO

The Oxygen Isotopic Composition of Water in the Inner Solar System

A dissertation submitted in partial satisfaction of the requirements for the degree
Doctor of Philosophy

in

Chemistry

by

Morgan Heath Nunn

Committee in charge

Professor Mark H. Thiemens, Chair
Professor Alison Coil
Professor John Crowell
Professor Josh Figueroa
Professor Judy Kim

2015

The dissertation of Morgan Heath Nunn is approved, and it is acceptable in quality and form for publication on microfilm and electronically:

_____

_____

_____

_____

_____
Chair

University of California, San Diego

2015

DEDICATION

To all of my teachers – family, friends, and educators – past, present, and future – thank you for sharing the beauty of understanding with me. I am especially grateful to my parents, Jim and Anne Prettyman, whose unending love and support provided the foundation for me to fearlessly explore this and other worlds.

To my first teacher, my mother, Anne Cushman Prettyman, I dedicate this dissertation. Your exuberance, gratitude, curiosity, and compassion shaped the person I am and enriched my experience of this life in countless ways. I can still feel how proud of me you are.

EPIGRAPH

“I am grateful.” -Mom

“In one drop of water are found all the secrets of all the oceans; in one aspect of You are found all the aspects of existence.” –Kahlil Gibran

“If there is magic on the planet, it is contained in the water.” –Loren Eisley

“A man who carries a cat by the tail learns something he can learn in no other way.” -Mark Twain

TABLE OF CONTENTS

LIST OF FIGURES

LIST OF TABLES

LIST OF SUPPLEMENTARY FILES

In Chapter 2, references to supplementary figures and tables can be found in the Science publication's Supplementary Materials. Morgan Nunn Chapter 2 Supplementary Materials: nunn_chapter_2_supplementary_materials.pdf.

In Chapter 3, references to supplementary figures and tables can be found in the Science publication's Supplementary Materials. Morgan Nunn Chapter 3 Supplementary Materials: nunn_chapter_3_supplementary_materials.pdf.

ACKNOWLEDGEMENTS

I thank my research advisor, Dr. Mark H. Thiemens, and my friend and mentor, Dr. Candace Kohl, whose constant support and belief in me made all the difference in the world. I am grateful for many wonderful conversations with colleagues in the Thiemens Group, especially Dr. Subrata Chakraborty and Teresa Jackson. I would like to thank my colleague and friend, Dr. Gerardo Dominguez, for his invaluable support and guidance during my time at UCSD.

Chapter 2, in full, is a reprint of the material as it appears in Science 2012. Peter Jenniskens, Marc D. Fries, Qing-Zhu Yin, Michael Zolensky, Alexander N. Krot, Scott A. Sandford, Derek Sears, Robert Beauford, Denton S. Ebel, Jon M. Friedrich, Kazuhide Nagashima, Josh Wimpenny, Akane Yamakawa, Kunihiko Nishiizumi, Yasunori Hamajima, Marc W. Caffee, Kees C. Welten, Matthias Laubenstein, Andrew M. Davis, Steven B. Simon, Philipp R. Heck, Edward D. Young, Issaku E. Kohl, Mark Thiemens, Morgan H. Nunn, Takashi Mikouchi, Kenji Hagiya, Kazumasa Ohsumi, Thomas A. Cahill, Jonathan A. Lawton, David Barnes, Andrew Steele, Pierre Rochette, Kenneth Verosub, Jérôme Gattacceca, George Cooper, Daniel P. Glavin, Aaron S. Burton, Jason P. Dworkin, Jamie E. Elsila, Sandra Pizzarello, Ryan Ogliore, Phillipe Schmitt-Kopplin, Mourad Harir, Norbert Hertkorn, Alexander Verchovsky, Monica Grady, Keisuke Nagao, Ryuji Okazaki, Hiroyuki Takechi, Takahiro Hiroi, Ken Smith, Elizabeth A. Silber, Peter G. Brown, Jim Albers, Doug Klotz, Mike Hankey, Robert Matson, Jeffrey A. Fries, Richard J. Walker, Igor Puchtel, Cin-Ty A. Lee, Monica E. Erdman, Gary R.

Eppich, Sarah Roeske, Zelimir Gabelica, Michael Lerche, Michel Nuevo, Beverly Girten, Simon P. Worden (the Sutter's Mill Meteorite Consortium). *Science* **338**, 1583, 2012 (DOI: 10.1126/science.1227163). Reprinted with permission from AAAS. The dissertation author was a co-investigator and co-author of this paper.

Chapter 3, in full, is a reprint of the material as it appears in Science 2013. Carl B. Agee, Nicole V. Wilson, Francis M. McCubbin, Karen Ziegler, Victor J. Polyak, Morgan H. Nunn, Stephen M. Elardo, Zachary D. Sharp, Yemane Asmerom, Mark H. Thiemens, Marilyn L. Fogel, Andrew Steele. *Science* **339**, 780, 2013 (DOI: 10.1126/science.1228858). Reprinted with permission from AAAS. The dissertation author was a co-investigator and co-author of this paper.

Chapter 5, in part, is currently being prepared for submission for publication of the material. Morgan H. Nunn and Mark H. Thiemens. The dissertation author conducted the experiments described and is the author of this material.

Chapter 6 describes experiments designed and carried out by Morgan H. Nunn and Gerardo Dominguez. The work was funded by the NASA Cosmochemistry grant. The dissertation author was a co-investigator and is the author of this material.

Chapter 7, in part, is currently being prepared for submission for publication of the material. Morgan H. Nunn, Subrata Chakraborty, Mark H. Thiemens. The dissertation author conducted the experiments described and is the primary author of this material.

I thank the NASA Earth and Space Sciences Fellowship, Zonta International Amelia Earhart Fellowship, ARCS scholarship, and AWIS scholarship for financial support of the research described in this dissertation.

VITA

2008	Bachelor of Science, Georgia Institute of Technology, Atlanta, GA
2009 - 2010, 2012	Teaching Assistant, Department of Chemistry and Biochemistry, University of California, San Diego
2012	Master of Science, University of California, San Diego
2010 - 2015	Research Assistant, University of California, San Diego
2015	Doctor of Philosophy, University of California, San Diego

GRANTS AND FELLOWSHIPS

2012 - 2015	NASA Earth and Space Sciences Fellowship
2011 - 2015	Achievement Rewards for College Scientists (ARCS) Scholarship
2011 & 2013	Zonta International Amelia Earhart Fellowship
2012	Association for Women in Science (AWIS) Scholarship

PUBLICATIONS

Jenniskens, P., et al. (Dissertation author is author 25 of 70 of this publication.) "Radar enabled recovery of the Sutter's Mill Meteorite, a carbonaceous chondrite regolith breccia." (2012) *Science,* **338**, 1583.

Agee, C. B., et al. (Dissertation author is author 6 of 12 of this publication.) "Unique meteorite from the early Amazonian epoch on Mars: Water-rich basaltic breccia Northwest Africa 7034." (2013) *Science,* **339***,* 780.

ABSTRACT OF THE DISSERTATION

The Oxygen Isotopic Composition of Water in the Inner Solar System

by

Morgan Heath Nunn

Doctor of Philosophy in Chemistry

University of California, San Diego, 2015

Professor Mark H. Thiemens, Chair

Where there is water, there can be life. Improving our understanding of how life, as we know it, arose uniquely in our solar system on Earth depends critically on our understanding of the history of water in the solar system. Better characterizing the sources of water to the Earth-Moon system is crucial in

constraining this history and motivated the experiments described in this dissertation.

The oxygen isotopic composition of water in lunar samples in addition to meteorites from Mars and several asteroids, which have delivered significant material to the Earth-Moon system, were characterized. The ordinary chondrite (OC) samples, Bjurböle matrix, Bjurböle chondrules, and ALHA77216, contain ^{17}O-enriched water with, Δ^{17}O up to 1.5‰, released by high temperature heating. Water liberated from the carbonaceous chondrite (CC), Murchison, by heating to high temperatures (≤ 1000˚C) possess Δ^{17}O approaching -1.5‰. Low-temperature fractions of water from these OC and CC samples is mass-dependently fractionated (Δ^{17}O ≅ 0‰). The eucrite, PCA 91006 releases water upon heating to 50-350˚C with Δ^{17}O ≅ 1‰ and 600-1000˚C with as low as -11‰. The martian meteorite, NWA 7034, contains water with an average Δ^{17}O = 0.32‰. The lunar samples analyzed (10049, 10057, 10060, 12021, 12039, 14163, 14305, 79035) possess water with average Δ^{17}O = 0.18‰. The oxygen isotopic composition of a whole rock sample of a carbonaceous chondrite (CC) meteorite, Sutter's Mill, was also measured, and possesses Δ^{17}O = -1.8‰. The 1σ error on these Δ^{17}O values is 0.011‰. These results reveal that delivery of water by OCs and CCs could account for almost all of the lunar water isotopic compositions measured.

Complementary studies measuring the isotopic composition of ozone (O_3), an important precursor to water, formed in experiments performed under

analogous conditions to those that existed early in the formation of the solar system were also conducted. Additionally, experiments characterizing the isotopic composition of O_2 involved in ion-molecule reactions which dominate molecule-formation processes occurring in cold regions of interstellar molecular clouds were also conducted. These complementary studies help define and explain the isotopic composition of oxygen-bearing reservoirs, especially water, in the present-day inner solar system.

The Oxygen Isotopic Composition of Water in the Inner Solar System

Chapter. 1 Introduction

1.1 The Stable Isotopes of Oxygen

1.1.1 Abundance, Nucleosynthesis, and Stability

Oxygen is the most abundant element, by mass, in the terrestrial planets and appears in many distinct chemical phases on each of these bodies. Oxygen naturally exists as three stable isotopes (^{16}O, ^{17}O, ^{18}O), which each contains 8 protons and 8, 9, or 10 neutrons, respectively. In our solar system, ^{16}O is, by far, the most abundant isotope of oxygen, making up 99.7% of all oxygen on Earth. The much rarer ^{17}O and ^{18}O comprise 0.037% and 0.19% of Earth's oxygen, respectively [1].

The relative abundance of oxygen isotopes reflects the ^{16}O, ^{17}O, and ^{18}O endogenous to the solar system as well as the relative nuclear binding energies of these nuclides. The binding energy per nucleon of ^{16}O, ^{17}O, and ^{18}O is 7.98, 7.75, and 7.77MeV, respectively. The energy required to undergo nuclear fission increases with increasing binding energy. Nuclides with higher binding energies should consequently be less likely to undergo nuclear fission, and they should be more abundant. The trend in abundance of ^{16}O, ^{17}O, and ^{18}O predicted by

comparing their binding energies is $^{16}O > ^{18}O > ^{17}O$, and this is, in fact, what is observed in nature.

Stars use nuclear fusion reactions to convert nuclear energy to thermal energy, creating sufficient pressure to balance the inward force of gravitational contraction while radiating energy outward on relatively long timescales. Distinct nuclear fusion reactions occurring in stars during different epochs of their lives produce ^{16}O, ^{17}O, and ^{18}O so measurement of their relative amounts in a sample sheds light on the stellar region in which the sample formed [2].

Oxygen-16 is predominantly made in the late stages of helium burning, while hydrogen burning and early stage helium burning dominate the production of ^{17}O and ^{18}O [2]. Oxygen-16 is unique among oxygen's stable isotopes in that it is a primary isotope, meaning it can be produced in stars initially comprised only of hydrogen. Synthesis of the secondary isotopes ^{17}O and ^{18}O occurs in stars that received seed nuclei from older, nearby stars via supernovae. The vast majority of the ^{16}O, and thus the vast majority of the total oxygen, in the Milky Way Galaxy was produced by massive stars ≥ 10 times the mass of our Sun [3].

Oxygen's isotopes of mass 16, 17, and 18 are stable, meaning they do not undergo radioactive decay on a timescale comparable to the age of the Earth (4.5 Gy) [4]. General guiding rules that apply to all nuclides are responsible for the stability of ^{16}O, ^{17}O, and ^{18}O.

The most stable isotopes are those with the same number of protons and neutrons, and stability generally decreases with increasing numbers of neutrons.

Isotopes with even numbers of neutrons are generally more stable than those with odd numbers. The Oddo-Harkins Rule summarizes the relationship between stability and number of nucleons (protons and neutrons). This rule states nuclei containing an even number of nucleons are more stable than either odd numbered nuclide containing one more or less neutron because of enhanced nuclear stability [5], [6].

1.1.2 Oxygen Isotopic Ratios

The distinct physical and chemical properties of ^{16}O, ^{17}O, and ^{18}O and oxygen-bearing species have led to distinct ratios of these isotopes in each oxygen-bearing phase on each celestial body (e.g., [7], [8]). Characterization of oxygen isotopic ratios is, therefore, an effective tool in elucidating the planetary parentage, composition of the source reservoir, and the processes that have led to the formation of an extraterrestrial sample.

Variability in the amounts of the rare isotopes (^{17}O, ^{18}O) relative to ^{16}O revealing differing contributions from diverse processes is often extremely small relative to the total amount of ^{16}O. Oxygen isotopic composition, therefore, is conveniently described by delta (δ) notation, where the amount of a rare isotope (^{17}O or ^{18}O) relative to the most abundant isotope (^{16}O) is presented in permil (‰) units with respect to a standard of known isotopic composition:

$$\delta^{17,18}O\ (‰) = [(R_{SA}/R_{ST})-1] * 1000$$

where R_{SA} = $^{17,18}O/^{16}O$ of the sample, R_{ST} = $^{17,18}O/^{16}O$ of the standard.

1.2 Isotopic Fractionation Processes

Reactions that fractionate isotopes yield products with different isotopic compositions than the reactant species. Physical and chemical processes induce fractionations in isotopic ratios. Oxygen isotopic fractionation is either mass-dependent or mass-independent so ^{18}O production or depletion is either proportional or equal to the ^{17}O production or depletion. In other words, oxygen undergoes mass-dependent or –independent fractionation (MDF, MIF), respectively, in these processes.

Kinetic and equilibrium processes induce MDF, while chemical and nuclear processes give rise to MIF. MIF oxygen on the surface of the Earth is rare, but it is relatively abundant in the terrestrial atmosphere and elsewhere in the solar system. MIF oxygen was first identified in the refractory calcium-aluminum-rich inclusions (CAI), the first condensates from gas in the protoplanetary disk that existed early in the solar system's formation and the most ^{16}O-rich solids in the solar system, within the Allende meteorite [9].

The $\Delta^{17}O$ value is used to describe the mass-independence of an oxygen-bearing species by reflecting the deviation from MDF, which produces $\delta^{17}O$ = 0.52 * $\delta^{18}O$. The $\Delta^{17}O$ value is defined by the following relationship:

$$\Delta^{17}O\ (‰) = \delta^{17}O - 0.52 * \delta^{18}O$$

[10], [11].

1.2.1 Mass-Dependent Fractionation Processes

Mass-dependent fractionation occurs in kinetic and equilibrium processes, the theoretical foundation of which was laid by Urey (1947) and Bigeleisen and Mayer (1947) [12], [13].

Kinetic Fractionation

The differences in mass between ^{16}O, ^{17}O, and ^{18}O result in different rates of reaction for each isotope in physical and chemical processes. Mass differences in isotopes affect relative reaction rates by the differential velocities of the isotopologues. Classical mechanics tells us kinetic energy is determined by temperature by the following relation:

$kT = 1/2mv^2$

where k = Boltzmann constant, T = absolute temperature, m = molecular mass, and v = average molecular velocity. It is clear from this relationship that, assuming ideal gas behavior, molecules at a given temperature possess the same kinetic energy regardless of the isotopic composition of the molecules.

Comparing the kinetic energy expressions for light and heavy isotopologues reveals their relative velocities are different though:

$v_1/v_2 = \sqrt{(m_2/m_1)}$

where the subscripts 1 and 2 refer to molecules substituted with light and heavy isotopes, respectively. As a consequence of the above relationship, the rate of diffusion and frequency of collision of heavier isotopologues are lower than for their lighter counterparts, and this results in slower reaction rates, in general, for heavier isotopologues. Kinetic processes induce MDF because the relative velocities of isotopically substituted molecules are proportional to the inverse square-root of their masses.

Equilibrium Fractionation

The source of mass-dependence in equilibrium fractionation processes is best described using an example of an isotope exchange reaction. Equilibrium isotope exchange reactions can be represented as:

$aX_1 + bX_2 \rightleftharpoons aX_2 + bX_1$ (Eqn. 1)

where 1 and 2 refer to the light and heavy isotopes, respectively, and aX_1 and aX_2 refer to isotopologues of element X [14].

The magnitude of differences in isotopic composition is conveniently expressed in terms of the fractionation factor (α), defined as:

$\alpha^{a\text{-}b} = R_a / R_b = ((X_2/X_1)_a / (X_2/X_1)_b) = K_{eq} = [Q(aX_2)Q(bX_1)] / [Q(aX_1)Q(bX_2)]$

where K_{eq} = equilibrium constant of the isotope exchange reaction, Q = partition function of the specified isotopologue.

Unlike kinetic fractionation processes, which are described by a classical treatment, quantum factors must be considered to accurately describe the fractionation affected by equilibrium isotope exchange reactions. Among these quantum factors are differences in vibrational, rotational, and intramolecular zero point energies, as well as symmetry considerations. Both the classical and quantum mechanical aspects of the description of isotope exchange reactions involving two isotopologues can be considered by evaluating the ratio of their partition functions:

$(Q_2/Q_1) = f * \Pi(\text{over } l)[(m_{2,l})/ (m_{1,l})]^{3/2}$ (Eqn. 2)

[13] where Q_i = partition function for isotopologue i, m_i = mass of isotope i, l = isotope atoms. The f value in Eqn. 2 is the total quantum contribution to the ratio of partition functions. The distinct momenta of the isotopologues are taken into account by the classical part of Eqn. 2, the ratio $[(m_{2,l})/ (m_{1,l})]^{3/2}$, which cancels out in the case of isotope exchange reactions, like Eqn. 1. The K_{eq} for these reactions may be calculated more simply as:

$K_{eq} = f(aX) / f(bX)$

where f(aX) and f(bX) are the quantum portions of the ratio of partition functions of isotopologues aX and bX.

Kinetic and equilibrium fractionation processes induce MDF by varying contributions from classically-derived and quantum mechanically-derived isotopic factors.

1.2.2 Mass-Independent Fractionation Processes

Early research theorized mass independent fractionation occurred exclusively from nuclear processes; however, later studies revealed a chemical process capable of producing MIF [15]. Hulston and discovered non-mass-dependently fractionated (NMDF) sulfur (S) in iron meteorites. They concluded that a nuclear process must have produced the NMDF S because all known physical and chemical processes fractionated isotopes mass-dependently [16]. They concluded cosmic-ray spallation produced the NMDF meteoritic S. However, corroborating evidence was not discovered: Non-mass-dependent fractionation would also be expected in cogenetically produced species, such as Mg and Si, but these anomalies have not been found. In the absence of a chemical process that could potentially explain non-mass-dependently fractionated oxygen, Clayton and colleagues concluded nuclear processes must have caused the MIF observed in CAIs [9].

Thiemens and Heidenreich were the first to show that a chemical process could induce non-mass-dependent fractionation when they produced isotopically enriched O_3 from O_2. They invoked self-shielding of $^{16}O_2$ to explain the formation of O_3 that is equally enriched in ^{17}O and ^{18}O [17]. Self-shielding is the photochemical process whereby light of the wavelength necessary to dissociate the relatively abundant ^{16}O-bearing species to make them reactive is attenuated before that required for the dissociation of ^{17}O or ^{18}O-bearing species. This

results in the disproportionate formation of ^{17}O and ^{18}O-bearing species, like CAIs, in most of the disk. Some groups still credit self-shielding of oxygen-bearing species for the existence of the observed heterogeneities in isotopic compositions in the solar system, but the absence of corroborating evidence has led many to search for a more consistent explanation. Recent, analogous studies of the isotopic effect of UV photodissociation of N_2 have been performed to better understand the potential for and significance of self-shielding in the protoplanetary disk [18]. These studies revealed that, although self-shielding may account for some mass-independently fractionated species, other photochemical processes are necessary to produce the observed isotopic compositions in N_2. Self-shielding of oxygen-bearing species is, therefore, not likely to be deterministic of the oxygen isotopic composition of solar system components. It may be concluded from the aforementioned studies that both nuclear and chemical processes can produce MIF.

Recent models have been proposed to explain the mass-independently fractionated oxygen in O_3 and CAIs. It was discovered that the isotopic selection that produces MIF O_3 occurs in the recombination reaction:

$$O + O_2 + M \rightarrow O_3 + M$$

[19].

In the formation of O_3, substitution of ^{16}O with the heavier isotopes of oxygen (^{17}O and ^{18}O, represented by Q) to the reactive oxygen species (O_2 and O) can produce asymmetric O_3 isotopomers (QOO or OOQ). Vibrationally-excited

QOO* or OOQ* have a greater density of reactive quantum states than their symmetric counterparts, O_3* or OQO* [20]. Excited O_3* either redissociates (to form O and O_2) or stabilizes (to form O_3), and the increased density of quantum states results in increased probability of stabilization for asymmetric species. This increased probability is equal, regardless of whether the asymmetry is created by the substitution of ^{17}O or ^{18}O, resulting in the production of isotopically anomalous, ^{17}O- and ^{18}O-rich, ^{16}O-poor O_3 [21]. It is important to note that although this model was created to explain MIF O_3, the results are equally true for any species with symmetric and asymmetric isotopologues.

Other models have been developed to explain the source of the mass-independent isotope anomaly observed in O_3. A quantum mechanics-derived model was developed by Babikov, and this model suggests isotopic selection that results in MIF O_3 occurs in the mechanism of energy transfer [22].

A model has been proposed to explain the production of MIF O_3 that is based on the differences in zero-point energy between isotopically substituted reactive oxygen species that form O_3 and the correlation of those differences with their different O_3 formation reaction rate coefficients [23]. Refinement and isolation of the most accurate model of mass-independently fractionated O_3 production will require the development and execution of extremely high precision isotopic studies of O_3 produced from isotopically substituted reactive oxygen species.

The symmetry-based effect described above for O_3 was expanded to explain the ^{16}O-rich CAIs found in meteorites [20, p. 2]. This model is notably different from that invoked to explain MIF O_3 in that the recombination that produces the isotopic anomaly occurs on the surface of nascent CAI grains, instead of in the gas phase, as is the case for O_3 (Fig. 1.1).

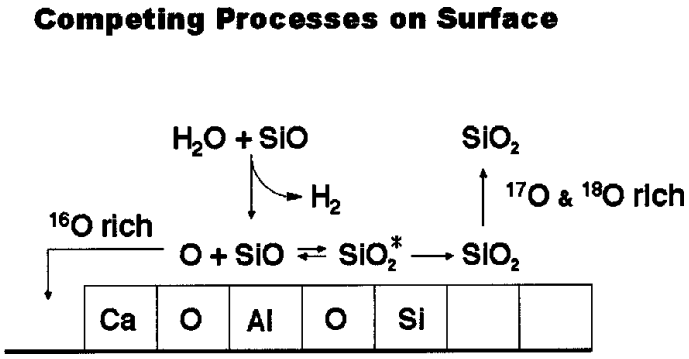

Figure 1.1 Schematic showing processes occurring on the surface of a developing calcium, aluminum-rich inclusion (CAI) grain. Figure taken from Marcus 2004 [20].

In the model presented in Marcus 2004, the isotopic anomaly in CAIs develops by the disproportionate condensation and incorporation of ^{16}O, relative to ^{17}O and ^{18}O, into the forming CAI grain (Fig. 1.1) [20]. The theoretical basis for the symmetry effect described above for O_3 is also true in this context and explains the disproportionate desorption of ^{17}O- and ^{18}O-containing SiO_2. In this model, isotopic selection occurs in the $O + SiO \rightleftharpoons SiO_2^* \rightarrow SiO_2$ reaction, where asymmetric SiO_2^* has a longer lifetime than symmetric SiO_2^* because of the former's increased density of reactive quantum states. The anomalously long

lifetime of asymmetric SiO_2* results in its having an increased probability of collisional relaxation, relative to symmetric SiO_2*. The difference in lifetimes of isotopically substituted SiO_2* leads to the ^{17}O and ^{18}O enrichment of desorbed SiO_2 and concomitant ^{16}O enrichment of condensed O. This mechanism accounts for the ^{16}O-rich, MIF oxygen found in CAIs and a relatively ^{17}O- and ^{18}O-enriched SiO reservoir that would later give rise to the bulk rock comprising the celestial bodies in our solar system [20].

1.2.3 Isotopic Effects of Formation and Exchange of Oxygen-Bearing Species in Meteorites

Reactions that produce oxygen-bearing species and govern their isotopic exchange can induce MDF and MIF, thereby causing a shift in the oxygen isotopic composition of the species. It is not possible to measure the oxygen isotopic composition of the proto-molecular cloud that gave rise to our solar system because nearly all endogenous oxygen has undergone sufficient processing to erase the primordial isotopic signature [8]. The primordial isotopic signature may be inferred, though, from modern abundances and consideration of the evolutionary history of a sample.

Studies of the constituent phases in meteorites, particularly the primitive chondrites, have led many groups to conclude both an ^{16}O-rich and an $^{17,18}O$-rich gas reservoir existed in the inner solar nebula [8]. Mixing of these reservoirs is

believed to be responsible for the observed oxygen isotopic heterogeneity in the solar system [7]. Refractory inclusions like CAIs and amoeboid olivine aggregates (AOAs) are enriched in ^{16}O ($\Delta^{17}O < -20‰$), suggesting the existence of an ^{16}O-rich gas reservoir (e.g., [24]–[26]. Observed $^{17,18}O$ enrichments of chondrules and alteration products in chondrites imply an $^{17,18}O$-rich gas reservoir also existed in the inner solar nebula [27]–[30].

Gas and dust in cold, dense molecular clouds within nebulae gravitationally collapse to form protoplanetary disks, which will eventually become planetary systems, around a central protostar. Gas and dust in the disk rotate around the protostar at different velocities, eventually resulting in the inward drift of dust grains [31], [32]. Solids drift inward toward the protostar until evaporation occurs, forming a band where the vapor concentration of the species is elevated relative to the rest of the disk.

Models have been developed to characterize the water and silicate evaporation fronts, which are highly applicable to the interpretation of analyses of these phases [33], [34]. The distribution and isotopic composition of water and silicate vapor and solid phases change as the disk evolves by processes such as evaporation, condensation, destruction by collision, and accretion, [8]. Gas-dust fractionation occurs during the settling of solids to the disk mid-plane and the transport of $^{17,18}O$-enriched water to the inner disk by ice migration [35]. Published models describe how the oxygen isotopic heterogeneity observed in

the inner solar system (See Section 1.3) could have been produced by exchange between relatively ^{17,18}O-rich gas and ^{17,18}O-poor silicate minerals [35].

Many MDF and MIF processes can affect the isotopic composition of oxygen-bearing phases of meteorites and their parent bodies subsequent to their formation. The MDF processes like this form oxygen-bearing species and govern their isotopic exchange. Examples of these MDF processes include evaporation and condensation of water; isotopic exchange reactions involving water and rock phases; and mineral formation. Photochemical processes and condensation of mineral grains are among the theorized sources of the mass-independent anomaly [15]. Many of the fractionation processes believed to have been involved in the creation of the oxygen isotopic compositions of inner solar system materials are described in Sections 1.2 and 1.4

Mineral Formation

Oxygen in terrestrial silicates is mass-dependently fractionated, reflecting the mass-dependent nature of the reactant reservoirs and fractionation induced by the silicate formation reaction [36]. Silicate oxygen in samples of other bodies in the inner solar system is non-mass-dependently fractionated to varying degrees. This isotopic anomaly could be inherited from a non-mass-dependently fractionated precursor and/or MIF processes enabled by physical conditions on the parent body.

Evidence from recent experimental studies has indicated MIF of oxygen isotopes can occur in the oxidation in silicon monoxide (SiO) to form silicon dioxide (SiO_2) [37]. This process could be responsible for producing the observed, diverse oxygen isotopic anomalies in inner solar system bodies.

The formation of secondary (aqueous) alteration products such as carbonates and phyllosilicates are generally MDF processes [38], [39]. As kinetically-controlled processes, their fractionation factors depend strongly on temperature. This results in large fractionations in minerals formed at low temperatures. Oxygen in terrestrial, soil carbonates are mass-dependently fractionated [38]. The oxygen isotopic composition of some carbonates and sulfates in SNC meteorites do not obey MDF laws, and their isotopic anomalies ($\Delta^{17}O \cong 0.7\text{-}1.4‰$) may result from photochemical processes on the surface or in the atmosphere of Mars [40], [41].

The large, positive mass-independent isotopic anomalies found in carbonates in SNC meteorites and aerosols from the terrestrial atmosphere can be explained by the inheritance of a MIF anomaly from O_3 to carbonate [40], [41]. The model proposed to explain the anomalous terrestrial carbonates involves the transfer of $^{17,18}O$-enrichment from atmospheric O_3 to surface carbonates via a hydrogen peroxide precursor.

Evaporation and condensation

The reversible physical processes of evaporation and condensation are kinetically controlled because the products and reactants are not in equilibrium:

$H_2{}^{18}O(g) + H_2{}^{16}O(l) \rightleftharpoons H_2{}^{18}O(l) + H_2{}^{16}O(g)$ (Eqn. 3)

$H_2{}^{17}O(g) + H_2{}^{16}O(l) \rightleftharpoons H_2{}^{17}O(l) + H_2{}^{16}O(g)$ (Eqn. 4)

where K_{eq}(Eqn. 3) > K_{eq}(Eqn. 4). The difference in equilibrium constants for eqns. 3 and 4 arises from the lower diffusion velocity and lower intramolecular zero point energy of $H_2{}^{18}O$, relative to $H_2{}^{17}O$.

Gas-Solid Exchange

A two-stage exchange model was developed by Clayton to better understand the isotopic effects of interactions of oxygen-bearing species in the gas and solid phases under the conditions expected on the parent body [39]. In this model, solids are comprised primarily of $MgFeSiO_4$ and the gas phase is made up of H_2O and CO. The predicted olivine to gas fractionation is $\Delta^{17}O$ = -1.10‰. Results of modeling high-temperature exchange of silicates and formation of secondary (aqueous) alteration products at low temperatures are consistent with the oxygen isotopic composition of some phases in meteorites [39].

Equilibrium is approached in most processes that form water and minerals on Earth, so most of these processes induce MDF [14]. Varying contributions from equilibrium and kinetic fractionation processes produce the observed mass-

dependence in the terrestrial water and rock oxygen reservoirs ($\Delta^{17}O \cong 0‰$). The isotopic effect of the occurrence of these processes under non-equilibrium conditions could be reflected in the oxygen isotopic anomalies found in extraterrestrial samples.

Solar Wind

Oxygen comprises a non-negligible fraction of the SW particles that bombard every body in the inner solar system and is implanted in the surface layers of regolith. Implanted SW oxygen exchanges with surrounding oxygen-bearing reservoirs, like water or minerals. Analyses of SW made by NASA's Genesis Mission discovered SW oxygen to be mass-independently enriched in ^{16}O [42].

Solar wind interaction with oxygen-bearing minerals on the surface of celestial bodies is believed to produce water [43]. Many groups agree the water found in the equatorial regions of the lunar surface is most consistently explained by its production in the solar wind [44]–[46]. In the model of Starukhina, oxygen-bearing minerals on the lunar surface are the source of oxygen in the production of water by solar wind. These minerals are comprised of mass-dependently fractionated oxygen and the reaction of mineral to form water is expected to induce MDF so solar wind-derived water on the lunar surface is hypothesized to be made up of mass-dependently fractionated oxygen.

1.3 Oxygen Isotopic Heterogeneity in the Inner Solar System

A measured oxygen isotopic composition reflects the primordial component of the sample as well as any shifts induced by physical and chemical processes that fractionate oxygen isotopes. Meteorites are made up of material ejected from an impact site on the surface of a body. Samples of other bodies, such as the Moon and Mars, analyzed in situ or returned to Earth for analysis were all collected on the surface of the body. The world's collection of extraterrestrial material therefore originates on the surface of a celestial body, and keeping this in mind when interpreting experimental results is important.

Evolutionary history is deterministic of oxygen isotopic composition. Mars, the Moon, and the other achondritic meteorite parent bodies are the known differentiated bodies that have produced meteorites found on Earth. Differentiation is the process that occurs on molten celestial bodies whereby the constituents are approximately homogenized by melting and then separated by gravitational forces based on their physical and chemical properties. The result is a body comprised of concentric spheres of approximately homogeneous composition with the least dense layer at the surface of the body and the densest layer at the core. The differentiated nature of achondritic meteorite parent bodies can be seen in the homogenous composition of these meteorites.

The structure of differentiated bodies is distinct from that of undifferentiated bodies, which have approximately equal composition at all radial

distances from the gravitational center. The parent bodies of chondritic meteorites are undifferentiated, so samples of chondrites contain many phases that are compositionally distinct. These components include matrix, chondrules, refractory inclusions like CAIs, and secondary alteration products, as well as many others. These phases are uniquely distinct in samples of undifferentiated bodies because these bodies never experienced high temperature exchange and equilibration, unlike differentiated bodies. The absence of homogenization on their parent bodies makes chondrites the most primitive meteorites, and some of their constituent phases are studied to gain information about conditions in the solar nebula.

Celestial bodies have unique endogenous, oxygen isotopic compositions as well as variation in the significance and effect of isotopic fractionation processes, such as those described in Section 1.2. Variation in the endogenous and process-driven components is responsible for the diverse oxygen isotopic compositions measured in the bulk rock forming the surface material on each of the solid bodies in our solar system, as inferred from the composition of meteorites (Fig. 1.2). In general, achondrites occupy $\delta^{17}O$-$\delta^{18}O$ space closer to the TFL than the chondritic meteorites.

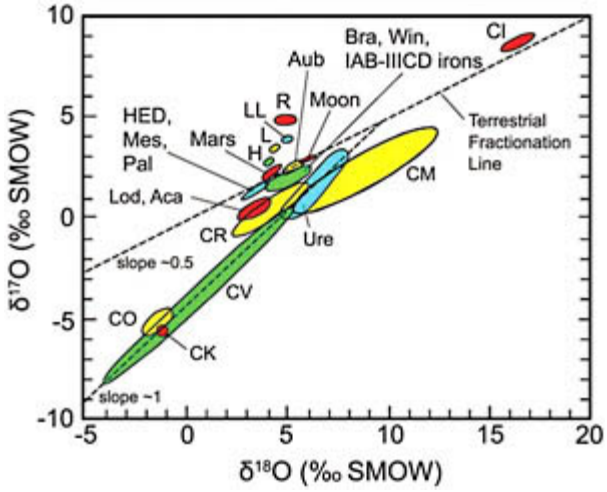

Figure 1.2 Oxygen isotopic composition ($\delta^{17}O$ vs. $\delta^{18}O$, ‰) of the constituent minerals of each class of meteorite, the Moon, and Mars. Compositions are with respect to Standard Mean Ocean Water (SMOW). Aca = Acapulcoite, Aub = Aubrite, Bra = Brachinite, CO, CK, CV, CR, CM, CI = Carbonaceous chondrites, HED = Howardite, Eucrite, Diogenite, H = High iron ordinary chondrite, L = Low iron ordinary chondrite, LL = Low-Low iron ordinary chondrite, Lod = Lodranite, Mes = Mesosiderite, Pal = Pallasite, R = Rumuruti chondrite, Ure = Ureilite, Win = Winonite.

In addition to the endogenous component and effects of differentiation, the oxygen isotopic composition of a sample from an inner solar system body depends on the prevalence of processes that fractionate isotopes. The MDF or MIF induced by those processes is described in detail in Section 1.2. The isotopic effect of these processes depends on their relative rates, local physical conditions, the mass-dependent or –independent nature of their fractionation factors, and the proportion of the oxygen-bearing reservoir made up of the products and reactants of these processes.

The variability in oxygen isotopic composition in the solar system shown in Figure 1.2 can be explained by the existence of an isotopically heterogeneous

oxygen reservoir or input of pure ^{16}O from a nearby supernova into an isotopically homogeneous oxygen reservoir. Mass-dependently fractionated oxygen found in samples from the inner solar system was most likely produced by a mixture MDF processes, such as isotopic exchange between water and rock phases; oxygen-bearing mineral formation; and evaporation and condensation of water. The MDF processes described in detail in Sections 1.2.3 and 1.2.4 account for the mass-dependently fractionated oxygen in the analyzed sample. Mass-independently fractionated oxygen could result from mineral condensation, photochemical processes in planetary atmospheres or on grain surfaces, and/or other possible physical and chemical processes. MIF processes that could affect the oxygen isotopic composition of meteorite components are described in detail in Section 1.2.2.

1.3.1 Oxygen Isotopic Heterogeneity on Earth

On Earth, processes in the atmosphere, hydrosphere, lithosphere, asthenosphere, and mantle, such as equilibration, reaction and exchange with other oxygen-bearing species, photochemical reactions, and phase changes fractionate oxygen isotopes and shift the isotopic ratios. The range of oxygen isotopic compositions on Earth are shown in Fig. 1.3. The dominant pathway for oxygen in the atmosphere is photochemistry, a MIF process, so most of that oxygen is MIF and obeys a 1:1 ^{17}O:^{18}O relationship. Terrestrial reservoirs that are

MDF, like atmospheric H_2O and air O_2, are dominated by MDF processes, like evaporation and photosynthesis.

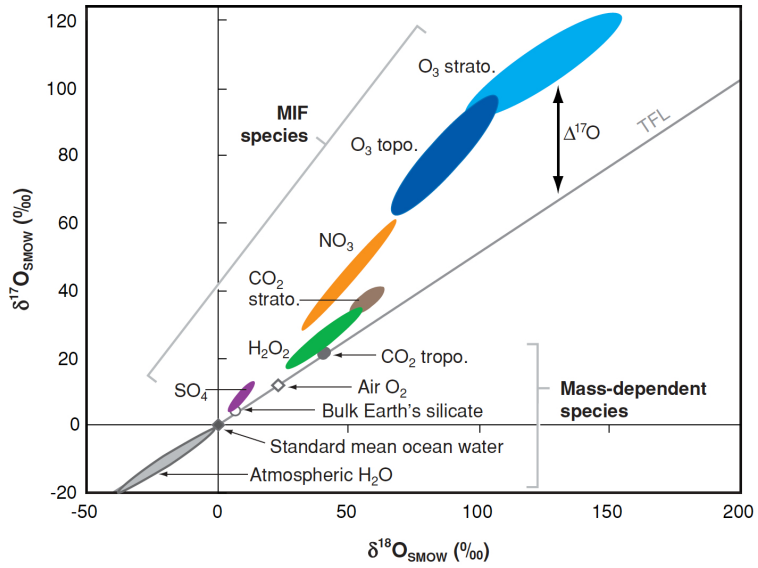

Figure 1.3 Oxygen isotopic composition ($\delta^{17}O$ versus $\delta^{18}O$, ‰) of oxygen on Earth. Compositions are with respect to Standard Mean Ocean Water (SMOW). The Terrestrial Fractionation Line (TFL), where $\delta^{17}O = 0.52 * \delta^{18}O$, is shown for reference [15].

1.3.2 Oxygen Isotopic Heterogeneity on Mars

On other solar system bodies as on Earth, oxygen isotopic composition is heterogeneous across the planet. Although our limited sampling of other bodies makes this more difficult, fractionation processes operate the same, regardless of body, under a given set of conditions, so inferences may be drawn. The varied isotopic compositions of many elements in many forms and phases on Mars

have been characterized and substantiate this [47]–[50]. The in situ measurements of the surface composition of Gusev Crater by the Spirit Rover and gamma-ray spectrometer measurements on the Odyssey Orbiter of the composition of Martian crust are inconsistent with measured compositions of the SNC suite of meteorites, which is widely agreed to represent the Earth's Martian meteorite collection [47]–[49].

On average, SNC meteorites possess $\Delta^{17}O \cong 0.3‰$ [51]. An exception to this is the Martian basaltic breccia NWA 7034, the $\Delta^{17}O$ value of which is 0.58‰ [52]. The compositions of many elements and mineral phases in NWA 7034 are within the range of the Spirit and Odyssey measurements, making it still more unique among the world's collection of Martian meteorites. Studies of the oxygen isotopic composition of water in NWA 7034 were performed by the dissertation author and are presented in Chapter 2.

The oxygen isotopic composition ($\Delta^{17}O$) of 13 Martian meteorites is presented in Figure 1.4. The bulk rock comprising these meteorites is distinct from samples of other celestial bodies, and its $\Delta^{17}O$ value varies little from the average ($\Delta^{17}O = 0.32‰$).

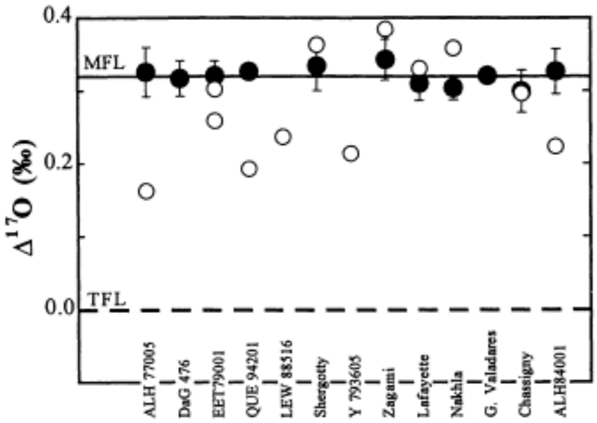

Figure 1.4 Oxygen isotopic composition of 13 Martian meteorites, presented as $\Delta^{17}O$ (‰). The $\Delta^{17}O$ values are with respect to Standard Mean Ocean Water (SMOW). Lines at $\Delta^{17}O$ = 0 and 0.32‰ represent the terrestrial fractionation line (TFL) and the Martian fractionation line (MFL), respectively. Filled circles mark analyses made by Franchi et al. and open circles show data from Clayton and Mayeda [53], [54].

Oxygen in water and secondary alteration products in SNC meteorites is isotopically heterogeneous, as evidenced by the large range of $\Delta^{17}O$ and $\delta^{18}O$ values measured in these phases (Fig. 1.5).

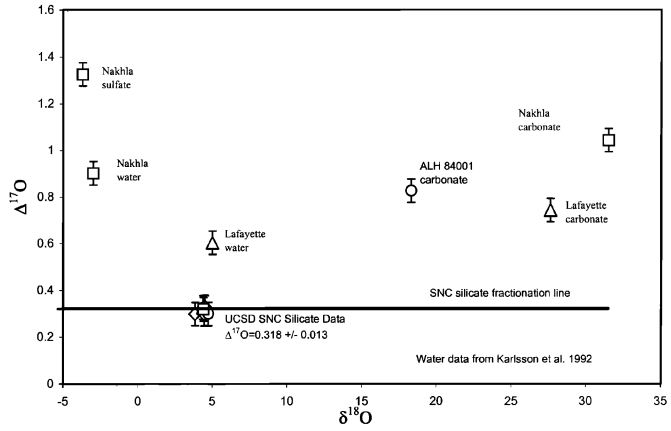

Figure 1.5 Oxygen isotopic composition of water and secondary alteration products in Martian meteorites (Nakhla, Lafayette, ALH 84001), presented as $\Delta^{17}O$ versus $\delta^{18}O$ (‰). Compositions are with respect to Standard Mean Ocean Water (SMOW). Terrestrial control analyses are shown for reference. Lines at $\Delta^{17}O$ = 0.32‰ represent the Martian fractionation line (MFL) [40], [53], [55].

The range in isotopic composition of alteration products shown in Figure 1.5 implies these oxygen reservoirs are not in equilibrium with the surrounding silicate rock, which has $\Delta^{17}O \cong 0.32‰$. Based on the many studies described above as well as others, the existence of several oxygen-bearing reservoirs that were not in isotopic equilibrium on Mars is hypothesized [40], [51], [53], [55].

1.3.3 Oxygen Isotopic Heterogeneity in Ordinary Chondrites

The three classes of ordinary chondrites (OCs) are H, L, and LL, reflecting the high iron, low iron, and low iron/low total metal abundance in these meteorites. The oxygen isotopic compositions of H, L, and LL chondrites are distinct, and, based on this line of evidence among others, the OCs are believed

to originate on three distinct parent bodies (Fig. 1.6). As a reference in the discussion of oxygen isotopic compositions in meteorite components, workers such as Clayton et al. used a line of best fit to the compositions of OCs shown in Figure 1.6, which they termed the Equilibrated Chondrite Line (ECL). The ECL is described by the equation $\delta^{17}O = 1.074 * \delta^{18}O - 1.53$.

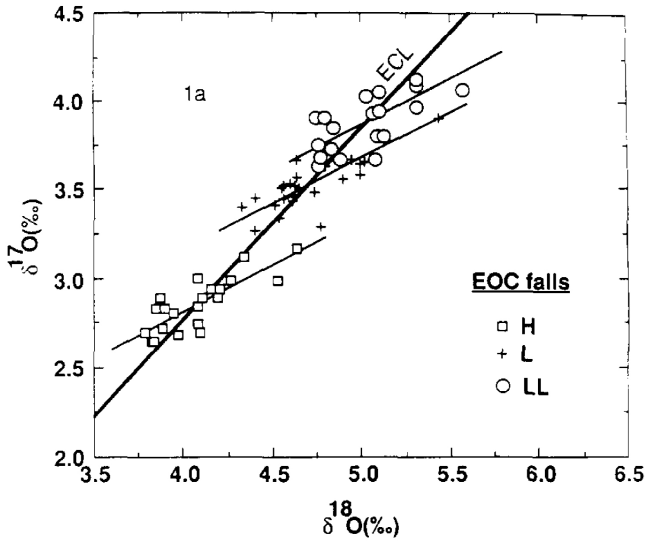

Figure 1.6 Isotopic composition of oxygen in ordinary chondritic (OC) meteorites, presented as $\delta^{17}O$ versus $\delta^{18}O$ (‰). H = high iron OC, L = low iron OC, LL = low iron and low metal. Compositions are with respect to Standard Mean Ocean Water (SMOW). The Equilibrated Ordinary Chondrite Line (ECL) at $\delta^{17}O = 1.074 * \delta^{18}O - 1.53$ is shown for reference. The mass-dependently fractionated nature of oxygen is shown by lines through the average of H, L, and LL chondrites where $\delta^{17}O = 0.5 * \delta^{18}O$ [56].

The oxygen isotopic composition of chondrules in H, L, and LL chondrites spans the range of the average, whole rock composition of these meteorites but are randomly distributed around the averages (Fig. 1.7). This reflects a common source reservoir for oxygen in the chondrules of all types of OCs.

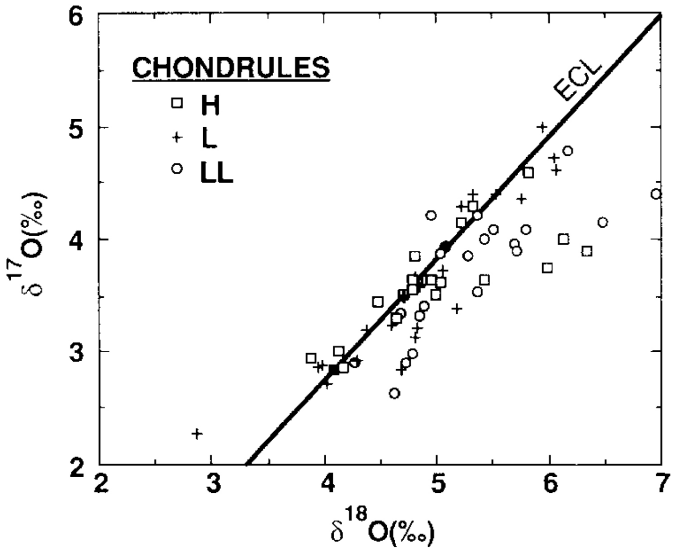

Figure 1.7 Isotopic composition of oxygen in individual chondrules in ordinary chondritic (OC) meteorites, presented as $\delta^{17}O$ versus $\delta^{18}O$ (‰). H = high iron OC, L = low iron OC, LL = low iron and low metal. Compositions are with respect to Standard Mean Ocean Water (SMOW). Filled symbols represent the average, whole rock composition of H, L, and LL equilibrated chondrites. The Equilibrated Ordinary Chondrite Line (ECL) at $\delta^{17}O = 1.074 * \delta^{18}O - 1.53$ is shown for reference [56].

1.3.4 Oxygen Isotopic Heterogeneity in Carbonaceous Chondrites

Carbonaceous chondrites (CCs) are a class of stony meteorite that originated from undifferentiated asteroids that once contained a large amount of water, relative to other asteroidal meteorite parent bodies. Recovered CCs are also relatively rich in organic compounds, such as amino acids. The CC class consists of 8 groups, which are named for the most representative meteorite of that group: Ivuna (CI), Vigarano (CV), Mighei (CM), Renazzo (CR), high metal

(CH), Bencubbin (CB), Karoonda (CK), Ornans (CO). Each of the eight groups of CCs is believed to have a unique parent body, and this is suggested by the different oxygen isotopic compositions of meteorites belonging to these groups (Fig. 1.8).

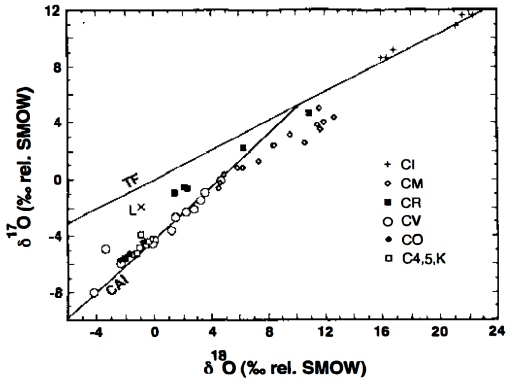

Figure 1.8 Oxygen isotopic composition of carbonaceous chondrite meteorites (CI, CM, CR, CV, CO, C4,5K), presented as $\delta^{17}O$ versus $\delta^{18}O$ (‰). Compositions are with respect to Standard Mean Ocean Water (SMOW). Lines representing terrestrial, mass-dependent fractionation (TF) and mass-independent fractionation observed in refractory inclusions (CAI) are shown and possess slopes of 0.52 and 1, respectively [7].

Meteorites belonging to the eight groups of CCs possess different oxygen isotopic compositions, with some overlap in the compositions of the groups (Fig. 1.8). Most oxygen in the CCs studied is mass-dependently fractionated, which could have been induced by low temperature formation. The pattern of oxygen isotopic compositions measured in these CCs is consistent with high temperature exchange of CAIs and chondrules with gas in the nebula and low temperature silicate-water exchange [7].

The Murchison meteorite is a CM2 carbonaceous chondrite, which, because of its large mass of over 100kg, has been studied by many groups. Analyses of the oxygen isotopic composition of water in Murchison were performed by the dissertation author and will be presented in Chapter 4. Mineral phases in Murchison display a range of oxygen isotopic compositions that are mass-dependently and –independently fractionated to varying degrees (Fig. 1.9).

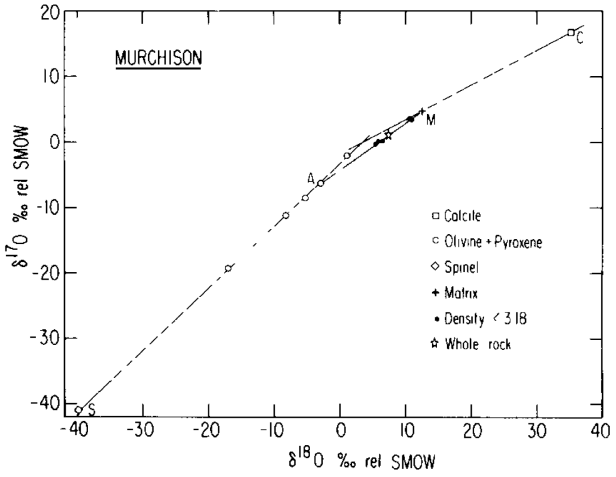

Figure 1.9 The oxygen isotopic composition of the whole rock and separated fractions of calcite, olivine & pyroxene, spinel, and matrix of the Murchison meteorite are presented as $\delta^{17}O$ versus $\delta^{18}O$ (‰). Compositions are with respect to Standard Mean Ocean Water (SMOW). Point A shows the weighted average composition of the anhydrous silicates. Lines SA and MC have slopes of 1 and ½, respectively [39].

The oxygen isotopic composition of Murchison is shown in Figure 1.9 as $\delta^{17}O$ versus $\delta^{18}O$ (‰). In Figure 1.9, high temperature minerals fall along the slope = 1 line, SA, representing MIF. Low temperature minerals in Murchison possess MDF oxygen, as evidenced by the proximity of their compositions to the

slope = ½ line, MC. These data imply at least two isotopically distinct, oxygen-bearing reservoirs contributed to the formation of the carbonaceous chondrite parent body. Solid-gas interactions in a temperature dependent exchange model like that described in Section 1.2.3 could explain the observed oxygen isotopic fractionation patterns [39].

1.3.5 Oxygen Isotopic Heterogeneity in Eucrites

Eucrites are a class of achondritic meteorites originating from a large, differentiated asteroid, possibly 4 Vesta [57], [58]. Eucrites are stony meteorites comprised primarily of pyroxene, pigeonite, and calcic plagioclase [59]. The larger class of howardites, eucrites, and diogenites (HEDs) is used to reflect the widely held belief that all HEDs have a common parent body [51], [60]. On average, HEDs have a $\Delta^{17}O \cong -0.3‰$ [51].

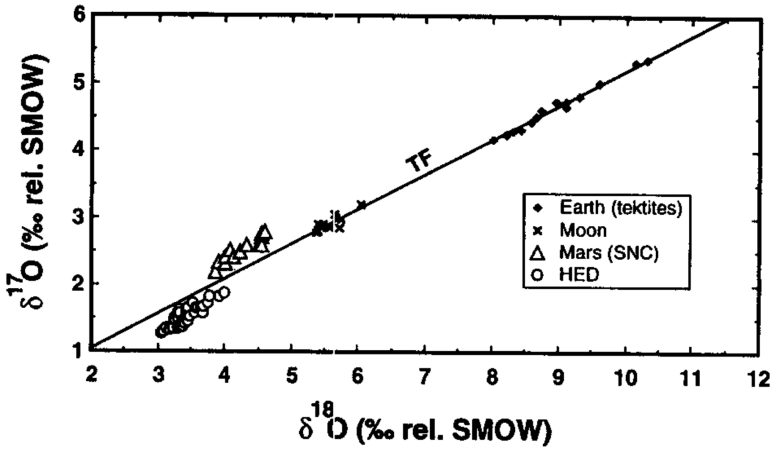

Figure 1.10 Oxygen isotopic composition of terrestrial tektites, the Moon, Mars (SNC meteorites), and HEDs, presented as $\delta^{17}O$ versus $\delta^{18}O$ (‰). Compositions are with respect to Standard Mean Ocean Water (SMOW). The terrestrial, mass-dependent fractionation line (TF) is shown for reference and has a slope of 0.52 [54].

The range of oxygen isotopic compositions in the eucrites studied by Clayton and Mayeda is $\delta^{17}O$ = 1.29 – 2.00‰ and $\delta^{18}O$ = 2.90 - 4.00 ‰ (Figure 1.10) [54]. The oxygen isotopic composition of the eucrites studied is clearly distinct from that of the Moon, Mars (SNCs), HEDs, and the Earth (tektites). The discrete oxygen isotopic compositions reflect the unique planetary parentage of these samples. The deviation in these compositions from MDF is not readily apparent in Figure 1.10, given the large scale. The isotopically anomalous compositions are more clearly shown in the comparison of $\Delta^{17}O$ and $\delta^{18}O$ (Fig. 1.11).

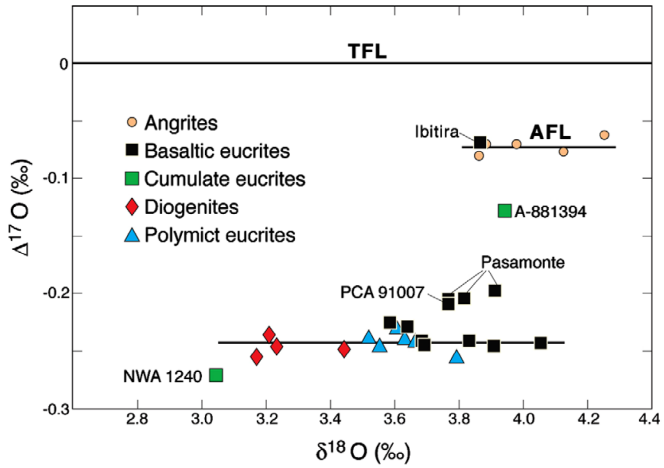

Figure 1.11 Oxygen isotopic composition of eucrites, presented as $\Delta^{17}O$ (‰) versus $\delta^{18}O$ (‰). The mean $\Delta^{17}O$ value of the eucrites analyzed is represented by the line at $\Delta^{17}O = -0.242 \pm 0.004$‰. The terrestrial fractionation line (TFL) at $\Delta^{17}O = 0$‰ is shown for reference [61].

The $\Delta^{17}O$ values of all the eucrites studied by Clayton and Mayeda and Scott et al. lie close to the mean [54], [61]. This small range in $\Delta^{17}O$ values implies the eucrite parent body is isotopically homogenous.

1.4 Water in the Inner Solar System

A significant fraction of the water in the inner solar system was inherited from a presolar source [62]. There is evidence to suggest this presolar water is isotopically enriched in ^{2}H, ^{17}O and ^{18}O [62], [63]. This oxygen isotopic effect can be seen in the $^{17,18}O$-rich compositions of asteroidal and molecular cloud H_2O in Figure 1.12.

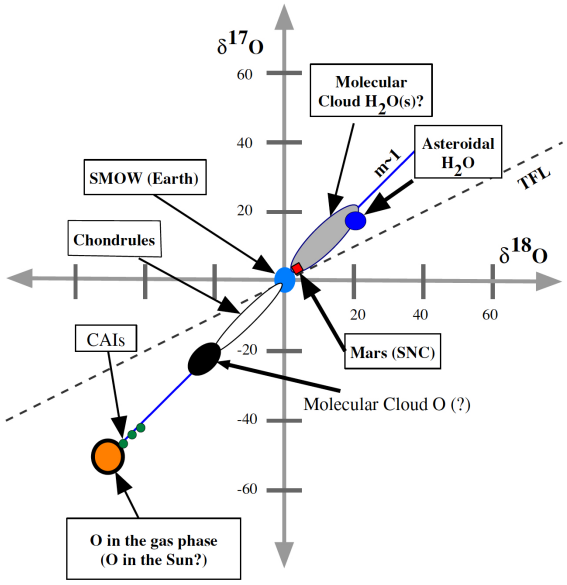

Figure 1.12 Oxygen isotopic composition ($\delta^{17}O$ versus $\delta^{18}O$, ‰) of selected oxygen reservoirs in the solar system. Reservoirs shown include molecular cloud H_2O, asteroidal H_2O (inferred), Standard Mean Ocean Water (SMOW), chondrules, Mars (SNCs), molecular cloud O, CAIs, and solar O [64].

1.4.1 Oxygen Isotopic Fractionation of Reactions which Formed the Primordial Water in the Solar System

The oldest solid materials in the solar system, CAIs and chondrules, are components of primitive meteorites and contain approximately equal amounts of ^{17}O and ^{18}O [9]. This places their oxygen isotopic compositions on a slope ~1 line in $\delta^{17}O$ versus $\delta^{18}O$ space, often referred to as the carbonaceous chondrite anhydrous meteorite (CCAM) or Allende CAI line [9]. Interstellar (IS) dust grains make up most of the solid material in dense molecular clouds (DMCs), the birthplace of stars and planetary systems [65]. Models of the chemistry occurring

on the surface of IS dust grains indicate on long timescales (10^5-10^6 years), a significant fraction of the oxygen in DMCs is water ice produced by one of the following processes (a or b):

a)

$$O + O \rightarrow O_2 \quad (1)$$

$$O + O_2 \rightarrow O_3 \quad (2)$$

$$H + O_3 \rightarrow O_2 + OH \quad (3)$$

$$H_2 + OH \rightarrow H + H_2O \quad (4)$$

or

$$H + OH \rightarrow H_2O \quad (5)$$

b)

$$H + O_2 \rightarrow HO_2 \quad (6)$$

$$H + HO_2 \rightarrow H_2O_2 \quad (7)$$

$$H + H_2O_2 \rightarrow H_2O + OH \quad (8)$$

[66]–[68].

In DMCs, dust grains could increase the probability of reaction 2 in the above scheme by providing a third body:

$$O(s) + O_2(s) + M\ (surface) \rightarrow O_3 + M\ (surface)$$

[64]. The effect of a third body on the rate of the O_3 formation reaction has been characterized [69]–[71]. It has long been known that photodissociation of O_2(s) by mercury-lamp generated, 184.5nm photons leads to production of O_3 [72].

The relative significance of processes *a* and *b* is not clear, but precursors to water in both of these processes (HO_2 and O_3) are known to be mass-

independently fractionated (in $\delta^{17}O$ versus $\delta^{18}O$ space, slope ~0.84 and ~1, respectively) [17], [73]. Reaction of MIF HO_2 and O_3 would result in the production of isotopically anomalous H_2O. Consequently, characterization of the oxygen isotopic fractionation induced in H_2O produced via HO_2 and O_3 in the parent molecular cloud is crucial in understanding the observed oxygen isotopic composition of water in the solar system.

1.4.2 Lunar Water

The relatively well-characterized mineral phases in meteorites describe much of the geological history of a sample and its parent body, but analysis of the rare water phase could elucidate the source of water on Earth by exposing the compositions of the potential water sources. The Earth and Moon are believed to have a common source of water. Most endogeneous, terrestrial water likely degassed to space following The Giant Impact, when Theia, a body roughly 2/3 Earth's diameter, collided with the proto Earth, resulting in the formation of the Earth and Moon [74], [75]. The primordial water composition of the Earth has long since been erased by physical processes like evaporation and precipitation or by reaction or interaction with other chemical species. The absence of these processes as well as plate tectonics on the Moon mean the primordial water may be well preserved.

Water found on the present day surface of the Earth and Moon is thought to primarily result from delivery by comets and asteroids or interaction with solar wind or radiation, or cosmic radiation. Spectroscopic studies of comets and asteroids and sample analyses of meteorites reveal the isotopic composition of the potentially impacting bodies. Measured abundances of cosmogenically produced radionuclides in lunar surface samples inform models that predict the effects of interaction with cosmic radiation.

The contribution of extraterrestrial material to the Earth-Moon system can be approximated using measured meteorite compositions, spectroscopically determined parent body compositions, and the flux of each type of potential impactor. Meteorites fall in an even distribution across the Earth's surface, and to estimate this flux, the abundant and well preserved collection of Antarctic meteorites, curated by the National Aeronautics and Space Administration (NASA) Astromaterials Research and Exploration Science (ARES), is taken as representative. This collection also displays the approximate meteorite flux to the Moon. Using this information, the mass and composition of meteoritic material delivered to the Moon may be estimated.

1.4.3 Water on Mars, Asteroids, and Comets

A paucity of measurements of water in extraterrestrial samples prompted this broad study of the isotopic composition of water in the inner solar system.

Oxygen isotopic studies of water on Mars are abundant relative to the few measurements of water in asteroids and comets. Martian meteorites, SNCs, have been analyzed to determine the oxygen isotopic composition of water on Mars (Figure 1.13, See Chapter 3).

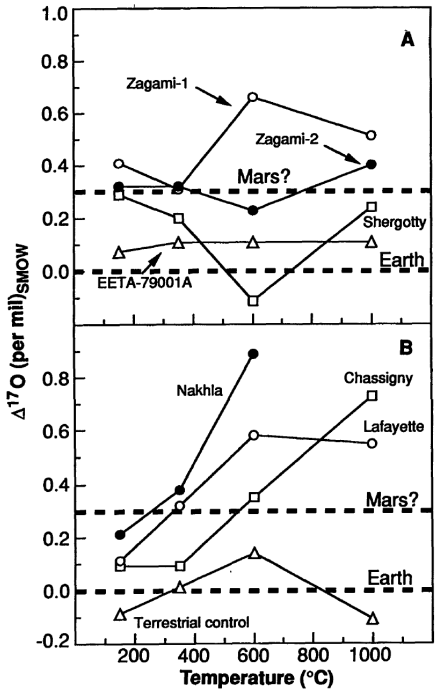

Figure 1.13 Oxygen isotopic composition ($\Delta^{17}O$, ‰) of water evolved during stepwise heating of SNC meteorites. Results reflect analyzed water liberated from samples of several SNCs (Zagami, Shergotty, EETA 79001A, Nakhla, Chassigny, and Lafayette) and a terrestrial control while heating stepwise to 150, 350, 600, and 1000˚C. Compositions are with respect to Standard Mean Ocean Water (SMOW). Dotted lines at $\Delta^{17}O$ = 0.0 and 0.3‰ represent the average composition of Earth and Mars, respectively [55].

Water in SNCs is isotopically heterogeneous within a sample and between samples of different SNCs. Some fractions of this water are ^{17}O-enriched relative to the bulk rock comprising Mars and the TFL. These results imply the Martian

water reservoir is isotopically heterogeneous and not in equilibrium with the oxygen-bearing mineral reservoir.

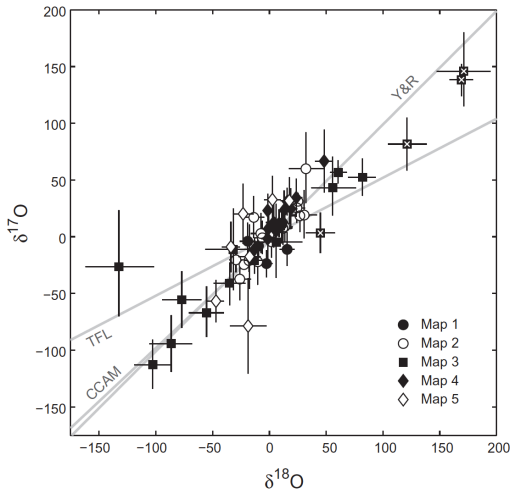

Figure 1.14 Oxygen isotopic composition ($\delta^{17}O$ versus $\delta^{18}O$, ‰) of particles from comet 81P/Wild2. Results reflect analyses of 63 particles in the bulb of a single track collected from the comet on NASA's Stardust mission. The terrestrial fractionation line (TFL), Young and Russell line (Y&R), and carbonaceous chondrite anhydrous mineral line (CCAM) are shown for reference. Error bars shown are 2σ [76].

NASA's Stardust mission collected and returned to Earth samples of the comet 81P/Wild2, which belongs to the Jupiter-family class of comets some workers have proposed delivered a significant amount of Earth's water. As is evident in Figure 1.14 mineral fragments found in comet 81P/Wild2 possess a wide range of oxygen isotopic compositions ($-70‰ \leq \Delta^{17}O \leq +60‰$). The Young and Russell line (Y&R) and carbonaceous chondrite anhydrous mineral line (CCAM) are the lines of best fit to the oxygen isotopic compositions of primitive

chondrite meteorites and refractory Calcium-Aluminum-rich Inclusions (CAIs) and have slopes of 1.0 and 0.94, respectively [77], [78].

The large range in oxygen isotopic compositions of mineral fragments found in comet 81P/Wild2 (Fig. 1.14) should not be neglected in the discussion of sources of water in the inner solar system. Oxygen in minerals delivered as comets makes up a large fraction of the oxygen reservoir on the surface of some bodies, and this cometary oxygen can form and isotopically exchange with water [43].

Chapter 2. Radar-Enabled Recovery of the Sutter's Mill Meteorite, a Carbonaceous Chondrite Regolith Breccia

2.1 Abstract

Doppler weather radar imaging enabled the rapid recovery of the Sutter's Mill meteorite after a rare 4-kiloton of TNT–equivalent asteroid impact over the foothills of the Sierra Nevada in northern California. The recovered meteorites survived a record high-speed entry of 28.6 kilometers per second from an orbit close to that of Jupiter-family comets (Tisserand's parameter = 2.8 ± 0.3). Sutter's Mill is a regolith breccia composed of CM (Mighei)–type carbonaceous chondrite and highly reduced xenolithic materials. It exhibits considerable diversity of mineralogy, petrography, and isotope and organic chemistry, resulting from a complex formation history of the parent body surface. That diversity is quickly masked by alteration once in the terrestrial environment but will need to be considered when samples returned by missions to C-class asteroids are interpreted.

2.2 Introduction

On 22 April 2012, the KBBX (Beale Air Force Base, California), KDAX (Sacramento, California), and KRGX (Reno, Nevada) weather radars of the U.S. National Climatic Data Center's NEXRAD network detected radial Doppler shifts in four sweeps, following a fast-moving daytime fireball seen over much of California and Nevada at 14:51:12 to 17 UTC (Fig. 2.1) [79]. The falling meteorites were identified from a downward sequence of subsequent detections, small-scale turbulence, and widely variable spectrum width values correlated in time, location, and direction with eyewitness reports of the fireball.

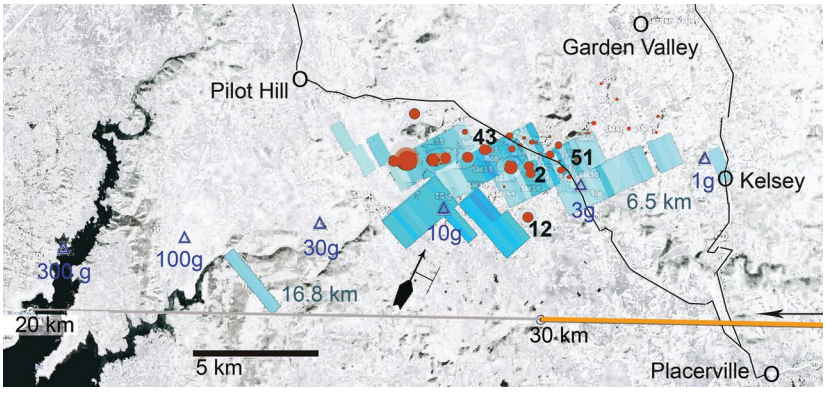

Figure 2.1 Map of ground-projected fireball trajectory solution, radar Doppler reflectivity, and meteorite find locations near Sutter's Mill. Ground-projected fireball trajectory solution is shown by the orange line. Radar Doppler reflectivity is shown in light blue; –5 dBZ for pale blue to +15 dBZ for deepest blue. Meteorite find locations near Sutter's Mill are reflected by red dots, where size is proportional to mass; relevant finds are labeled with SM number. Blue triangles are the calculated impact locations for breakup at 48 km and wind drift from 13 m/s winds to azimuth 27° between 18 and 2 km altitude.

Under the radar footprint over the townships of Coloma and Lotus in El Dorado County, California, the first three pieces of the meteorite were recovered on 24 April, before heavy rain hit the area. One meteorite fell at Sutter's Mill (SM), the gold discovery site that initiated the California Gold Rush. Two months after the fall, SM find numbers were assigned to the 77 meteorites listed in table S3, with a total mass of 943 g (see Section 2.3). The biggest meteorite is 205 g.

This is a tiny fraction of the pre-atmospheric mass, based on the kinetic energy derived from infrasound records. Eyewitnesses reported hearing a loud boom followed by a deep rumble. Infrasound signals (table S2A) at stations I57US and I56US of the International Monitoring System, located ~770 and ~1080 km from the source, are consistent with stratospherically ducted arrivals. The combined average periods of all phase-aligned stacked waveforms at each station of 7.6 s correspond to a mean source energy of 4.0 (–2.2/+3.4) kT of TNT, using the multistation period yield relation from (Ens 2012). This was the most energetic reported bolide falling on land globally since the 1.2-kT impact of asteroid 2008 TC_3 over Sudan in 2008 [80], [81].

Seismic data suggest a point source altitude of 54.8 ± 10.9 km above mean sea level, estimated from impulsive phase arrivals of the air blast at eight seismograph stations by applying a simple half-space sonic velocity model and direct ray paths to a standard earthquake location code (table S2B) [82].

This altitude corresponds to a persistent flare detected in a set of three photographs from Rancho Haven, north of Reno, Nevada (fig. S1). Triangulation

with videos from Johnsondale, California, and Incline Village, Nevada (figs. S2 and S3), shows that the bolide was first detected at 90 km approaching from the east, had a broad peak in brightness around 56 km, and detonated at 47.6 ± 0.7 km (Table 2.1). Even in the daytime sky, a great many fragments were detected down to 30 km.

Table 2.1 Atmospheric trajectory and pre-atmospheric orbit for the SM and Maribo CM chondrites. Angular elements are for equinox J2000.0.

Atmospheric trajectory	**SM**	**Maribo**	**Pre-atmospheric orbit**	**SM**	**Maribo**
Hb (beginning height - km)	90.2 ± 0.4	111.8 ± 0.4	TJ (Tisserand's parameter)	2.81 ± 0.32	3.04 ± 0.32
Hm (broad maximum - km)	~56	~58	a (semimajor axis - AU)	2.59 ± 0.35	2.34 ± 0.29
Hf (disruption - km)	47.6 ± 0.7	37.3 ± 0.6	e (eccentricity)	0.824 ± 0.020	0.795 ± 0.026
He (end height - km)	~30.1	~32	q (perihelion distance - AU)	0.456 ± 0.022	0.481 ± 0.010
V∞ (entry speed - km/s)	28.6 ± 0.6	28.0 ± 0.7	w (argument of perihelion - °)	77.8 ± 3.2	99.0 ± 1.4
h (entry elevation angle - °)	26.3 ± 0.5	30.2 ± 0.5	W (longitude of ascending node - °)	32.77 ± 0.06	117.64 ± 0.05
az (entry azimuth angle from south - °)	272.5 ± 0.4	276.2 ± 0.2	i (inclination - °)	2.38 ± 1.16	0.72 ± 0.98
Vg (geocentric entry speed - km/s)	26.0 ± 0.7	25.4 ± 0.8	Q (aphelion distance - AU)	4.7 ± 0.7	4.2 ± 0.6
Rag (geocentric right ascension of radiant - °)	24.0 ± 1.3	124.6 ± 1.0	Tp (perihelion time)	2012-03-09.1	2008-12-03.6
Decg (geocentric declination of radiant - °)	12.7 ± 1.7	18.8 ± 1.6	Epoch (UT)	2012-04-22.620	2009-01-17.798

The entry speed is twice that of typical triangulated falls from which meteorites have been recovered (table S1). SM has the highest disruption

altitude on record. With an entry velocity of 28.6 km/s, the infrasound-derived kinetic energy corresponds to a pre-atmospheric mass of ~40,000 (range 20,000 to 80,000) kg. Counter to intuition, the catastrophic disruption was key to meteorite survival from this fast entry [81]. So far, ~0.1 kg/km has been recovered along the trend line, for an estimated total fallen mass ≥1.7 kg. This is far less than that recovered from the similar-sized but slower-impacting 2008 TC_3: 1.2 kg/km and 39 kg [81]. An airship search did not find impact scars from falling kilogram-sized meteorites.

The pre-atmospheric orbit (Table 1) had low inclination and high eccentricity, with aphelion close to the orbit of Jupiter and perihelion (*q*) approaching the orbit of Mercury (fig. S5). Semimajor axis, eccentricity, and inclination are strikingly similar to the preliminary values reported for the CM-type carbonaceous chondrite Maribo by Haack *et al*. [83], [84]. The entry conditions, too, were much alike. Upon request, W. Singer and G. Stober provided the seven Juliusruh radar head-echo range and direction positions of the early 112- to 79-km altitude part of this fall (table S1), which translated into the orbital elements listed in Table 1. SM and Maribo have lower perihelion distance and higher-eccentricity orbits than all other known (mostly ordinary chondrite) falls (table S1).

That distinction may be due to a bias toward a more recent evolution into Earth-crossing orbits for this population. SM has a cosmic ray exposure (CRE) age at the extreme low end of the CM2 chondrite CRE age distribution, which as a group is younger than all other classes of meteorites except lunar meteorites

[85]. An age of 0.10 ± 0.04 million years (My) was obtained from the measured ^{26}Al activity (with a 0.705 million-year half-life) of 3.8 ± 0.8 dpm/kg in SM36 (table S20). He and Ar isotopic ratios in SM43 and SM51 show no clear excess of a cosmogenic noble gas component, but a small excess of cosmogenic Ne is observed as deviations from two mixing lines between the trapped components; solar Ne – P3 Ne and P3 Ne – Ne E (fig. S27) [86]. The low concentration of cosmogenic ^{21}Ne [1.02 ± 0.11 × 10^{-10} cm^3/g at standard temperature and pressure (STP)] indicates a very short CRE age of 0.051 ± 0.006 My (the average of four ages in table S18), if a production rate of 2 × 10^{-9} cm^3/g/My at STP for the near surface of a large object is adopted [87].

The SM and Maribo orbits have a Tisserand's parameter with respect to Jupiter (T_J) that borders those of asteroids (T_J >3) and Jupiter family comets (T_J = 2 to 3). Visual observations of Murchison (CM) also point to approach on a low-inclined orbit [88]. A possible Jupiter-family comet origin is intriguing [84] [for a review, see [88]], especially because the CM-like micrometeorites are dynamically linked to Jupiter-family comets [89]. Finding two asteroids on orbits at q = 0.47 astronomical unit (AU) could mean that both are part of an old ~0.1-My-old meteoroid stream, perhaps related to 2P/Encke, but only if CM chondrites survive longer than typical Taurid meteoroids [84].

Until other evidence of hydrothermal alteration in Jupiter-family comets is found, an origin in the asteroid belt is more likely [88]. The asteroid-family source has low inclination and is close to the 3:1 mean motion resonance with Jupiter,

the CRE age leaving little time for thermal drag forces to move the semimajor axis of a main-belt asteroid into resonance at 2.5 AU. A suitable candidate is the (495) Eulalia family, recently proposed as a source of near-Earth C-class asteroids [90]. Unlike ordinary chondrites ejected from the 3:1 resonance, which tend to collide with Earth on higher-impact-probability perihelion distance $q \sim 1$ AU orbits of lower eccentricity (table S1), the fractured CM chondrites may disintegrate too rapidly to evolve into such orbits. The short exposure age of SM as compared to other CM chondrites could mean it had already broken from a larger precursor while evolving into an SM-like orbit.

The reflectance spectrum of SM12 (fig. S8) is a good match to the Hayabusa 2 mission's target, asteroid 1999 JU_3, over the measured 0.38- to 0.92-μm range when normalized at 0.55 μm (fig. S8). The meteorite's albedo at 0.55 μm is low, 2.5 to 4.0% at the standard 30° incidence and 0° emergence angles. Carbonates are abundant in this sample and produce strong infrared absorption bands near 1450 and 875 cm^{-1}, stronger than those seen in CM2 Murchison.

SM12 has a compression strength of 82 ± 6 MPa, as compared to ~30 MPa for other CM2s [91]. The impacting asteroid fragmented at a dynamic pressure of only 0.9 MPa at 48 km, presumably because of internal cracks [92]. X-ray computed tomography scanning of SM3, 9, 18, 51, 54, and 73 at the 12- to 30-μm/voxel edge showed abundant fractures through stones and abundant fractures within some lithic fragments, terminating at the fragment edges (fig.

S28) [93]. Volume measurements (table S19) yielded densities of 2.27 ± 0.07 g/cm^3, similar to an average CM2 density of 2.20 g/cm^3 (range 1.88 to 2.47) [94]. He ideal-gas pycnometry of SM19 gave a bulk density of 2.31 ± 0.04 g/cm^3, a grain density of 3.34 ± 0.02 g/cm^3, and a high porosity of 31.0 ± 1.4% (Britt et al 2012).

This density and the infrasound-derived kinetic energy yield an asteroid diameter of 2.5 to 4.0 m. Concentrations of the cosmogenic radionuclide ^{60}Co in three fragments—SM18, SM36 (table S20A), and SM43—and model calculations confirm that the asteroid's pre-atmospheric size was >0.9 m [95]. The fireball's peak luminosity (–18 to –20 magnitude) at the first broad maximum suggests a size of 1.8 to 3.5 m.

2.3 Textural and Compositional Variety

Because of its large size, SM provides insight into the variety of materials present at the surface of its parent body. Individual SM meteorites have differing magnetic susceptibilities (χ in 10^{-9} m^3/kg). Ten different stones (table S4) suggest a bimodal distribution clustering around $\log_{10}\chi$ = 4.03 and 4.26. The primary magnetic mineral is magnetite (Fe_3O_4), with concentrations of 2.0 and 3.3 weight % (wt %), respectively. These magnetite concentrations are intermediate between typical CM2s (~1 wt %) and magnetite-rich C2s or anomalous CMs (>6 wt %) [96]. SM2 has a stable natural remnant

magnetization, probably extraterrestrial in origin, corresponding to a magnetic field paleointensity of ~3 μT, comparable to other carbonaceous chondrites [97].

SM is a regolith breccia. Like all CM chondrites, SM contains Ne from solar wind implantation in a surface regolith (fig. S27) [98]. Unlike most other CM chondrites, the brecciated nature of that regolith is evident: SM2, 18, 47, 48, 51, and 54 contain angular to rounded clasts embedded in a fine-grained comminuted matrix seen visually (Fig. 3.2A), by x-ray and backscattered electron mapping (Fig. 3.2B and fig. S13), and by x-ray and neutron computed tomography (figs. S28 and S30).

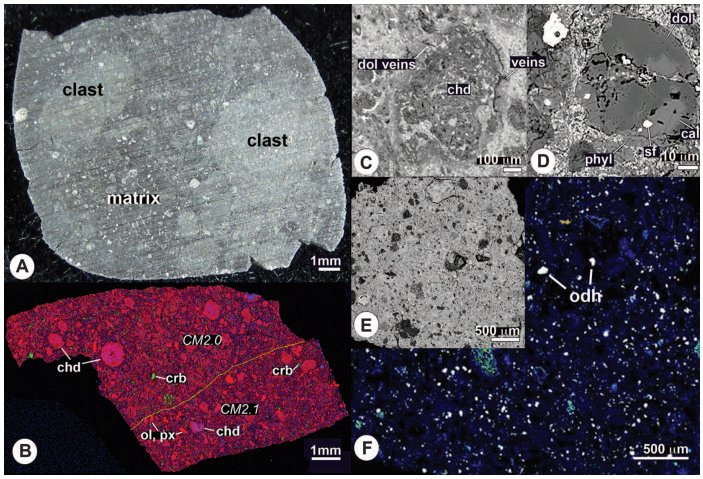

Figure 2.2 Samples of the Sutter's Mill meteorite shown in visible light, combined elemental map, x-ray maps, and backscattered electron images. (A) Slice of SM48 in visible light, showing light clasts in a dark matrix. (B) Combined elemental map in Mg (red), Ca (green), and Al (blue) Ka x-rays of the sample SM51-1 composed of two extensively aqueously altered CM2.0 and CM2.1 lithologies, with a sharp boundary (yellow dashed line). Both lithologies contain complete chondrule pseudomorphs (chd) embedded in a phyllosilicate-rich matrix and abundant carbonate grains (crb). In addition, the CM2.1 lithology contains rare olivine (ol) and pyroxene (px) grains of incompletely hydrated chondrules, amoeboid olivine aggregates (AOAs), and Ca-Al–rich inclusions (CAIs). (C) Backscattered electron (BSE) image of a chondrule pseudomorph (chd) composed mainly of phyllosilicates in SM51-1. The fine-grained rim around the chondrule is crosscut by veins of dolomite (dol), indicating in situ aqueous alteration. (D) BSE image of a carbonate grain composed of closely intergrown dolomite (dol) and calcite (cal) with inclusions of Fe,Ni-sulfide (sf) in SM51-1. The grain is rimmed by phyllosilicates (phyl). (E) BSE image of a small chip from sample SM2-5 with (F) corresponding Ca-S composite x-ray map (Ca, blue; S, green); all light spots in the map correspond to oldhamite (CaS; odh).

The classification of SM as a CM chondrite is confirmed by whole-rock chemistry (Fig. 2.3) and by O (Fig. 2.4 and fig. S21), Os (supplementary text S2.6), and Cr (supplementary text S2.7) isotopic compositions. The Os isotopic compositions and highly siderophile element abundances are well within the range of CM chondrites (figs. S16 and S17). However, the Re-Os isotopic

systematics indicate minor, what was probably recent, open-system behavior of these two elements, as seen in other chondrites [99]. SM plots in the field of CM chondrites on the diagram of $\varepsilon^{54}Cr$ versus $\Delta^{17}O$ (fig. S20) [100]. Using ^{53}Mn-^{53}Cr chronometry (^{53}Mn decays to ^{53}Cr with a half-life of 3.7 My), the data place the accretion time of SM at 4566.57 ± 0.66 million years ago (Ma) (fig. S19) [100].

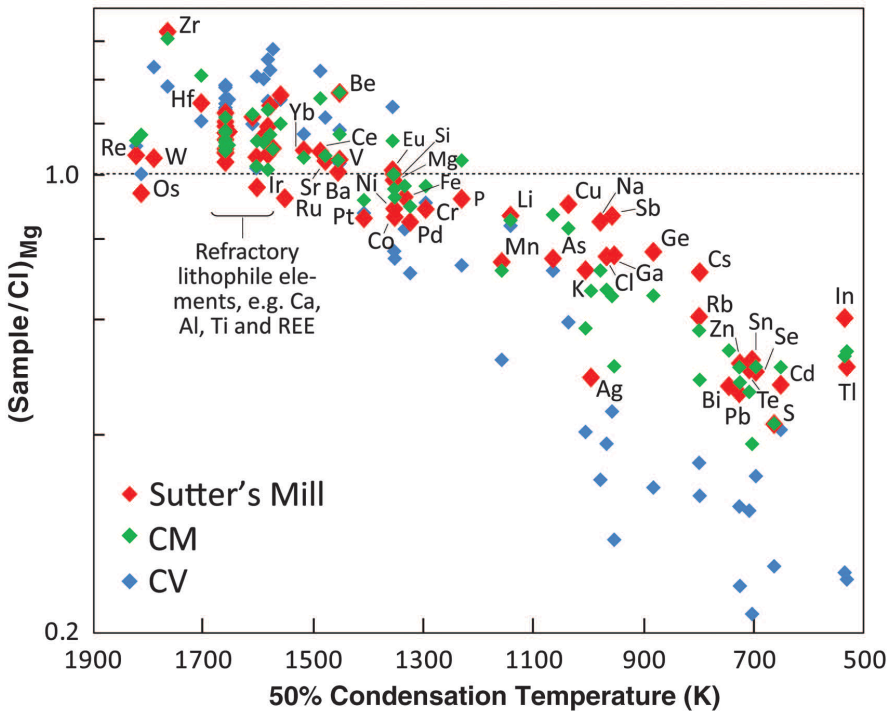

Figure 2.3 Elemental composition of the Sutter's Mill meteorite. Average elemental composition of SM meteorite (table S7) compared to averages for CI (Ivuna type), CM, and CV (Vigarano type) groups of carbonaceous chondrites. Data are normalized to CI and Mg and plotted against 50% condensation temperatures of the elements [101]. Data sources: CI [101], CV [102], and CM [103].

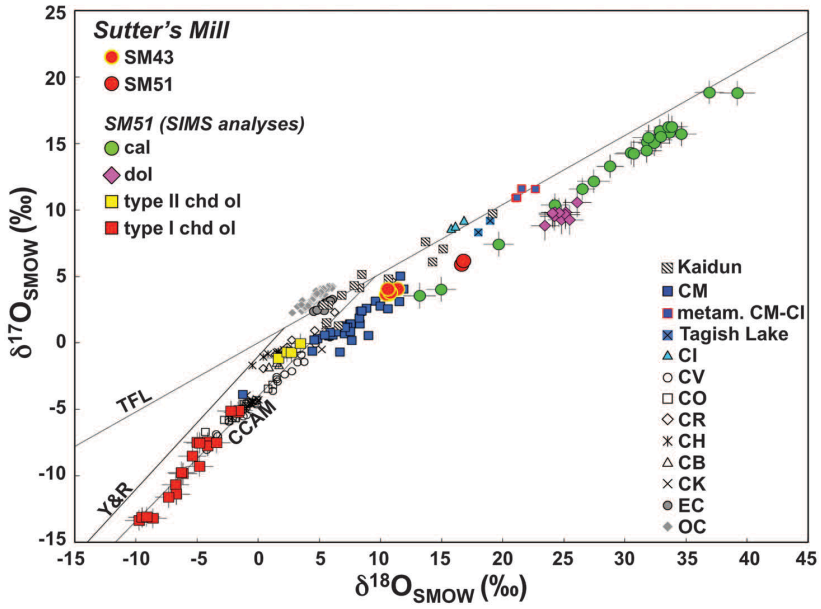

Figure 2.4 Oxygen isotopic composition ($\delta^{17}O$ versus $\delta^{18}O$, ‰) of SM and other carbonaceous chondrites. SM43 and SM51 extend the currently known CM field in the three O-isotope diagram. Data for ordinary, enstatite, and carbonaceous chondrites and for Kaidun chondritic regolith breccia are from [39], [56], [103]–[105]. TFL, terrestrial fractionation line; CCAM, carbonaceous chondrite anhydrous mineral line [104]; Y&R, Young and Russell line [77]. SMOW, standard mean ocean water.

SM contains CM lithologies (from CM2.0 to 2.1, Fig. 2.2B) with varying histories of aqueous alteration and thermal metamorphism. The abundances of thermally labile elements, such as Se, Te, Zn, Sn, and Tl (Fig. 2.3 and table S7), known to be sensitive to open-system heating and volatilization, indicate that most of SM avoided metamorphic (on a million-year time scale) heating above 400° to 500°C [106]. Like other CM chondrites, both lithologies of SM51 (Fig. 2.2B) and some of those in SM2 contain abundant carbonate grains and complete chondrule pseudomorphs embedded in a phyllosilicate-rich matrix (Fig. 2.2, B and C). Sample SM2-5 contains clasts of incompletely altered CM

material, whose matrix consists largely of submicrometer-sized olivine pseudomorphs after phyllosilicates and troilite (Fig. 2.2D and fig. S14). This and the complete lack of carbonates and tochilinite indicate that this particular clast has experienced thermal metamorphism to ~500°C; all other metamorphosed CMs are finds [107].

Thermoluminescence (TL) measurements of SM2-1d (fig. S35) show heating to 300° ± 20°C within the last 0.2 My (fig. S36), and it has induced TL similar to low-metamorphic-grade CO and CV chondrites and unlike other CM chondrites [108]. Raman spectra of macromolecular carbon (fig. S33) suggest that SM2-9 experienced only 153° ± 27°C, whereas a sample of SM12 experienced 268° ± 42°C on a million-year time scale (using the method in [109]).In a Raman G-band center–versus-width diagram (fig. S33), SM2-9 plots between CM2 and CO3 chondrites, whereas SM12 trends closer to polycrystalline C observed in CV3 chondrites.

There are various potential sources for the observed heating. The fast entry would have heated the meteorite surface to >700°C for up to 1.5 s, but it is unclear that this would offer enough time to alter the meteorite deeper inside. At 0.47 AU from the Sun, small tumbling asteroids warm up to ~200°C, more at the surface, less inside. Alternatively, the recent heating could have been related to the impact that liberated the meteorite from the asteroid surface ≥0.05 Ma. Annealing above 300°C may also have occurred on the parent body during the first 1 My after accretion, the most probable cause being the decay of live ^{26}Al.

SM, like Kaidun, shows large variations in O isotope compositions, reflecting the presence of diverse types of lithologies in both regolith breccias (Fig. 2.4). The aqueous alteration that produced carbonates and phyllosilicates caused variation in $\delta^{18}O$ along an approximately fixed $\Delta^{17}O$ ($=\delta^{17}O - 0.52 \times \delta^{18}O$) fractionation line (Fig. 2.4). This requires water-rock reaction involving flowing water as a result of a temperature gradient [110]. Individual SM fragments plot at different positions along this line. The carbonates exhibit a very large range in $\delta^{18}O$ value [+13 to +39‰] with $\Delta^{17}O = -1.9 \pm 1.5$‰ (fig. S21). A trend line regressed through the calcite data, $\delta^{17}O = -4.88 + 0.62 \times \delta^{18}O$, is nearly identical to that reported by [111] based on CM calcites.

SM has the lowest N/C ratio and $\delta^{15}N$, as compared to other CM2 chondrites (fig. S24), suggesting that it contains different N-bearing organic components. C and N isotopic compositions vary widely between fragments, with $\delta^{13}C$ and $\delta^{15}N$ values ranging between –13‰ and +28.5‰ and between –0.6‰ and +16.7‰, respectively. Bimodality in C release suggests two separate organic components, a volatile-rich and a volatile-poor component, the former being isotopically lighter and more cross-linked. Added to these components is CO_2 from the decomposition of carbonates. The maximum in $\delta^{13}C$ of +65‰ is likely to be from the decomposition of calcite; $\delta^{13}C$, however, may be underestimated because of contamination by isotopically lighter components. About 2% of the total C combusts above 1000°C and reaches a $\delta^{13}C$ of +130‰. This is a well-known feature of carbonaceous chondrites, produced by the

combustion of ^{13}C-enriched ($\delta^{13}C \sim +1400‰$) presolar silicon carbide grains [112]. Apparently, SM contains a significant abundance of presolar grains.

2.4 Reactive Compounds

The rapid pre-rain recovery of SM offers a rare glimpse of what reactive minerals and organic compounds may be present at the surface of asteroids. Unseen in other CM chondrites, abundant CaS grains were found in SM2-4 (Fig. 2.2E). A powder Laue pattern of these CaS grains proved to index as oldhamite (fig. S16). Oldhamite is quickly lost to moisture. The oldhamite grains are set within fine-grained comminuted matrix, containing also olivine, enstatite, Fe-Ni-Zn sulfides, Fe-Ni-Cr phosphides, and grains of reduced C, suggesting admixture of a reduced component, possibly xenolithic enstatite chondrite material. It is interesting that the comminuted matrix of SM contains fragments of such a rare meteorite type, rather than the far more abundant ordinary chondrites, probably implying interactions between C- and E-type asteroids.

In comparison to SM2 (pre-rain), the SM12 sample (post-rain) shows strong alteration effects, demonstrating rapid reaction between terrestrial water and reactive S-bearing species. Fourier transform ion cyclotron resonance mass spectra (FTICR-MS) of SM's methanol soluble fraction showed only hundreds of mass signals with comparatively low intensity, high aliphaticity, and, different from the thousands analyzed in other carbonaceous chondrites, many highly

oxygenated species and polysulfur-rich compounds (fig. S31) [113]. Nuclear magnetic resonance (NMR) spectroscopy of the same extracts showed abundant highly branched, singly oxygenated aliphatics and a considerable diversity of unsaturated compounds in an intensity ratio of near 40:6:1 (fig. S32). Both NMR and FTICR-MS signals confirmed convergence with structures recently observed in rather highly thermally altered meteorites.

Water-soluble organic compounds and inorganic salts can be formed, mobilized, and altered by aqueous alteration and terrestrial weathering. Ion chromatography of ≤20 mg of water-extracted pre-rain SM2 showed formate at 80 parts per million (ppm) and acetate at 700 ppm, whereas post-rain interior SM12 had trace formate and only ~100 ppm acetate [114]. Detected inorganic anions in SM2 were sulfate (1300 ppm) and chloride (262 ppm), again with only trace amounts present in interior SM12. Murchison (presumably more aqueously altered) has a 20 times higher soluble sulfate abundance (26,000 ppm) than SM2 [114]. Sodium was the dominant cation (on a per-mole basis) at ~1900 ppm in SM2, followed by calcium (2080 ppm) and magnesium (117 ppm).

Water extracts of SM2 were analyzed by gas chromatography mass spectrometry for ammonia and amines; amino, hydroxyl, and dicarboxylic acids; and, for amino acids, also by liquid chromatography with fluorimetric detection and time-of-flight mass spectrometry [115], [116]. The most abundant water-soluble compounds detected by these methods included glycine, β-alanine, γ-amino-*n*-butyric acid, and, in some analyses only, ε-amino-*n*-caproic acid (table

S21). The highest total amino acid abundances were found in a fragment of SM12 at a depth of 9 to 12 mm from the crust. Exterior portions of SM2 and SM12 contained predominantly contaminant L-amino acids, and both samples were highly depleted in amino acids overall. The pH values of SM water extracts ranged from 8.90 to 9.65, which are higher than for other CMs.

Dichloromethane/methanol (9:1 volume to volume) extracts also showed variably low amounts of soluble hydrocarbon (fig. S34). SM2 contained naphthalene, methylnaphthalenes, dimethylnaphthalenes, anthracene/phenanthrene, a series of linear 15-C to 22-C alkanes, and very little S, usually abundant in comparable CM extracts [117]. The SM12 extracts were instead dominated by cyclic octatomic S, dimethyltrisulfide, and dimethyltetrasulfide, the latter two for about a combined 1 mmole/g; the fragment contained in addition only naphthalene at 2 to 8 nmol/g, plus methylnaphthalenes and biphenol in subnanomole amounts, but no alkanes or anthracene/phenanthrene.

The SM meteorite demonstrates that the complexity of C-class asteroid surfaces is greater than previously assumed. Rapid terrestrial alteration probably erases many vestiges of the internal and external processes on the asteroid that remain to be explored in spacecraft sample-return missions.

2.5 Supplementary Materials

Oxygen Isotopes

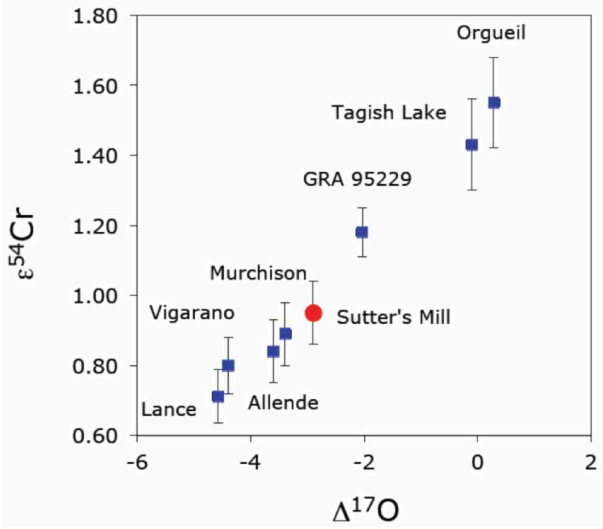

Figure 2.5 Diagram of $\varepsilon^{54}Cr$ excess versus $\Delta^{17}O$ excess among different carbonaceous chondrites. Data sources: Solid red circle (this work). Solid blue squares [100]. See Eq. S1 in section 2.8 for the definition of $\Delta^{17}O$.

Compared to the D'Orbigny age anchor, the slope of $^{53}Mn/^{55}Mn$ = (5.90±0.67) x 10^{-6} defined by Sutter's Mill and other carbonaceous chondrites (Fig. S20) translates into an absolute age of 4,566.57± 0.66 My. This suggests a nebula-wide, moderately volatile element depletion event has occurred within ±0.66 My. It constrains the timescale of accretion and compaction of the carbonaceous chondrite parent bodies, including that of Sutter's Mill (this work), to within ~ 1 Ma after CAI formation at 4,567.60 ± 0.36 My [100], [118], [119]. This suggests the first stage of planet formation from dust to planetesimals is completed within ~1 My [100], [120]. The nuclear anomaly of $\varepsilon^{54}Cr$ *vs.* $\Delta^{17}O$ plot

(Fig. S20) places Sutter's Mill squarely in the CM field [100]. ^{54}Cr, together with few other nuclear anomalies, is becoming a tool on par with $\Delta^{17}O$ to classify meteorites [121].

Laser Fluorination

The oxygen isotopic compositions of silicates in SM43 were measured using the laser fluorination technique of Farquhar and Thiemens at UC San Diego [40]. SM43 was separated into 1-2mg aliquots, which were laser fluorinated in a single session. Data were normalized to the NBS-28 quartz standard, samples of which were analyzed immediately before and after the meteorite analyses. The isotopic compositions of the product O_2 were measured on a Finnigan MAT 253, and average uncertainty in $^{18}O/^{16}O$ is ± 0.03‰ (1σ) and $^{17}O/^{16}O$ is ± 0.06‰ (1σ).

Oxygen isotope data from both UCSD and UCLA are consistently reported in Table 2.2 as $\delta^{17}O'$ and $\delta^{18}O'$ defined as: $\delta^{xx}O + 1000 * \ln(1 + \delta^{xx}O /1000)$, where ^{xx}O refers to either ^{17}O or ^{18}O, respectively, and $\delta^{xx}O$ in turn is parts per 1,000 deviations from Standard Mean Ocean Water (SMOW) as the reference, $\delta^{xx}O = [(^{xx}O/^{16}O)Sample/(^{xx}O/^{16}O)_{SMOW} – 1] * 1000$. The $\Delta^{17}O$ values reported are relative to a mass fractionation curve passing through the origin on the Standard Mean Ocean Water scale with an exponent *b* which relates the mass fractionation factors for $^{17}O/^{16}O$ and $^{18}O/^{16}O$ according to the relation

$\alpha_{17} = \alpha_{18}^{\beta}$ (*96*), where $\alpha_{17} = (^{17}O/^{16}O)_{Sample}/(^{17}O/^{16}O)_{SMOW}$, and $\alpha_{18} = (^{18}O/^{16}O)_{Sample}/(^{18}O/^{16}O)_{SMOW}$. Thus $\Delta^{17}O$ is calculated consistently and accurately as:

$$\Delta^{17}O = \delta^{17}O' - \beta * \delta^{18}O' = 1000[\ln(\alpha_{17}) - \beta * \ln(\alpha_{18})] \quad \text{(Eq. S1)}$$

which is used to assess the deviation from the empirically defined Terrestrial Fractionation Line (TFL) as in [122]. $\Delta^{17}O$ calculated using $b = 0.528$ (UCLA) and $b = 0.5247$ (UCSD) are both shown in Table 2.2 in two separate columns. The tank O_2 used as an internal standard in this study at UCLA was calibrated against air O_2 ($\delta^{18}O_{SMOW} = 23.5‰$, $\Delta^{17}O = -0.35‰$) and San Carlos olivine ($\delta^{18}O_{SMOW} = 5.2‰$, $\Delta^{17}O = 0.00‰$).

Table 2.2 Oxygen isotopic composition of Sutter's Mill meteorite: Laser Fluorination using BrF_5. Isotopes relative to SMOW, measured isotopic compositions have been corrected for contribution from blank in laser fluorination system and have been compared to measured compositions of laser fluorinated samples of NBS-28 quartz standard (UCSD) and of San Carlos olivine standard (UCLA).

Sample ID	$\delta^{17}O$ (‰)	±1s (‰)	$\delta^{18}O$ (‰)	±1s (‰)	$\Delta^{17}O$ (‰) *b*=0.528	$\Delta^{17}O$ (‰) *b*=0.5247	±1s (‰)	Lab
SM43-2	4.034	0.044	11.351	0.028	-1.960	-1.922	0.029	UCSD
SM43-3	3.630	0.073	10.658	0.044	-1.997	-1.962	0.050	UCSD
SM43-4	3.643	0.058	10.436	0.013	-1.867	-1.833	0.051	UCSD
SM43-6	3.757	0.052	10.763	0.037	-1.926	-1.890	0.033	UCSD
SM43-8	4.033	0.053	10.564	0.023	-1.545	-1.510	0.041	UCSD
SM51-1	5.898	0.010	16.657	0.011	-2.898	-2.843	0.007	UCLA
SM51-2	6.167	0.018	16.824	0.003	-2.716	-2.660	0.018	UCLA

2.6 Acknowledgements

Chapter 2, in full, is a reprint of the material as it appears in Science 2012. Peter Jenniskens, Marc D. Fries, Qing-Zhu Yin, Michael Zolensky, Alexander N. Krot, Scott A. Sandford, Derek Sears, Robert Beauford, Denton S. Ebel, Jon M. Friedrich, Kazuhide Nagashima, Josh Wimpenny, Akane Yamakawa, Kunihiko Nishiizumi, Yasunori Hamajima, Marc W. Caffee, Kees C. Welten, Matthias Laubenstein, Andrew M. Davis, Steven B. Simon, Philipp R. Heck, Edward D. Young, Issaku E. Kohl, Mark Thiemens, Morgan H. Nunn, Takashi Mikouchi, Kenji Hagiya, Kazumasa Ohsumi, Thomas A. Cahill, Jonathan A. Lawton, David Barnes, Andrew Steele, Pierre Rochette, Kenneth Verosub, Jérôme Gattacceca,

George Cooper, Daniel P. Glavin, Aaron S. Burton, Jason P. Dworkin, Jamie E. Elsila, Sandra Pizzarello, Ryan Ogliore, Phillipe Schmitt-Kopplin, Mourad Harir, Norbert Hertkorn, Alexander Verchovsky, Monica Grady, Keisuke Nagao, Ryuji Okazaki, Hiroyuki Takechi, Takahiro Hiroi, Ken Smith, Elizabeth A. Silber, Peter G. Brown, Jim Albers, Doug Klotz, Mike Hankey, Robert Matson, Jeffrey A. Fries, Richard J. Walker, Igor Puchtel, Cin-Ty A. Lee, Monica E. Erdman, Gary R. Eppich, Sarah Roeske, Zelimir Gabelica, Michael Lerche, Michel Nuevo, Beverly Girten, Simon P. Worden (the Sutter's Mill Meteorite Consortium). *Science* **338**, 1583, 2012 (DOI: 10.1126/science.1227163). Reprinted with permission from AAAS.

The dissertation author was a co-investigator and co-author of this paper. Dissertation author is responsible for the oxygen isotopic analyses of the Sutter's Mill Meteorite described in Jenniskens et al. 2012. See page 1585 of Jenniskens, P., et al. 2012 and pages 35-37 of associated *Supplementary Materials* for dissertation author's contributions.

Chapter 3. Unique Meteorite from Early Amazonian Mars: Water-Rich Basaltic Breccia Northwest Africa 7034

3.1 Abstract

We report data on the martian meteorite Northwest Africa (NWA) 7034, which shares some petrologic and geochemical characteristics with known martian meteorites of the SNC (i.e., shergottite, nakhlite, and chassignite) group, but also has some unique characteristics that would exclude it from that group. NWA 7034 is a geochemically enriched crustal rock compositionally similar to basalts and average martian crust measured by recent Rover and Orbiter missions. It formed 2.089 ± 0.081 billion years ago, during the early Amazonian epoch in Mars' geologic history. NWA 7034 has an order of magnitude more indigenous water than most SNC meteorites, with up to 6000 parts per million extraterrestrial H_2O released during stepped heating. It also has bulk oxygen isotope values of $\Delta^{17}O = 0.58 \pm 0.05‰$ and a heat-released water oxygen isotope average value of $\Delta^{17}O = 0.330 \pm 0.011‰$, suggesting the existence of multiple oxygen reservoirs on Mars.

3.2 Introduction

The only tangible samples of the planet Mars available today for study in Earth-based laboratories are the so-called SNC (shergottite, nakhlite, and

chassignite) meteorites and a single cumulate orthopyroxenite (Allan Hills 84001) [123]. The SNCs currently number 110 named stones and have provided a treasure trove for elucidating the geologic history of Mars [124]. But, because of their unknown field context and geographic origin on Mars and their fairly narrow range of igneous rock types and formation ages, it is uncertain to what extent SNC meteorites sample the crustal diversity of Mars [125]. In fact, geochemical data from NASA's orbiter and lander missions suggest that the SNC meteorites are a mismatch for much of the martian crust exposed at the surface [126]. For example, the basalts analyzed by the Mars Exploration Rover Spirit at Gusev Crater are distinctly different from SNC meteorites, and Odyssey Orbiter gamma-ray spectrometer (GRS) data show that the average martian crust composition does not closely resemble SNC [47]–[49].

NWA 7034, on deposit at the Institute of Meteoritics in Albuquerque, was purchased by Jay Piatek from Aziz Habibi, a Moroccan meteorite dealer, in 2011. It is a 319.8-g single stone, porphyritic basaltic monomict breccia, with a few euhedral phenocrysts up to several millimeters and many phenocryst fragments of dominant andesine, low-Ca pyroxene, pigeonite, and augite set in a very fine-grained, clastic to plumose, groundmass with abundant magnetite and maghemite; accessory sanidine, anorthoclase, Cl-rich apatite, ilmenite, rutile, chromite, pyrite, a ferric oxide hydroxide phase, and a calcium carbonate were identified by electron microprobe analyses on eight different sections at the University of New Mexico (UNM). X-ray diffraction (XRD) analyses conducted at

UNM on a powdered sample and on a polished surface show that plagioclase feldspar is the most abundant phase (38.0 ± 1.2%), followed by low-Ca pyroxene (25.4 ± 8.1%), clinopyroxenes (18.2 ± 4.0%), iron oxides (9.7 ± 1.3%), alkali feldspars (4.9 ± 1.3%), and apatite (3.7 ± 2.6%). The x-ray data also indicate a minor amount of iron sulfide and chromite. The data are also consistent with magnetite and maghemite making up ~70% and ~30%, respectively, of the iron oxide detected (see Section 3.9).

3.3 Petrology and geochemistry

Numerous clasts and textural varieties are present in NWA 7034, including gabbros, quenched melts, and iron oxide– and ilmenite-rich reaction spherules (figs. S1 to S4) (see Section 3.9). However, the dominant textural type is a fine-grained basaltic porphyry with feldspar and pyroxene phenocrysts. NWA 7034 is a monomict brecciated porphyritic basalt that is texturally unlike any SNC meteorite. Basaltic breccias are common in Apollo samples, lunar meteorites, and HED meteorites but are wholly absent in the world's collection of SNC meteorites [127]. The absence of shock-produced SNC breccias seems curious at face value, because nearly all of them show evidence of being subjected to high shock pressures, with feldspar commonly converted to maskelynite. Martian volcanic breccias are probably not rare, given the observed widespread occurrence of volcanism on Mars. However, launch and delivery of such

materials to Earth as meteorites has not been observed [127]. Although NWA 7034 is texturally heterogeneous, both in the hand specimen and microscopically (Fig. 3.1), it can be considered a monomict breccia because it shows a continuous range of feldspar and pyroxene compositions that are consistent with a common petrologic origin (figs. S5 and S6). We find no outlier minerals or compositions that would indicate the existence of multiple lithologies or exotic components. We also see no evidence for polymict lithologies in either the radiogenic or stable isotope ratios of NWA 7034 solids. However, many clasts and some of the fine-grained groundmass have phases that appear to have been affected by secondary processes to form reaction zones. We observed numerous reaction textures, some with a ferric oxide hydroxide phase; this phase and apatite are the main hosts of the water in NWA 7034 (fig. S2). Impact processes are likely to have affected NWA 7034 by virtue of the fact that this meteorite was launched off of Mars, exceeding the escape velocity—presumably by an impact—although the shock pressures did not produce maskelynite. One large (1-cm) quench melt clast that was found could originate from shock processes (fig. S3). On the other hand, the very fine groundmass with the large phenocrystic feldspars and pyroxenes strongly suggests an eruptive volcanic origin for NWA 7034; thus, it is likely that volcanic processes are a source of the brecciation.

It has been shown that Fe-Mn systematics of pyroxenes and olivines are an excellent diagnostic for classifying planetary basalts [128]. The Fe-Mn systematics of NWA 7034 pyroxenes, as determined by electron microprobe

analyses, most resemble the trend of the SNC meteorites from Mars (Fig. 2); other planetary pyroxenes such as in lunar samples and basalts from Earth are poor matches for NWA 7034. Furthermore, feldspar compositions (fig. S5) and compositions of other accessory phases in NWA 7034 are consistent with mineralogies commonly found in SNC meteorites but not with any other known achondrite group (see Section 3.9, [129]. However, the average bulk chemical composition of NWA 7034 does not overlap in major element space with SNC; instead, it is remarkably similar to the geochemistry of the rocks and soils at Gusev Crater and the average martian crust composition from the Odyssey Orbiter GRS (Fig. 3.3 and figs. S7 and S8). NWA 7034, Gusev rocks, and the GRS average martian crust all have higher concentrations of the alkali elements sodium and potassium than do SNC meteorites. Other major and minor element ratios such as Mg/Si, Al/Si, and Ni/Mg have similarly good matches between NWA 7034 and Gusev Crater rocks (figs. S7 and S8). Although some work has been conducted to link martian meteorites to surface rocks analyzed by the Mars Exploration Rovers, and aside from the exotic “Bounce Rock” at Meridiani Planum and a hypothesized martian soil component in Tissint melt pockets, there has been no direct link between the bulk chemical com- positions of martian meteorites and surface rocks to date [130]–[134].

The rare-earth element (REE) abundances of NWA 7034 were determined by multicollector inductively coupled plasma mass spectrometry (Neptune MC-ICP-MS) at UNM. They are enriched relative to chondritic abundances, with a

marked negative europium anomaly (Eu/Eu* = 0.67) (fig. S9 and table S2). The REE pattern has a negative slope, and light rare-earth elements (LREE) are elevated relative to the heavy rare-earth elements (HREE) [CI-chondrite normalized lanthanum-ytterbium ratio (La/Yb)N = 2.3]. Bulk SNC meteorites are much less enriched in REE than is NWA 7034 (fig. S10); although LREE enrichment relative to HREE and REE patterns with negative slopes are seen in nakhlites, only magmatic inclusions and mesostasis in nakhlites and estimated nakhlite parent magmas have LREE enrichments comparable to those of NWA 7034 [135], [136]. We observed ubiquitous, relatively large (up to ~100 mm) Cl-rich apatite grains in NWA 7034 that presumably harbor a substantial fraction of the REEs in this meteorite, as neither merrillite nor whitlockite were identified in any of the investigated thin sections or probe mounts.

3.4 Radiometric age

A five-point isochron gives an Rb-Sr age for NWA 7034 of 2.089 ± 0.081 billion years ago (Ga) [2σ; mean square weighted deviation (MSWD) = 6.6], an initial $^{87}Sr/^{86}Sr$ ratio of 0.71359 ± 54 (Fig. 4), and a calculated source $^{87}Rb/^{86}Sr$ ratio of 0.405 ± 0.028 (Fig. 3.5).

The Sm-Nd data for the same samples result in an isochron of 2.19 ± 1.4 Ga (2σ). The high uncertainty in the latter is due to minimal separation between the data points generated from analysis of mineral separates. The small error on

the Rb-Sr age may come from the abundance and variety of feldspar compositions in NWA 7034 (fig. S5). Furthermore, we are confident that the Rb-Sr isochron and variations in the $^{87}Sr/^{86}Sr$ values are the result of the time-integrated radiogenic growth from ^{87}Rb and not the results of mixing between end members with different $^{87}Sr/^{86}Sr$ values (figs. S11 to S14). The combined REE and isotopic data show that NWA 7034 is an enriched martian crustal rock (Fig. 3.5). The whole rock has $^{143}Nd/^{144}Nd = 0.511756$ and $^{147}Sm/^{144}Nd = 0.1664$, giving a calculated initial (source value) $^{143}Nd/^{144}Nd = 0.509467 \pm 0.000192$ (initial $\varepsilon_{Nd} = -9.1 \pm 1.7$, calculated using the Rb-Sr age). This requires that NWA 7034 was derived from an enriched martian reservoir, with an inferred time-integrated 147Sm/144Nd = 0.1680 ± 0.0061, assuming separation from a chondrite-like martian mantle at 4.513 Ga [136], [137]. Data for each of our analyses are available in table S3. An age of ~2.1 Ga for NWA 7034 would make it the only dated meteorite sample from the early Amazonian epoch in Mars' geologic history [137].

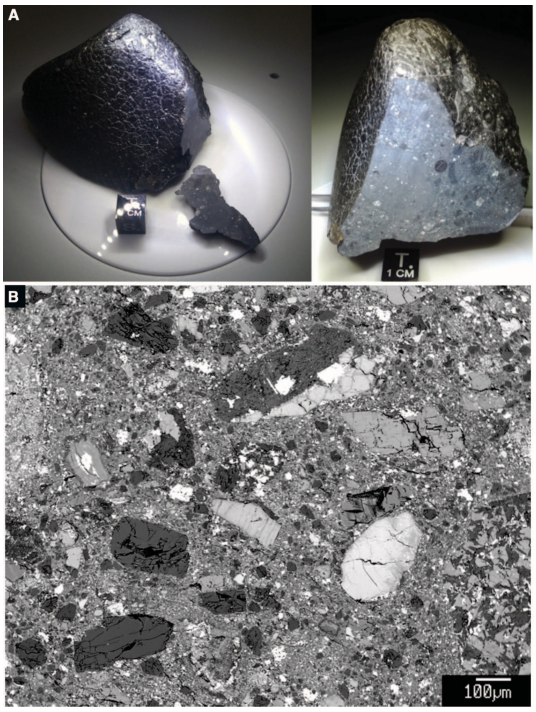

Figure 3.1 Photo and backscatter electron image of NWA 7034. (A) Two views of the NWA 7034 hand specimen. (B) Backscatter electron image of porphyritic texture in NWA 7034. Large dark crystals are feldspar; large light-colored crystals are pyroxene. A portion of a gabbroic clast is shown above the scale bar.

NWA 7034 is derived from the most enriched martian source identified to date; it is even more enriched than the most enriched shergottites (Fig. 3.5) [138], [138]–[140]. On the basis of REE enrichment, isotopic values, and match to rover elemental data, NWA 7034 may better represent the composition of Mars' crust than other martian meteorites. Although NWA 7034 may not be representative of a magmatic liquid, the negative europium anomaly and the absence of merrillite or whitlockite suggest either that the magma(s) parental to basaltic breccia NWA 7034 underwent plagioclase fractionation before eruption or that feldspar was left in the residuum during partial melting [141]. Because of the instability of plagioclase at high pressure, these processes would have

necessarily occurred in the crust or upper mantle of Mars [142]. Consequently, the geochemically enriched source that produced NWA 7034 could have originated from the martian crust or mantle, much like the geochemically enriched reservoir(s) that are recorded in the shergottites [143], [144], [144]–[146].

3.5 Carbon

Confocal Raman imaging spectroscopy conducted at the Carnegie Institution Geophysical Laboratory in Washington, DC, identified the presence of macromolecular carbon (MMC) within mineral inclusions in the groundmass minerals of NWA 7034 (see Section 3.9). This MMC is spectrally similar to reduced organic macromolecular carbon that has been identified in several shergottites and a single nakhlite meteorite (fig. S15), indicating that the production of organic carbon from abiogenic processes in the martian interior may not be unique to SNC-like source regions in Mars [144]. Steele *et al.* also demonstrated that the formation mechanism of MMC requires reducing magmatic conditions consistent with oxygen fugacities below the fayalite-magnetite-quartz (FMQ) buffer [147]. Consequently, much of the ferric iron in the oxides of NWA 7034, as evidenced by electron probe microanalysis and XRD, was likely a product of oxidation subsequent to igneous activity as a result of secondary processes.

Bulk carbon and carbon isotopic measurements on NWA 7034 were also carried out at Carnegie, using combustion in an elemental analyzer (Carlo Erba NC 2500) interfaced through a Conflo III to a Delta V Plus isotope ratio mass spectrometer (ThermoFisher) in the same manner as the data reported by [see Section 3.9] [147], [148]. These data indicate that carbon is present within mineral inclusions in NWA 7034 at concentrations of at least 22 ± 10 ppm, and that the $\delta^{13}C$ isotopic value of this carbon is –23.4 ± 0.73‰, which is very similar to previous bulk C and $\delta^{13}C$ analyses of carbon included in shergottite meteorites analyzed in the same manner [147], [148]. These data indicate that multiple geochemical reservoirs in the martian interior may have similarly light $\delta^{13}C$ values. The bulk C concentration in the untreated sample performed in these measurements was 2080 ± 80 ppm C, with a corresponding $\delta^{13}C$ value of –3.0 ± 0.16‰. Scattered carbonate veinlets from desert weathering were observed by backscatter electron imaging and element mapping with the electron microprobe, especially in the near-surface material but less frequently in the deeper interior slices of NWA 7034. Although this carbonate is below the detection limits of our XRD analyses of the bulk sample and is thus a minor phase within the meteorite, we believe that this weathering product is sampled in our bulk carbon and carbonate analyses (see Section 3.9) (fig. S16).

3.6 Oxygen isotopes

Measurements of oxygen isotopic composition were performed by laser fluorination at UNM on acid-washed and non-acid-washed bulk sample and at the University of California, San Diego (UCSD), on vacuum pre-heated (1000°C) bulk sample (table S4). The triple oxygen isotope precision on San Carlos olivine standard [$\delta^{18}O$ = 5.2‰ versus standard mean ocean water (SMOW); $\Delta^{17}O$= 0‰] analyzed during sessions at UNM was $\Delta^{17}O$ = ± 0.03‰; the precision at UCSD using NBS-28 quartz standard ($\delta^{18}O$ = 9.62‰) was also $\Delta^{17}O$ = ± 0.03‰. In total, we carried out 21 analyses of bulk NWA 7034 (Fig. 3.6). The mean value obtained at UNM was $\Delta^{17}O$ = 0.58 ± 0.05‰ (*n* = 13) for acid- washed samples and $\Delta^{17}O$ = 0.60 ± 0.02‰ (*n* = 6) for non–acid-washed samples; at UCSD the mean value was $\Delta^{17}O$ = 0.50 ± 0.03‰ (*n* = 2) for vacuum preheated samples that were dewatered and decarbonated. The combined data give $\Delta^{17}O$ = 0.58 ± 0.05‰ (*n* = 21). These interlab values of bulk samples are in good agreement but are significantly higher than literature values for SNC meteorites ($\Delta^{17}O$ range 0.15 to 0.45‰) [51], [53], [149], [150]. Figure 3.6 shows that the $\delta^{18}O$ values (5.5 to 7.0‰ versus SMOW) of NWA 7034 are higher than any determination from the SNC group. The $\Delta^{17}O$ values of the non–acid-washed samples measured at UNM are similar to and within error of the acid-washed samples; this indicates that NWA 7034 has, at most, only minor terrestrial weathering products, which would drive the non–acid-washed values closer to $\Delta^{17}O$ = 0.00‰. The slope of

the best-fit line to the combined UNM acid-washed and non–acid-washed data is 0.517 ± 0.025, which suggests that the oxygen isotopic composition of NWA 7034 is the result of mass-dependent fractionation processes.

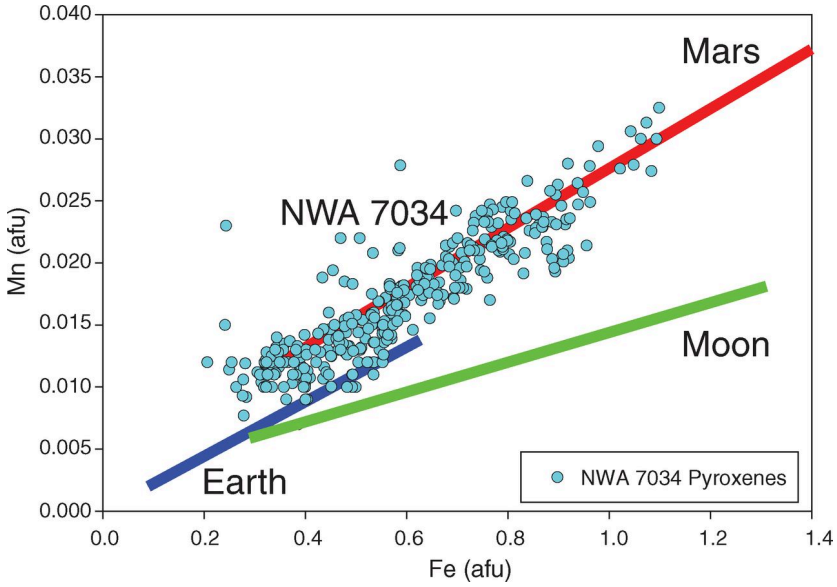

Figure 3.2 Fe versus Mn (atomic formula units) of pyroxenes in NWA 7034, Mars, the Moon, and Earth. The trend for all NWA 7034 pyroxenes (cyan dots, 349 microprobe analyses) and, for comparison, pyroxene trends from Mars (red), the Moon (green), and Earth (blue) are shown [128].

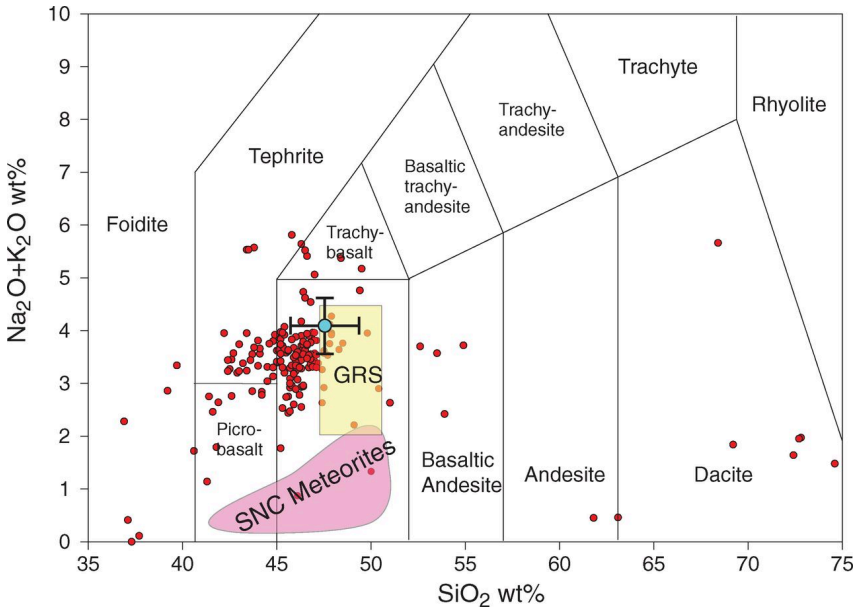

Figure 3.3 Volcanic rock classification scheme based on the abundance of alkali elements and SiO_2. Plot is modified after McSween *et al*. [126]. Red dots denote analyses of rocks and soils at Gusev Crater by the Alpha Particle X-ray Spectrometer (APXS) onboard the Spirit rover [48], [49]. The yellow rectangle is the average martian crust as measured by the GRS onboard the Mars Odyssey orbiter [47]. The pink field is the known range of martian meteorite (SNC) compositions. The cyan dot is the mean value of bulk NWA 7034 as determined by 225 electron microprobe analyses of fine-grained groundmass; error bars denote SD.

There are no other known achondrites or planetary samples with bulk oxygen isotope values similar to those of NWA 7034. Most achondrite groups have negative or near-zero $\Delta^{17}O$ values, as do rocks from Earth and the Moon. The oxygen isotope compositions of Venus and Mercury are currently unknown, but NWA 7034 is too oxidized and iron-rich to be derived from Mercury, and it seems to be a poor match for Venus because it experienced low-temperature alteration on its parent body and has significant indigenous water, which would not persist with the high surface temperatures on Venus [151]–[154]. The distinct

$\delta^{18}O$ and $\Delta^{17}O$ values relative to other martian meteorites can be explained by multiple reservoirs—either within the martian lithosphere or between the lithosphere and a surficial component—or by incorporation of exotic material [55], [155]. The idea of separate long-lived silicate reservoirs is supported by radiogenic isotope studies [139], [156]. The distinct $\Delta^{17}O$ and $\delta^{18}O$ values of the silicate fraction of NWA 7034 relative to all SNC meteorites measured to date further support the idea of distinct lithospheric reservoirs that have remained unmixed throughout martian history. A near-surface component with high $\Delta^{17}O$ values has been proposed on the basis of analysis of low-temperature alteration products, and this may in part explain the $\Delta^{17}O$ differences between the bulk and "water-derived" components of NWA 7034 [55], [155], [157]. However, the $\Delta^{17}O$ value of 0.58‰ for the bulk silicate is different from the $\Delta^{17}O$ value of 0.3‰ found in all SNC samples measured to date. If materials with a $\Delta^{17}O$ value other than 0.3‰ are attributed to a surficial (atmospheric) component, then the bulk of NWA 7034 would have necessarily undergone extensive exchange with this reservoir. This is a possibility, given the abundance of low-temperature iron oxides. The ramifications of distinct lithospheric reservoirs are very different from those attributed to a different surficial reservoir. The latter could be explained by photochemical-induced isotope fractionation and/or hydrodynamic escape, whereas the former is consistent with a lack of initial planet-wide homogenization and an absence of plate tectonics [40], [55], [110], [158]. Isolated lithospheric oxygen isotope reservoirs are inconsistent with a global magma ocean scenario

for early Mars, which would have very efficiently homogenized oxygen isotopes in the planet, as occurred for Earth and the Moon. Instead, Mars' differentiation could have been dominated by basin-forming impacts that left regional or even hemisphere-scale magmatic complexes with distinct and varied isotopic and geochemical characteristics [159].

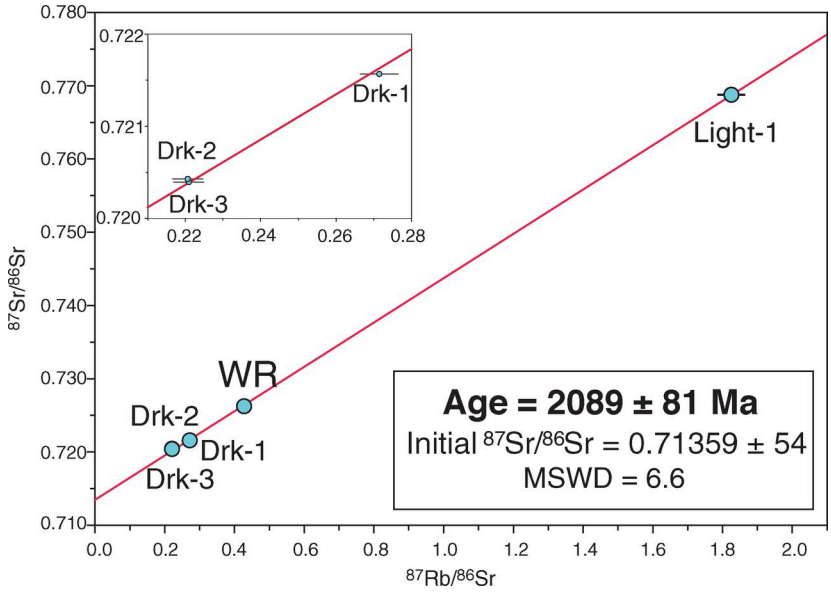

Figure 3.4 Rb-Sr whole-rock mineral isochron of NWA 7034. The mineral fractions are labeled as Light-1, Drk-1, Drk-2, and Drk-3 according to abundance of dark magnetic minerals. Light-1, with high $^{87}Rb/^{86}Sr$, was the least magnetic fraction. An MSWD value of 6.6 suggests that the small scatter in the values cannot be explained by analytical errors and may include slight isotopic heterogeneities in the rock. 2σ measurement errors were used for the $^{87}Sr/^{86}Sr$ data; 2% errors for the $^{87}Rb/^{86}Sr$ data were used for age calculation. Larger errors were assigned to the $^{87}Rb/^{86}Sr$ ratios because of the inability to perform internal mass fractionation on Rb isotopic measurements (Rb only has two isotopes). There was not enough Sm and Nd in the mineral fractions to provide a meaningful age.

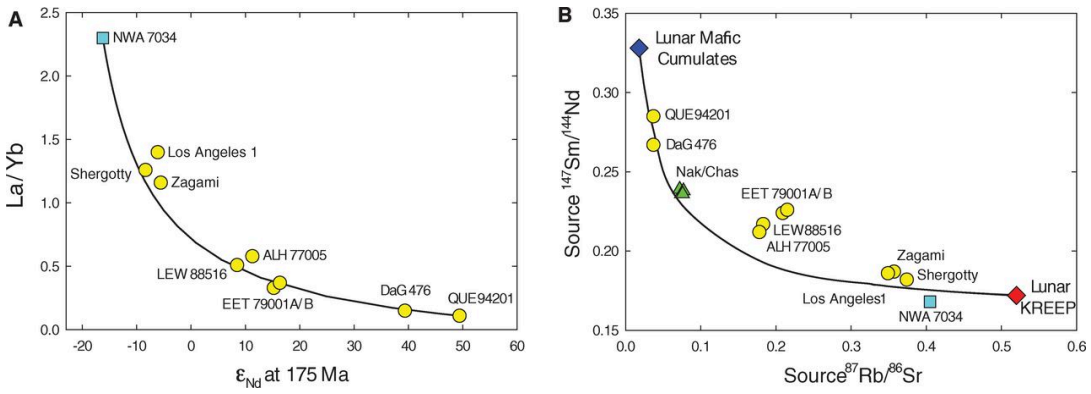

Figure 3.5 Plots of bulk rock La/Yb ratio versus ε_{Nd} and calculated parent/ daughter source ratios. (A) Plot of bulk rock La/Yb ratio versus ε_{Nd} calculated at 175 Ma for NWA 7034 and basaltic shergottites. Solid line represents two-component mixing line between NWA 7034 and QUE 94201. (B) Plot of calculated parent/ daughter source ratios for NWA 7034, basaltic shergottites, nakhlites including Chassigny (which has values similar to nakhlites) (Nak/Chas), and lunar mantle sources. Solid line represents two-component mixing line between depleted lunar mafic cumulates and lunar potassium, rare-earth elements, and phosphorus (KREEP). Depleted lunar mafic cumulates are estimated by [160]–[162]. Lunar KREEP is estimated by [162]. Data for basaltic shergottites, nakhlites, and Chassigny are from [140], [156] and references therein.

Another possibility is that NWA 7034 originally had oxygen isotope values similar to or the same as SNC, but a cometary component with higher $\delta^{18}O$, $\delta^{17}O$, and $\Delta^{17}O$ was mixed with it through impact processes on Mars, thus producing a $\Delta^{17}O$ excess relative to SNC. Until we find clear evidence of such an exotic component in NWA 7034, this scenario seems less likely than the other two.

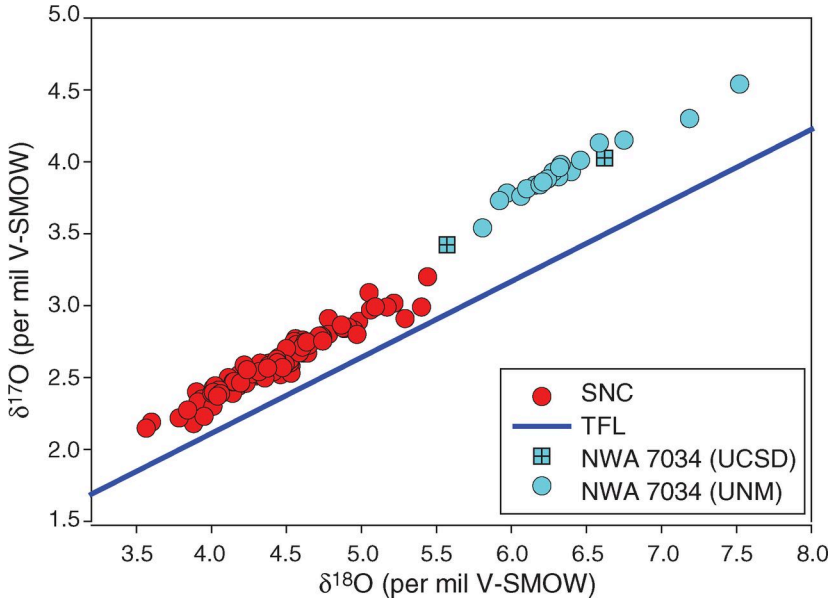

Figure 3.6 Oxygen isotope plot showing the values of NWA 7034 from this study. Cyan dots, 13 analyses of acid-washed and six analyses of non–acid- washed bulk samples (UNM); cyan squares, two analyses of dry, decarbonated bulk preheated to 1000°C (UCSD). Red dots are SNC meteorites from the literature [51], [53], [55], [149], [150]. TFL, terrestrial fractionation line (slope 0.528).

3.7 Water

The oxygen isotope ratio of water released by stepped heating in a vacuum at UCSD (table S5) shows that most, possibly all, of the water in NWA 7034 is extraterrestrial, with $\Delta^{17}O$ values well above the terrestrial fractionation line (Fig. 3.7). NWA 7034 water falls primarily within the range of values for bulk SNC meteorites, with a weighted mean value of $\Delta^{17}O = + 0.33 \pm 0.01‰$; $\delta^{18}O$ and $\delta^{17}O$ values give a slope of 0.52, indicating mass-dependent fractionation. Note that the $\Delta^{17}O$ value for NWA 7034 water is lower than, and outside the range of,

the $\Delta^{17}O$ for bulk NWA 7034, offering clear evidence that there are multiple distinct oxygen isotope sources for this sample. The $\Delta^{17}O$ value of the water released at the 500° to 1000°C range (+0.09‰) approaches terrestrial values, possibly because of decomposition of the terrestrial carbonate veins in the meteorite and equilibration of the produced CO_2 with the released water. Karlsson *et al*. reported oxygen isotope values of water from several SNC meteorites and also saw that they differed from the $\Delta^{17}O$ of the bulk SNC samples [55]. However, their observed $\Delta^{17}O$ relationship between bulk rock and water is reverse to the one seen in NWA 7034, with waters in general having more positive $\Delta^{17}O$ values than their respective host rocks (Nakhla, Chassigny, and Lafayette). Only two shergottites (Shergotty and EETA-79001A) have waters with $\Delta^{17}O$ values more negative than the host rock, and Nakhla has water similar to its host rock. Romanek analyzed iddingsite, an alteration product of olivine and pyroxene, in Lafayette and found the $\Delta^{17}O$ value is 1.37‰ for a 90% iddingsite separate, supporting the positive $\Delta^{17}O$ shift of Lafayette water relative to host rock [157]. Karlsson argued that this $\Delta^{17}O$ difference suggested a lack of equilibrium between water and host rock, with the lithosphere and hydrosphere having distinct oxygen isotopic reservoirs [55]. Our data support this conclusion but suggest that the $\Delta^{17}O$ value of the “water” reservoir is not always heavier than the rock reservoir.

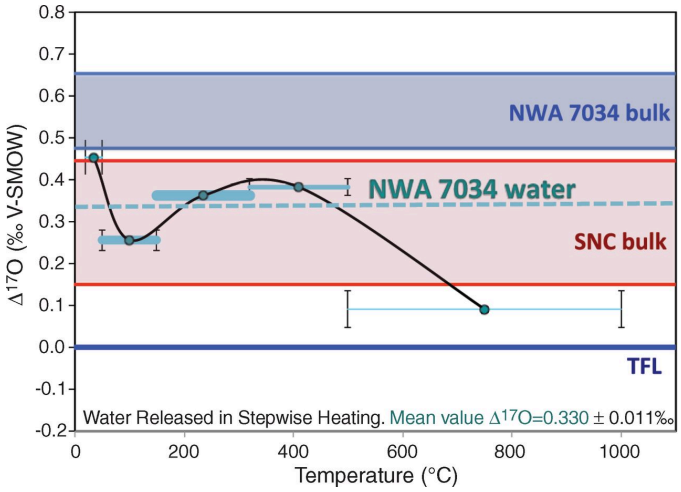

Figure 3.7 Plot of $\Delta^{17}O$ versus temperature, showing values for NWA 7034 water released by stepped heating. Vertical error bars are given for each data point; horizontal line segments show the temperature range for each step, and the thickness of the line segment indicates the relative proportion of water released at each step. Dashed line is the mean value of $\Delta^{17}O$ for NWA 7034 water. Also shown are ranges of $\Delta^{17}O$ for bulk NWA 7034 analyses and for bulk SNC values from the literature.

We determined the deuterium/hydrogen isotope ratio (δD value versus SMOW) and the water content of whole-rock NWA 7034 at UNM by both bulk combustion and stepped heating in a continuous-flow helium stream with high-temperature carbon reduction (Fig. 3.8 and table S6) [163]. Six whole-rock combustion measurements yielded a bulk water content of 6190 ± 620 ppm. The mean δD value for the bulk combustion analyses was +46.3 ± 8.6‰. The maximum δD values in two separate stepwise heating experiments were +319‰ and +327‰, reached at 804°C and 1014°C, respectively (table S6), similar to values seen in the nakhlites [164]. Figure 3.8 shows that most of the water in NWA 7034 is released between approximately 150° and 500°C, and that there are two plateaus of δD values, one around –100‰ at 50° to 200°C and a second around +300‰ at 300° to 1000°C. This suggests that there are two distinct δD components in NWA 7034: a low-temperature negative-value component and a high-temperature positive-value component. One possibility is that the low-temperature negative values are from terrestrial water contamination, although the Δ^{17}O values in water released at even the lowest temperature step of 50°C have a 0.3‰ anomaly (Fig. 3.7). It is also possible that protium-rich water is released at the lowest steps of dehydration, although such fractionation is not observed on terrestrial samples. Alternatively, the hydrogen but not the oxygen isotope ratios could have been affected by terrestrial alteration. Finally, it is possible that nearly all the released water from NWA 7034 is in fact martian and

not terrestrial. In this case, the hydrogen isotope ratios have fractionated as a function of temperature, or there are two distinct hydrogen isotope reservoirs.

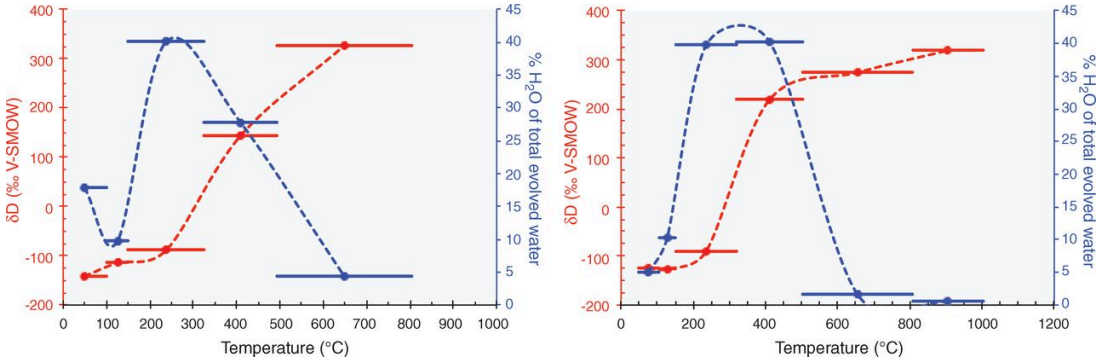

Figure 3.8 Plots of δD versus temperature, showing data for the NWA 7034 bulk sample during stepped heating. The horizontal solid lines represent the temperature intervals; circles are mid-interval temperatures. The two plots represent two aliquots of the NWA 7034 sample.

Our data show that NWA 7034 has more than an order of magnitude more indigenous water than most SNC meteorites. The amount of water released at high temperature (>320°C) is 3280 ± 720 ppm. Leshin *et al*. measured an average of 249 ± 129 ppm H_2O released above 300° to 350°C in seven bulk SNC meteorites, with the exception of the anomalous Lafayette nakhlite (which released 1300 ppm H_2O above 300°C) [164]. They argued that some of the water released at temperatures as low as 250°C could in fact be from martian alteration products [164]. Given our oxygen water analyses, this could also be the case for NWA 7034 at temperatures as low as 50°C. Hence, the total amount of martian water in NWA 7034 could be in the vicinity of 6000 ppm, possibly supporting hypotheses that aqueous alteration of near-surface materials on Mars occurred

during the early Amazonian epoch (2.1 Ga) either by magmatically derived or meteoric aqueous fluids [165]–[167].

3.8 Conclusions

The young crystallization age of NWA 7034, 2.1 Ga, requires that it is planetary in origin. Its major, minor, trace, and isotopic chemistry is inconsistent with originating from Earth, the Moon, Venus, or Mercury, and it is most similar to rocks from Mars. Nonetheless, NWA 7034 is uniquely different from any other known martian meteorite, as it is the most geo- chemically enriched rock from Mars found to date. Moreover, the bulk chemistry of NWA 7034 is strikingly similar to recently collected orbital and lander data collected at the martian surface, allowing for a direct link between a martian meteorite and orbital and lander spacecraft data from Mars. NWA 7034 is also distinct from the SNC meteorites because it has higher bulk $\delta^{18}O$ and $\Delta^{17}O$, suggesting the existence of multiple oxygen isotopic reservoirs within the lithologic portion of Mars.

3.9 Supplementary Materials

Methods

NWA 7034 Laser Fluorination Data from UCSD. Bulk solids dry and decarbonated to 1000˚C.

Table 3.1 Oxygen isotope data (relative to V-SMOW; precision of $\Delta^{17}O'$ values is 0.03‰).

	$\delta^{17}O'$	$\delta^{18}O'$	$\Delta^{17}O'$
	3.43	5.59	0.48
	4.03	6.64	0.53
Average	**3.73**	**6.12**	**0.50**
Stdev	**0.43**	**0.75**	**0.03**

Table 3.2 Oxygen Isotopic Composition of Water Extracted from NWA 7034 by Stepwise Heating (relative to V-SMOW; precision of $\Delta^{17}O$' values is 0.03‰.

Temperature (˚C)	Time heating		wt%	Oxygen		St.Dev.
50	1.5	16.2	0.024	$\delta^{18}O$ =	-21.780	0.045
				$\delta^{17}O$ =	-11.047	0.065
				$\Delta^{17}O$ =	0.453	
150	3	76.0	0.111	$\delta^{18}O$ =	-3.883	0.027
				$\delta^{17}O$ =	-1.794	0.039
				$\Delta^{17}O$ =	0.256	
320	1	91.0	0.133	$\delta^{18}O$ =	-4.729	0.030
				$\delta^{17}O$ =	-2.135	0.024
				$\Delta^{17}O$ =	0.362	
500	1	39.2	0.057	$\delta^{18}O$ =	-1.634	0.021
				$\delta^{17}O$ =	-0.481	0.031
				$\Delta^{17}O$ =	0.382	
1000	1	5.56	0.008	$\delta^{18}O$ =	11.019	0.037
				$\delta^{17}O$ =	5.909	0.064
				$\Delta^{17}O$ =	0.0910	
Total		228	0.333	$\Delta^{17}O$ =	0.330	0.011

3.10 Acknowledgements

Chapter 3, in full, is a reprint of the material as it appears in Science 2013. Carl B. Agee, Nicole V. Wilson, Francis M. McCubbin, Karen Ziegler, Victor J. Polyak, Zachary D. Sharp, Yemane Asmerom, Morgan H. Nunn, Robina Shaheen, Mark H. Thiemens, Andrew Steele, Marilyn L. Fogel, Roxanne Bowden, Mihaela Glamoclija, Zhisheng Zhang, Stephen M. Elardo. *Science* **339**, 780, 2013 (DOI: 10.1126/science.1228858). Reprinted with permission from AAAS. The dissertation author was a co-investigator and co-author of this paper.

Dissertation author conducted the laser fluorination experiments on whole rock samples of NWA 7034 to obtain the oxygen isotopic composition of the silicate material comprising the bulk of the rock. Dissertation author carried out water extraction experiments on NWA 7034 and determined the oxygen isotopic composition of water in NWA 73034. See pages 782-784 of Agee, C. B., et al. 2013 and pages 27-28 of associated *Supplementary Materials* for dissertation author's contributions.

Chapter 4. Oxygen isotopic composition of water in meteorite samples

4.1 Abstract

Meteorites belonging to many classes are believed to have formed from impacts on asteroids, and samples of these classes of meteorites can be studied to understand the compositions of the meteorite parent bodies. Oxygen's abundance in many phases in rocks from all bodies in the solar system and three stable isotopes (^{16}O, ^{17}O, ^{18}O) make it an ideal species of study in the exploration of other celestial bodies by sample analysis. The oxygen isotopic composition of the minerals comprising meteorite samples are well characterized, but few measurements of the isotopic composition of the relatively rare water phase have been made. Samples of a carbonaceous chondrite, a eucrite, separated matrix and chondrule fractions and whole rock samples of an ordinary chondrite were selected for water analysis to characterize the oxygen isotopic composition of asteroidal meteorite parent bodies and potential contributors to the water reservoir in the Earth-Moon system. The meteorite samples were chosen based on the flux of that class of meteorites to the Earth-Moon system and the oxygen isotopic composition of the class's constituent minerals (see Figures 5.1 and 1.2). I analyzed water in samples of the Bjurböle (L/LL4 ordinary chondrite, OC), ALHA 77216 (L3.7-3.9 ordinary chondrite), PCA 91006 (eucrite), and Murchison (CM2 carbonaceous chondrite) meteorites I extracted by stepwise heating to 50,

150, 350, 600, and 1000°C. Water in the meteorite samples was isotopically heterogeneous within a given class as well as within a given sample and possessed a $\Delta^{17}O$ value mostly in the range 1.6 to -1.6‰ and as low as -11‰ with respect to SMOW.

4.2 Extraction and Isotopic Analysis of Water

A rock/soil sample weighing 1-3g is crushed and loaded into a quartz tube on a stainless steel vacuum line, which is subsequently pumped to high vacuum ($P \leq 10^{-4}$Torr) to remove loosely bound, surface-adsorbed water (Fig. 4.1). Samples are heated step-wise between 50 and 1000°C while collecting evolved volatiles in a nickel reaction tube at liquid nitrogen temperature. The temperature, length of time, and total number of heat steps are optimized for each sample. The temperature at which water is evolved is proportional to the strength with which the water is bound in the sample and the relative difficulty of exchanging oxygen atoms in that water with surrounding species.

The number of heat steps is maximized to ensure the collection of extraterrestrial water separately from potentially terrestrial water contamination and allow water in the most possible mineral phases to be characterized. A limit on the number of heat steps is imposed by the minimum amount of water that can be liberated in each step and analyzed precisely (~0.1µmol). The temperature and number of heat steps used to extract water from each sample

differs and was decided on in light of the expected water release profile, based on expected hydration states of its constituent minerals and their respective dehydration temperatures.

Low temperature heat steps (T = 50, 150°C) remove surface-adsorbed water. If the sample contains any terrestrial water, it will be liberated in 150˚C and/or 50˚C heat step. Heating a sample at 350˚C releases interlayer water from phyllosilicates and water from low temperature alteration products. The 600˚C heat step liberates structural water (-OH) from phyllosilicates and high temperature igneous minerals as well as any remaining H_2O, which ensures the 1000˚C step represents pure, primordial water. The highest temperature heat step at 1000°C releases the water of principal interest because, as the least readily exchanged water, it is most likely to reflect primordial composition. Structural water from phyllosilicates, chlorites, and amphiboles, in addition to water trapped in vesicles or dissolved in glass is primarily released in the 1000˚C step.

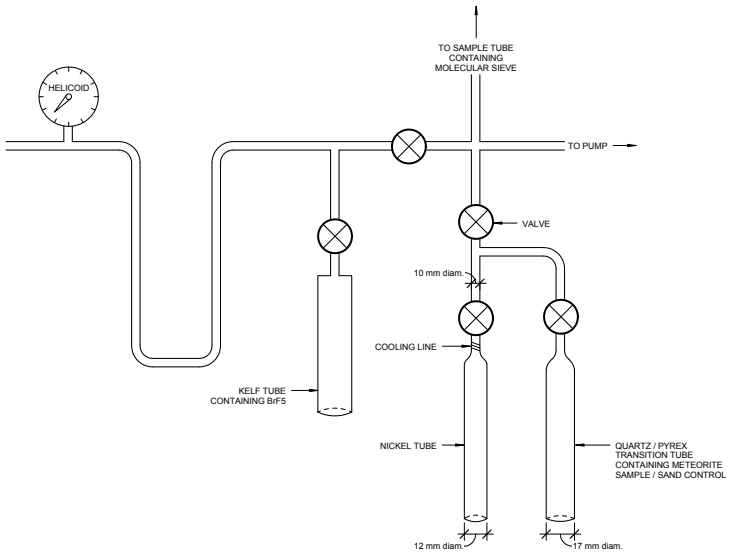

Figure 4.1 Schematic of vacuum system used to extract and fluorinate water from samples

Evolved water is selectively and quantitatively converted to molecular oxygen with bromine pentafluoride by the following reaction: $BrF_5 + H_2O \rightarrow BrF_3 + 2HF + ½O_2$. This fluorination reaction is specific for water, ensuring the resultant oxygen collected for isotopic analysis had water in the sample as its only source. Oxygen isotopic ratios ($^{17}O/^{16}O$ and $^{18}O/^{16}O$) are measured using a stable isotope ratio mass spectrometer (Thermo Finnigan MAT 253) with an ultra high purity oxygen (UHPO) reference gas of known isotopic composition.

The absence of a fractionation factor associated with the experimental procedure was verified by the analysis of a terrestrial control sample. Water extracted from the terrestrial control sample in all heat steps (T = 150, 350, 600, and 1000°C) had mass dependently fractionated oxygen, reflected by the $\Delta^{17}O \approx 0‰$. Conversely, meteoritic water (evolved at T = 1000°C) had $\Delta^{17}O$ as low as -

11‰ but was mostly in the 1.6 to -1.6‰ range. The advantages of this technique are evident in the high precision of isotopic ratio measurements. The high precision in even the smallest samples and large range in the size of samples that can be analyzed demonstrate the utility of this method and its potential for analysis of other samples.

4.3 Results and Discussion

4.3.1 Ordinary Chondrites: Bjurböle and ALHA 77216

Water extracted from 5 samples of low-iron ordinary chondrites (2 samples of Bjurböle matrix, 2 samples of Bjurböle chondrules, and 1 sample of ALHA 77216) by stepwise heating at (50,) 150, 350, 600, and 1000˚C is isotopically highly heterogeneous, even within a given sample, suggesting heterogeneity in the oxygen isotopic composition of water on the L chondrite parent body (Figure 4.2). The non-mass-dependently fractionated oxygen in nearly all the fractions of water in the extraterrestrial samples analyzed ($\Delta^{17}O \neq 0‰$) and predominantly mass dependently fractionated oxygen in water in the terrestrial control sample ($\Delta^{17}O \approx 0‰$) confirm the extraterrestrial nature of the water in the meteorite samples. The approach of the $\Delta^{17}O$ value of some of the high temperature fractions of water extracted from these OCs toward the bulk rock composition could reflect partial equilibration of water with host rock or, more likely given the

kinetic restraints imposed by the physical conditions on the parent body asteroid, a common oxygen source for these fractions of water and rock. However, the observed heterogeneity limits the conclusions that may be drawn from these results.

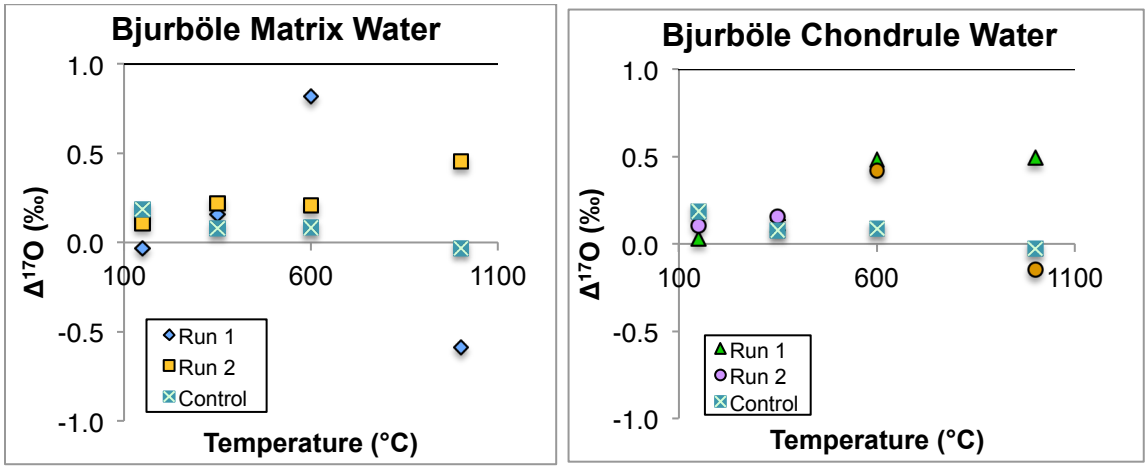

Figure 4.2 Oxygen isotopic composition ($\Delta^{17}O$, ‰) of water extracted from separated fractions of matrix and chondrule samples of the Bjurböle meteorite. Compositions are with respect to Standard Mean Ocean Water (SMOW). Results reflect analyses of water liberated from Bjurböle and a terrestrial control by stepwise heating to 150, 350, 600, and 1000˚C. Error in $\Delta^{17}O$ values is ±0.011‰ (1s). The bulk rock composition of Bjurböle is represented by a line at $\Delta^{17}O$ = 0.98‰ [56].

The $\Delta^{17}O$ value of each fraction of water extracted from Bjurböle matrix and chondrules (except matrix 1) lies between the TFL and the whole rock composition. These results suggest the $\Delta^{17}O$ value of the OC water reservoir is ≥ 0.5‰.

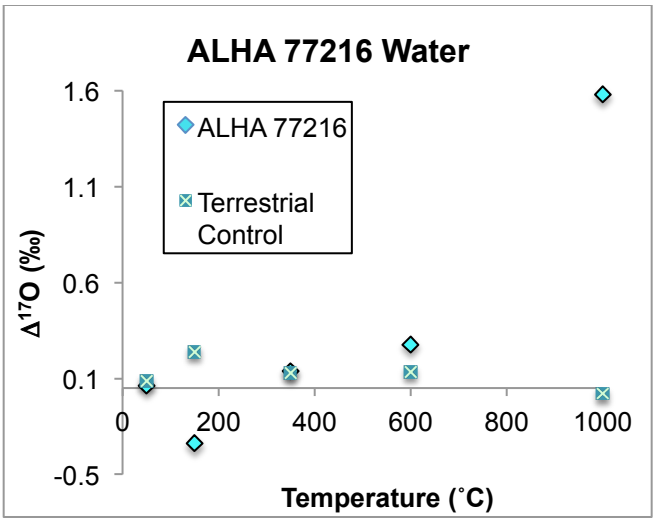

Figure 4.3 Oxygen isotopic composition ($\Delta^{17}O$, ‰) of water extracted from a sample of the ALHA 77216 meteorite. Compositions are with respect to Standard Mean Ocean Water (SMOW). Error in $\Delta^{17}O$ values is ±0.011‰ (1s). The average composition of L3 finds is $\Delta^{17}O$ = 0.92±0.14‰ [56].

The measured isotopic composition of the high temperature fraction of water extracted from ALHA 77216 is consistent with an OC water reservoir with a $\Delta^{17}O$ value ≥ 0.5‰.

All samples of OCs, with the exception of one fraction of Bjurböle chondrules, showed a maximum water release at 350˚C, suggesting the largest fraction of water in these OCs is held in low temperature alteration products. The water release profile (Fig. 4.4) displays the relative water yield produced by heating samples 150-1000˚C and is presented as the amount of water liberated in each heat step (wt%H_2O/OH) divided by the total amount of water extracted in all the steps and normalized to 100%.

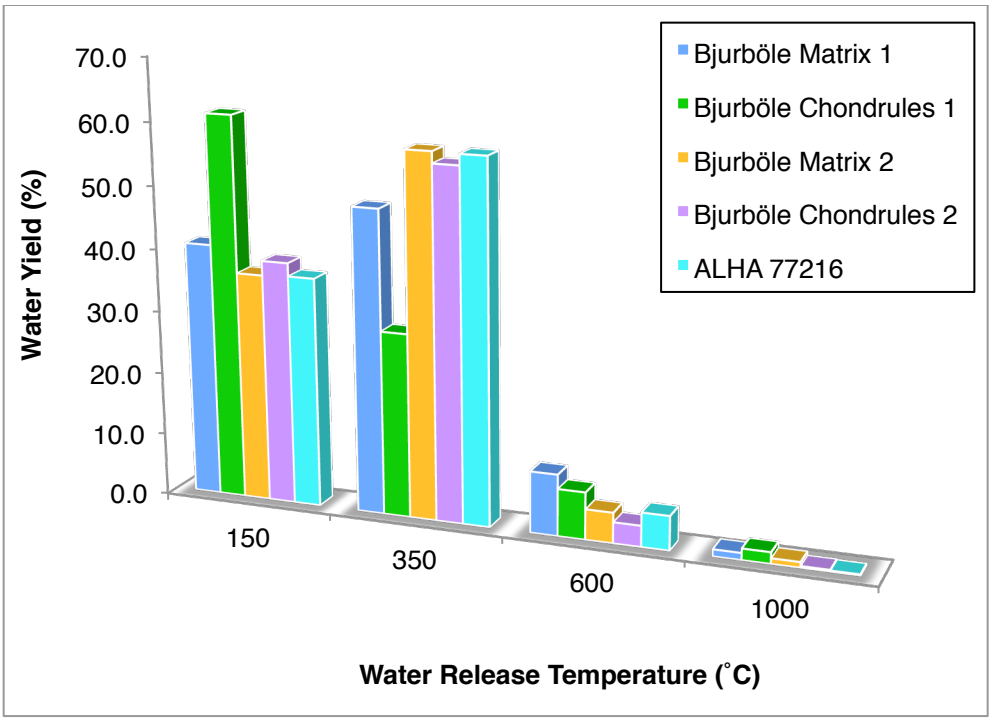

Figure 4.4 Water release profiles of ordinary chondrites Bjurböle and ALHA 77216. Separated matrix and chondrule fractions of Bjurböle and a whole rock sample of ALHA 77216 were heated stepwise to 150, 350, 600, and 1000˚C to liberate analyzed water.

The similarity in the water release profiles of all the OC samples studied suggests a relatively homogeneous distribution of the major water-bearing phases across the OC parent body. These phases may obtain water from different sources though, as the range in water oxygen isotopic composition implies.

4.3.2 Carbonaceous Chondrite: Murchison

Water in a sample of the carbonaceous chondrite meteorite Murchison was extracted by stepwise heating, and the oxygen isotopic composition of each fraction of water is presented in Figure 4.5. The 50˚C heat step removes physisorbed molecular water, so the proximity of the $\Delta^{17}O$ value of this fraction to 0‰ (the composition of atmospheric water vapor at sea level) suggests some terrestrial water may have been adsorbed on the meteorite sample or exchanged with the surrounding rock. The $\Delta^{17}O$ value of each water fraction increasingly approaches the bulk rock composition with increasing temperature. This steady approach is consistent with a significant amount of water-rock exchange and/or the formation of water and rock from an isotopically homogeneous oxygen reservoir. A considerable degree of aqueous alteration on the carbonaceous chondrite parent body has been posited by many workers in light of studies of carbonaceous chondrites, which is consistent with the latter explanation, but the possibility of the existence of a homogenous oxygen reservoir cannot be disregarded.

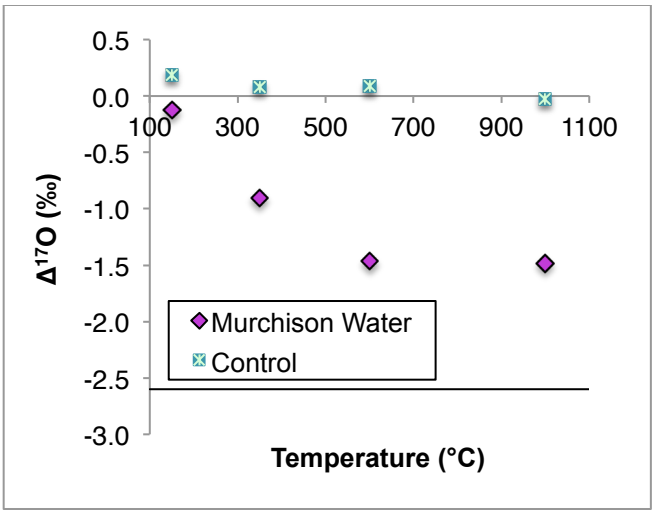

Figure 4.5 Oxygen isotopic composition ($\Delta^{17}O$, ‰) of water extracted from a sample of the Murchison meteorite. Results reflect analyses of water liberated from samples of Murchison and a terrestrial control by stepwise heating to 150, 350, 600, and 1000˚C. Compositions are with respect to Standard Mean Ocean Water (SMOW). Error in $\Delta^{17}O$ values is ±0.011‰ (1s). The bulk rock composition of Murchison is represented by a line at $\Delta^{17}O$ = -2.6‰ [56].

The largest fractions of water are released from Murchison during heating at 150 and 600˚C (Fig. 4.6), which can be explained, in light of the isotopic composition of these fractions, by the presence of some terrestrial water contamination and hydrated secondary alteration products.

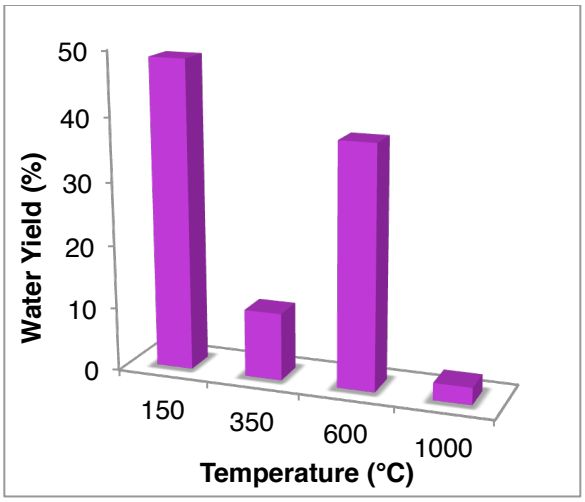

Figure 4.6 Water release profile of the Murchison meteorite. Analyzed water was collected during stepwise heating of a sample of the Murchison meteorite to 150, 300, 600, 1000˚C.

The proximity of the $\Delta^{17}O$ value of the 150˚C fraction (-0.122‰) to the terrestrial fractionation line (0‰) suggests a major source of this fraction is physisorbed, molecular water from the terrestrial atmosphere. The large 600˚C fraction could reflect the abundance of hydrated secondary alteration products which, considering its similar isotopic composition to the 1000˚C fraction (-1.5‰) could reflect a common oxygen source for water in alteration products as well as impact/volcanic glasses, (other phases that release at 1000˚C). Low temperature alteration products appear to be a less significant contributor to the water in Murchison than in the OCs.

4.3.3 Achondrite: PCA 91006, a Eucrite

The $\Delta^{17}O$ value of water extracted from the eucrite PCA 91006 by stepwise heating decreases with increasing temperature of extraction to -11‰. This value is significantly less than that of the average bulk rock of polymict eucrites (-0.25‰), suggesting water-rock exchange on Vesta, the eucrite parent body, was not deterministic of the final water isotopic composition [61]. The distinct $\Delta^{17}O$ value of the highest temperature fraction of water (1000˚C) implies Vesta had an isotopically distinct source of water after the asteroid was differentiated.

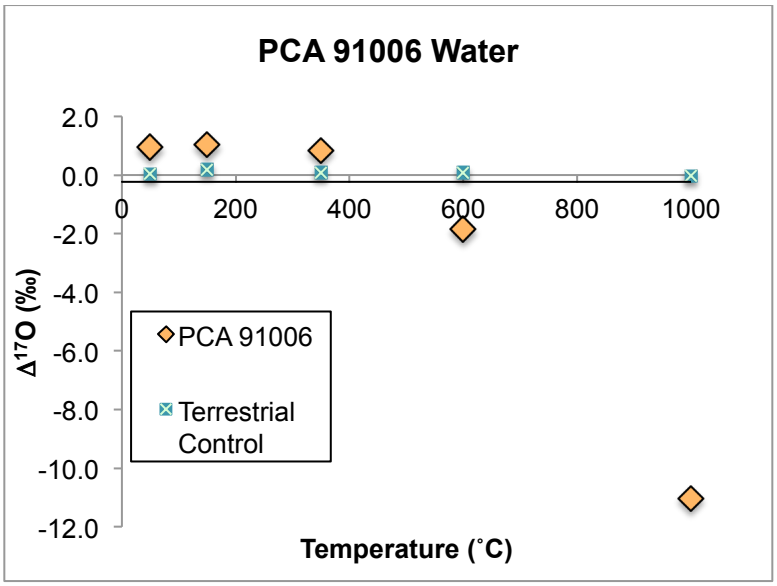

Figure 4.7 Oxygen isotopic composition ($\Delta^{17}O$, ‰) of water in the eucritic meteorite PCA 91006. Analyzed water was evolved from samples of PCA 91006 and a terrestrial control by stepwise heating to 50, 150, 350, 600, and 1000˚C. Error in $\Delta^{17}O$ values is ±0.011‰ (1s). The average bulk rock composition of polymict eucrites is represented by a line at $\Delta^{17}O$ = -0.23‰.

The largest fraction of water is liberated from PCA 91006 by heating to 150˚C, implying the existence of a significant amount of physisorbed molecular water, when considered with this fraction's oxygen isotopic composition ($\Delta^{17}O$ = 1.0‰) and its similarity to that of the 50˚C fraction ($\Delta^{17}O$ = 0.96‰).

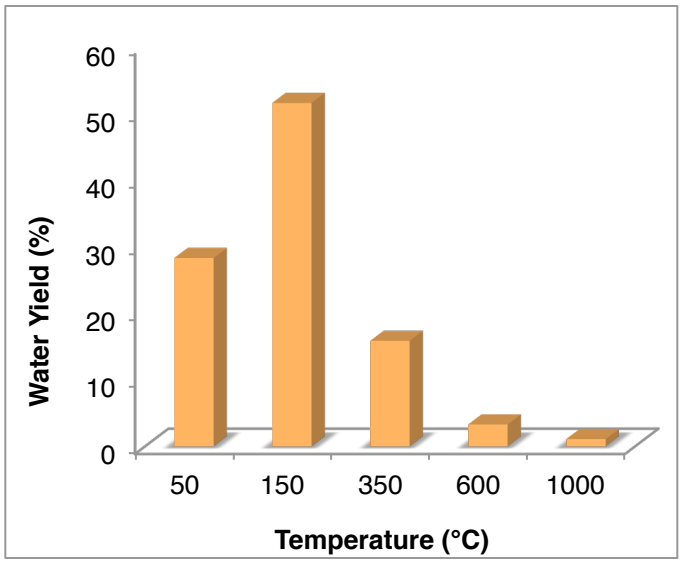

Figure 4.8 Water release profile of a sample of PCA 91006.

The relatively large fractions of the total water made up by the lower temperature heat steps (50-350˚C) could reflect a large amount of molecular water from either the terrestrial environment or an oxygen source that is isotopically similar to it. The relatively low water yield of the higher temperature heat steps (600-1000˚C) reflects the rarity of the water-bearing phases containing primordial oxygen.

4.4 Conclusions

The range observed in water release profiles for the meteorites Bjurböle, ALHA 77216, Murchison, and PCA 91006 displays the distinct petrologies or, more specifically, the variety of identities and abundances of water-bearing phases on the meteorite parent bodies. The range in oxygen isotopic composition of water extracted from these meteorites implies the existence of isotopically distinct water oxygen sources and/or multiple processes that lead to differentially fractionated water oxygen isotopes on each parent body. Distinct oxygen isotopic compositions of water extracted at the same temperature in different fractions of the OC Bjurböle reveal isotopic heterogeneity in the OC water oxygen reservoir. The oxygen isotopic compositions of water in the OCs are consistent with a primordial oxygen reservoir on the OC parent body with $\Delta^{17}O \geq 0.5‰$. A sample of Bjurbole chondrules and another sample of its surrounding matrix in addition to Murchison showed high temperature water fractions with $\Delta^{17}O$ approaching that of their host rock. Most samples (one sample of Bjurbole chondrules and another sample of its surrounding matrix, ALHA 77216, and PCA 91006) show a high temperature water fraction isotopically unlike their host rock, suggesting, in general, water-rock interaction on asteroidal meteorite parent bodies is often not significant and/or the water and rock oxygen source reservoirs are isotopically distinct.

Chapter 5. Oxygen Isotopic Composition of Lunar Water

5.1 Abstract

The origin of water in the Earth-Moon system is one of the most debated, unanswered questions in planetary science today, and if we are to understand the unique existence of life on Earth, we must understand the history of water in the inner solar system. The first quantitative evidence of the existence of water in the lunar interior and on the lunar surface was provided by recent discoveries of water in lunar volcanic glasses and reflectance spectroscopy studies of the lunar surface (Cassini, M3/Chandrayaan-1, Deep Impact).

Several sources of water in the present day Earth-Moon system have been proposed, and previous studies indicate the most likely origins of lunar water are in delivered asteroidal and cometary material, production from solar wind interaction, and a primordial lunar component. Reflectance spectra were interpreted to mean lunar surface water was produced by solar wind interaction [44]–[46]. Analyses of the concentration, in addition to the hydrogen and nitrogen isotopic composition (D/H and $\delta^{15}N$) of hydrated phases in lunar material have led several groups to suggest significant amounts of volatiles were delivered to the lunar surface by impacting asteroids (similar in composition to CI carbonaceous chondrites) and comets (Oort Cloud or Jupiter-Family). An

endogenous lunar water component has also been found in hydrous glasses [168]–[171].

Characterization of the oxygen isotopic composition of water provides unique information on the mass-dependence and independence of the sources and processes that gave rise to it, but the scarcity of lunar water and ^{17}O necessitated the development of a high precision analytical technique for the acquisition of informative results. We developed and employed such a technique in the analysis of water in a suite of samples collected on the lunar surface by the Apollo 11, 12, 14, and 17 missions (10049, 10057, 10060, 12021, 12039, 14163, 14305, and 79035). We present here the first measurements of the oxygen isotopic composition of water in bulk lunar surface material and discuss the implications of these results on the potential sources of this water.

5.2 Introduction

The moon is believed to have formed ~4.5 billion years ago from the debris produced by the impact of a proto-planet, Theia, with the proto-Earth, according to the giant impact hypothesis [74], [172]. The depletion in volatile species, including water, in lunar, relative to terrestrial, material has been interpreted to mean any primordial water accreted with the rest of the constituent lunar material has been lost to space through outgassing and desorption, but recent findings of water retained in volcanic glasses suggest an endogenous

lunar water component may have survived accretion and evolution to the present day [173]. Proposed explanations for water on the Moon include delivery by asteroids and comets, production on the lunar surface by solar wind, and (a primordial component [44]–[46], [168]–[170], [173]. Determination of the oxygen isotopic composition of water and comparison to the compositions of the potential extraterrestrial sources could shed light on the relative amounts of endogenous water and water delivered by each class of meteorite and comet. Plate tectonics ensure the isotopic composition of water on Earth evolves on long time scales as it is processed through the mantle, where it exchanges with oxygen-bearing minerals at high temperatures, gradually erasing the primordial oxygen isotopic signature. The absence of plate tectonics on the Moon implies the composition of water in lunar material reflects the sources and subsequent processing (such as diffusion, cosmic ray interaction, evaporation, photolysis, gardening). To better understand the sources of water in the Earth-Moon system, we made high precision measurements of the oxygen isotopic composition of water in 9 samples of lunar surface material brought back on NASA's Apollo missions.

Apollo-era analyses of the recently returned lunar samples concluded they contained no indigenous water [174]–[177]. Through the development of a more sensitive analytical technique, including the use of a more sensitive and precise mass spectrometer than was available at that time, we have successfully extracted water from several lunar samples and characterized the oxygen isotopic composition of that water. Reflectance spectroscopy measurements

made on the lunar surface by Cassini, M3/Chandrayaan-1, Deep Impact provided the first quantitative evidence of lunar surface water. Noting the diurnal variability of water in regions of the lunar surface exposed to solar radiation, these studies concluded the predominant source of water on the lunar surface being solar wind derived was the most consistent explanation for their observations [44]–[46]. Solar wind derived water would be produced from H/D in the solar wind and oxygen in lunar surface minerals, and consequently, it would posses the oxygen isotopic signature of the bulk moon [43]. Estimating how much, if any, of the current lunar water has its source in the solar wind is not possible by oxygen isotopic analyses because production of water by interaction with the solar wind and exchange of oxygen between water and the minerals that constitute the Moon would similarly shift the oxygen isotopic composition closer to that of the bulk Moon.

The presence of water in Cabeus, a permanently shadowed crater near the lunar south pole, was confirmed by NASA's Lunar CRater Observation and Sensing Satellite (LCROSS) mission [178]. The origin of water in Cabeus and other permanently shadowed regions is unclear, particularly in light of models describing the possibility for large-scale transport of volatiles from low latitude regions toward the poles. Up to 1400ppm water was discovered in lunar melt inclusions in an Apollo 17 olivine, the collection location of which suggests an endogenous origin [173]. Hydrogen isotopic characterization (δD) of water-

bearing lunar apatite led several groups to hypothesize water in the lunar mantle was delivered by (an) Oort Cloud comet(s) [167], [169], [171], [179].

Several approaches to understanding the relative contributions of cometary and meteoritic water to the current, terrestrial water reservoir have been made. Recent studies of the comet 103P/Hartley 2 found its hydrogen isotopic composition (D/H) to be similar to this Jupiter family comet, suggesting most of the water on Earth could have been delivered by comets originating in the Kuiper belt [170]. Taken in light of nitrogen isotopic evidence, Alexander et al. suggest the hydrogen isotopic composition of Earth's volatiles can be explained most completely by predominant contribution from CI chondritic meteorites [168].

Oxygen's three stable isotopes, ^{16}O, ^{17}O, ^{18}O, enable the elucidation of the mass-dependence or independence of the processes that gave rise to its host species. Additionally, the distinct formation processes and differential nuclear stabilities of ^{16}O, ^{17}O, and ^{18}O have led to distinct ratios of these isotopes in each oxygen-bearing phase on each celestial body. Oxygen is the most abundant element, by mass, in the terrestrial bodies of the inner solar system and appears in many distinct chemical phases on each of these bodies. Characterization of oxygen isotopic ratios is, therefore, an effective tool in determining the formation and equilibration history of an extraterrestrial sample.

Meteorites from Mars and all asteroid parent bodies, with the exception of the extremely rare aubrite class of meteorites, display bulk oxygen isotopic compositions that are distinct from the Earth and Moon (see Figure 1.2). The

Antarctic Meteorite Collection is believed to be representative of the relative flux of meteorites to the entire Earth and, therefore, approximately to the Moon [180]. Comparison of the oxygen isotopic composition of each type of potential impactor (these meteorites and comets), taking into account their relative fluxes (Figure 5.1), with that of lunar water can shed light on the relative amounts of water contributed to the lunar water reservoir by each type of impactor.

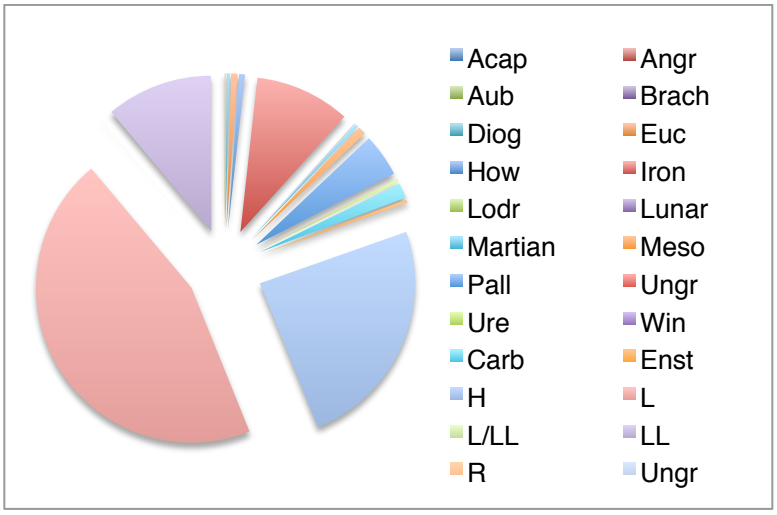

Figure 5.1 Relative amount, by mass, of meteorites of each class in the Antarctic Meteorite Collection. Statistics reflect the collection as of September 2012, as reported by the National Aeronautics and Space Administration (NASA) Astromaterials Research and Exploration Science (ARES) curator. (http://curator.jsc.nasa.gov/antmet/us_clctn.cfm) Acap = Acapulcoite, Angr = Angrite, Aub = Aubrite, Brach = Brachinite, Diog = Diogenite, Euc = Eucrite, How = Howardite, Lodr = Lodranite, Meso = Mesosiderite, Pall = Pallasite, Ungr = Ungrouped achondrite, Ure = Ureilite, Win = Winonite, Carb = Carbonaceous chondrite, Enst = Enstatite chondrite, H = High iron ordinary chondrite, L/LL = Low/Low-Low iron ordinary chondrite, LL = Low-Low iron ordinary chondrite, R = Rumuruti chondrite, Ungr = Ungrouped chondrite.

Oxygen may be delivered by asteroidal or cometary impacts in minerals (olivines and pyroxenes in greatest abundance; spinels, feldspars, phosphates, and secondary alteration products like phyllosilicates in lower abundance), organic compounds, and adsorbed and trapped volatiles (H_2O(l), H_2O(s, ice), and O_2), among other phases. Each of these has a distinct oxygen isotopic composition. Until the oxygen-bearing phases that would be retained during impact and would lead to the formation of water are better characterized (and their concentrations and oxygen isotopic compositions are better known), we will consider all delivered oxygen as a possible contributor to the lunar water reservoir.

Predominantly kinetic and thermodynamic/equilibrium fractionation processes affect the $\delta^{17}O$ and $\delta^{18}O$ values of oxygen-bearing species on the lunar surface, shifting the measured composition along a line representing mass-dependent fractionation, where $\delta^{17}O = 0.52*\delta^{18}O$. The $\Delta^{17}O$ value is used to describe the mass-dependence/-independence of an oxygen-bearing species by reflecting the deviation from mass-dependent fractionation:

$$\Delta^{17}O\ (‰) = \delta^{17}O - 0.52 * \delta^{18}O$$

[10], [11]. Because the change in $\Delta^{17}O$ during processing on the lunar surface is predominantly 0‰, analysis of the $\Delta^{17}O$ value could be a more accurate point of comparison for determination of sources of oxygen in lunar surface water. Mass-independently fractionated oxygen in terrestrial water is rare, but it is relatively abundant elsewhere in the solar system and was first identified in the refractory

calcium-aluminum-rich inclusions (CAI) within the Allende meteorite [9]. Perfectly mass-dependent fractionation has been represented by other groups by a $\delta^{17}O$ / $\delta^{18}O$ ratio of 0.5-0.528, but we have found a ratio of 0.52 most accurately represents the kinetic equilibrium fractionation process of mineral dehydration [56].

Mineral fragments from the bulb of a single Stardust track collected from comet 81P/Wild 2 display a large range in oxygen isotopic compositions (-70‰ < $\Delta^{17}O$ < 60‰) [76]. The flux of Oort Cloud or Jupiter-Family comets to the Earth-Moon system since the Moon formed is not known, but the range in oxygen isotopic composition of a small fraction of a single comet prevents constraints being placed on the amount or isotopic composition of oxygen delivered by comets.

Meteorites and comets have delivered oxygen to the lunar surface in the form of abundant minerals and (rarer) water, so the direct comparison of their oxygen isotopic compositions to that of lunar water for source elucidation is possible. Solar wind derived lunar water would have formed from the interaction of incoming, energetic H and D with surface minerals, and so the oxygen isotopic composition of that water would reflect that of the source minerals, i.e., bulk Moon [43].

The $\Delta^{17}O$ value is, therefore, an effective diagnostic for identifying classes of meteorites that contributed to the lunar water reservoir. The oxygen isotopic

composition of lunar water we measured will be presented and discussed in the context of the concentration and composition of water in potential impactors.

5.3 Methods

Water is extracted from lunar samples in stepwise heating experiments and converted to molecular oxygen (O_2) using a water fluorination technique. Each sample (1-3g) is first crushed to a homogenous, fine-grained powder, unless it was a soil and, thus, already like this. The sample is then loaded into a quartz sample tube in a stainless steel and glass vacuum system and pumped to a 10^{-4} Torr vacuum overnight (until degassing ceases). Samples are heated stepwise to 50, 150, and 1000°C to separately collect water bound in different phases. The temperature at which water is released from a sample is directly proportional to the strength with which it is bound to the constituent minerals of the samples. The 50˚C heat step succeeds in liberating physisorbed, molecular water (H_2O), which includes terrestrial atmospheric water vapor. The 150˚C heat step releases any remaining physisorbed, molecular water [55]. Water released upon heating a sample to 1000˚C, just below the annealing temperature of the most abundant phase, SiO_2, is primarily water trapped in glasses and, to a much lesser extent, structural water, -OH. Water liberated in the highest temperature heat step has the lowest probability of exchanging with surrounding oxygen-bearing reservoirs and, therefore, most likely reflects the oxygen isotopic

composition of a primitive water source. The 1000˚C fraction could include water trapped in the immediate aftermath of an impact (and would therefore reflect the impactor's composition) and in a volcanic eruption (and would therefore reflect the lunar mantle composition).

While heating samples to 50, 150, and 1000°C, all evolved volatiles are collected in a liquid nitrogen cold trap in separate experiments. In a reaction vessel isolated from the sample itself, these volatiles are allowed to react with bromine pentafluoride (BrF_5), a strong oxidizer which quantitatively converts water to O_2 and hydrogen fluoride (HF). Because this reaction is specific to water, a clean molecular oxygen sample is produced by using this reaction, instead of a water sample, whose properties make it difficult to work with in a vacuum system (i.e., fluorination is effectively a purification step). Furthermore, product O_2 is easily purified from the reagents and product HF. Molecular oxygen produced in the fluorination procedure is collected and its oxygen isotopic composition ($\delta^{17}O$ and $\delta^{18}O$) is measured on a Thermo Finnigan MAT 253 dual inlet isotope ratio mass spectrometer (IRMS). Blank experiments were performed before each heat step to ensure the experimental procedure contributed < 10% of minimum expected water yield, i.e., < 0.1mmole of water. Analogous stepwise heating studies performed on terrestrial sand (SiO_2) confirm the experimental procedure induces no mass independent isotopic fractionation. Accuracy and precision of mass spectrometric analyses is confirmed by comparison to a reference ultra high purity oxygen (UHPO) gas of known isotopic composition

$\delta^{17}O$ = 11‰ and $\delta^{18}O$ = 22‰ and zero enrichment mass spectrometer ratio equivalence tests before all analyses of lunar water.

Samples chosen for analysis are: 10049, 10057, 10060, 12021, 12039, 14163, 14305, 79035. These samples represent approximately the full range in geographic sampling locations on the lunar surface. These samples were also selected because they span the range in surface exposure ages of lunar samples and we sought to determine the effect of this variable on the oxygen isotopic composition of water in lunar surface samples (Fig. 5.2). Samples with distinct petrography were selected to see how these properties determine the relative and absolute frequency of different reactions/processes. To investigate the heterogeneity of the distribution of water bearing phases in 14305, the original ~3g sample was divided up and analyzed as a ~2g and a ~1g sample, referred to as “14305 (2g)” and “14305 (1g),” respectively.

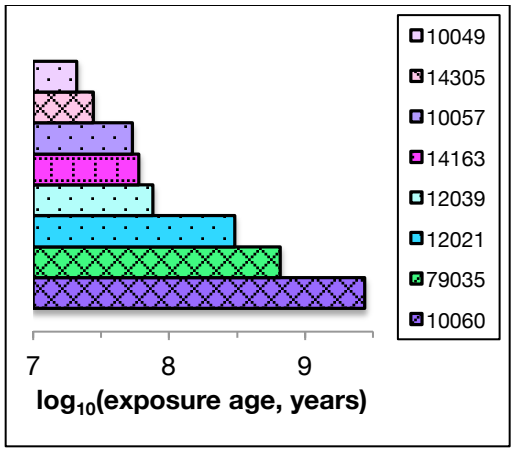

Figure 5.2 Cosmic ray exposure (CRE) ages of analyzed lunar samples. The range in CRE age is from 21 million years (10049) to 2.75 billion years (10060). Samples include basalts, breccias, and a soil. Patterns are indicative of sample type: series shown in a pattern of dots are basalts (10049, 10057, 12021, 12039), diamonds are breccias (10060, 14305, 79035), and squares is a soil (14163).

5.4 Results and Discussion

The amount of water evolved from each lunar sample during each heat step is presented in Figure 5.3 as a relative water yield, calculated by dividing the amount of water liberated in a given heat step by the total amount of water liberated from a given sample in the 50, 150, and 1000˚C steps. Relative water yields, more so than absolute water yields, enable more elucidative direct comparison of the highly heterogeneous lunar samples. Patterns indicate the sample type, i.e., series shown in a pattern of dots are basalts (10049, 10057, 12021, 12039), diamonds reflect breccias (10060, 14305, 79035), and squares represent a soil (14163). Lunar samples 10049, 10060, 12039, and 14305 (2g)

release the largest proportion of water during heating at 150˚C, whereas heating 10057, 14163, 14305 (1g), and 79035 at 1000˚C released the largest proportion of water. Sample 12021 uniquely showed its maximum water release at 50˚C. There is no observable correlation in sample type and water release profile, which indicates the identity and/or the concentration of the major water-bearing phases is not specific to/fixed for a given sample type. The difference in the water release profiles of the samples of 14305 (1g sample exposed to terrestrial atmosphere for 3 years 3 months longer than 2g sample) reveal the heterogeneous distribution of water-bearing phases in a single sample. The diversity in water release patterns among the lunar samples analyzed requires contributions from multiple, major water-bearing phases.

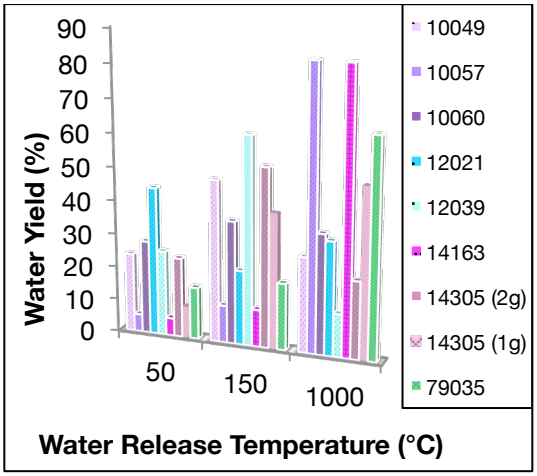

Figure 5.3 Water release profiles of lunar samples. The relative amount of water released by heating lunar samples 10049, 10057, 10060, 12021, 12039, 14163, 14305 (2g), 14305 (1g), and 79035 stepwise to 50, 150, and 1000˚C are shown. Patterns reflect sample type: series shown in a pattern of dots are basalts (10049, 10057, 12021, 12039), diamonds are breccias (10060, 14305, 79035), and squares is a soil (14163).

Water extracted from the lunar samples selected for this study by stepwise heating span a large range in oxygen isotopic composition ($\delta^{17}O$ and $\delta^{18}O$, Fig. 5.4) and possess small but distinct mass independent isotopic anomalies. The magnitude of the mass independent anomalies is outside the range of error or that expected from varying mass dependent slopes [11]. Because of the large ranges in $\delta^{17}O$ and $\delta^{18}O$, the anomalies are best plotted in terms of the $\Delta^{17}O$ value (Fig. 5.5). Measured $\delta^{17}O$ and $\delta^{18}O$ values have been corrected for the effect of ≥ 4.5% nitrogen contamination (see Ch. 7 for details).

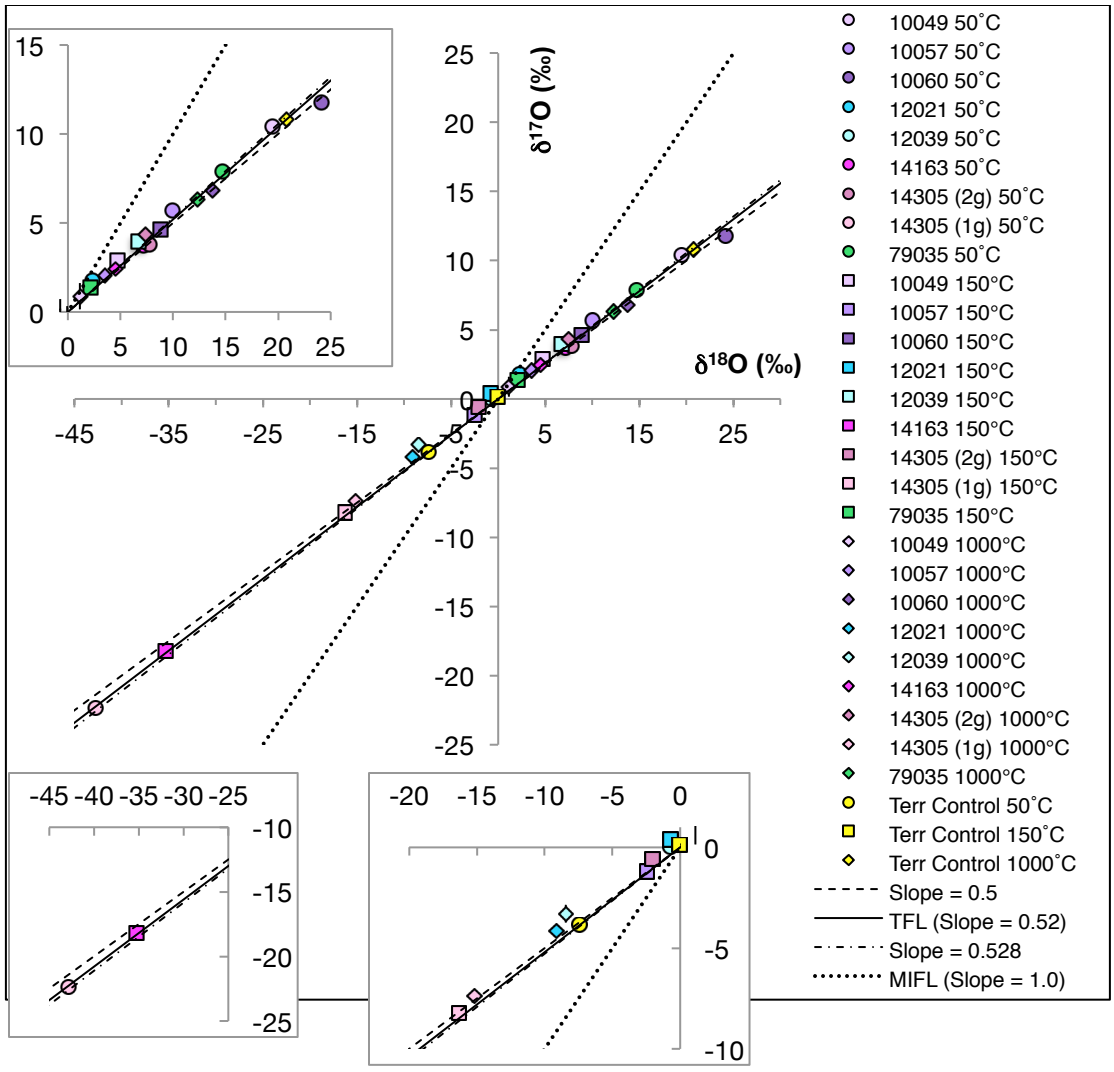

Figure 5.4 Oxygen isotopic composition ($\delta^{17}O$ vs. $\delta^{18}O$, ‰) of water extracted from lunar samples. Results reflect analyses of water liberated from lunar samples 10049, 10057, 10060, 12021, 12039, 14163, 14305 (2g), 14305 (1g), and 79035 by stepwise heating at 50˚C (circles), 150˚C (squares), and 1000˚C (diamonds). Compositions are with respect to Standard Mean Ocean Water (SMOW). 1σ error bars are plotted but almost all are smaller than the data point marker. Lines representing mass independent fractionation (MIFL, slope = 1.0), terrestrial fractionation (TFL, slope = 0.52), and mass dependent fractionation (slopes = 0.5 and 0.528) are shown for reference.

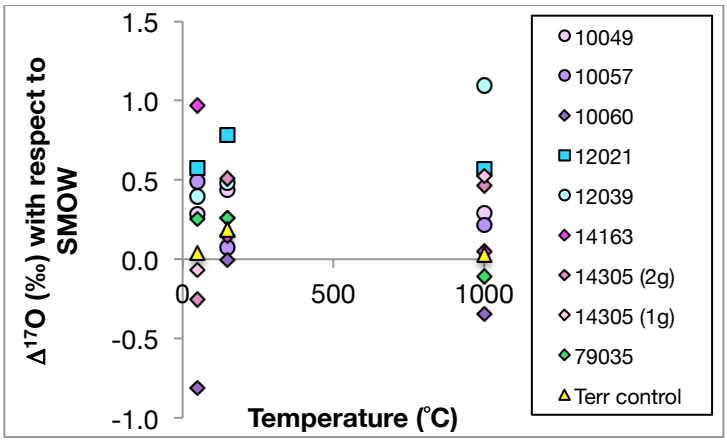

Figure 5.5 $\Delta^{17}O$ (‰) of water extracted from lunar samples. Water was released during stepwise heating experiments of lunar samples 10049, 10057, 10060, 12021, 12039, 14163, 14305 (2g), 14305 (1g), and 79035 at 50, 150, and 1000˚C. Compositions are relative to Standard Mean Ocean Water (SMOW).

The lunar samples analyzed display a large range in $\Delta^{17}O$ values across the 50˚, 150˚, and 1000˚C fractions (-0.81 to 1.1‰), and the average is 0.28‰. The average $\Delta^{17}O$ for the 50˚, 150˚, and 1000˚C fractions are 0.20, 0.33, and 0.31‰. The measured data are consistent with input of oxygen with a positive, mass-independent anomaly. Meteorites belonging to the H, L, and LL classes have a $\Delta^{17}O$ value of 0.98‰, and OCs make up ~80%, by mass, of meteorites [56]. The observed range however requires negative $\Delta^{17}O$ contribution from an endogenous source, including lunar water, solar-wind derived water, cometary material/water, and/or terrestrial contamination. The absolute value of measured $\Delta^{17}O$ values are a lower limit because any contamination by terrestrial atmospheric water vapor, which has $\Delta^{17}O$ = 0‰, would bring the measured $\Delta^{17}O$ closer to 0‰.

The 50˚C fraction of water extracted from lunar samples shows a larger range in $\Delta^{17}O$ values (-0.81‰ for 10060 to 0.97‰ for 14163) than the 150 and 1000˚C fractions. In Agee et al 2013, we reported that a Martian meteorite, which was exposed to the terrestrial atmosphere for orders of magnitude longer than the lunar samples, did not acquire a significant amount of terrestrial water [52]. It is highly unlikely the lunar samples absorbed much terrestrial water, and that contribution would only serve to dilute the anomalous component.

The 50˚C step releases loosely bound, physisorbed molecular water (H_2O) acquired primarily on the Moon and, possibly, some from the terrestrial atmosphere. The lunar component of the 50˚C fraction may have been delivered or produced by asteroidal and cometary impacts, in addition to solar wind-derived water and endogenous lunar water. Large variability in $\Delta^{17}O$ for the 50˚C step may reflect, in part, differential propensity to adsorb water vapor. This propensity is dependent upon porosity, binding affinity for H_2O, crystal structure of the constituent minerals, which vary widely among the lunar samples, and the length of time the sample was exposed to the H_2O source.

Samples 12039, 14163, and 14305 were stored under a nitrogen (N_2) atmosphere since their collection on the lunar surface at the Johnson Space Center (JSC) and were exposed to the terrestrial atmosphere only while being admitted into the vacuum system (<~1 hour). Samples 10049, 10057, 10060, 12021, and 79035 were exposed to the terrestrial atmosphere for 15 years in the safe storage at UCSD, contained within the JSC sample vials. The isotopic

composition of 50˚C water in the 1g portion of 14305, which was exposed to the terrestrial atmosphere for 3 years and 3 months, is -0.069‰, compared to -0.254‰ for the 2g portion of 14305, which was directly transferred from the clean N_2 atmosphere to the vacuum system. The difference in the isotopic composition of the portions of 14305 reflects heterogeneity within the sample and/or uptake of terrestrial atmospheric water vapor and subsequent exchange (wt% H_2O evolved in 50˚C step of 2g and 1g portions is approximately the same, 21 and 23ppm, respectively, suggesting adsorbed terrestrial H_2O is removed during chamber evacuation). The large range in positive and negative $\Delta^{17}O$ values of the 50˚C fraction of water across the lunar samples analyzed and the absence of correlations in sample type and water content and composition requires several oxygen-bearing sources and/or several processes that fractionate oxygen isotopes with varying degrees of mass independence.

Water liberated by heating samples at 150˚C shows the smallest range in $\Delta^{17}O$ values of all the fractions: 0.00‰ for 10060 to 0.78‰ for 12021. The $\Delta^{17}O$ of water extracted at 150˚C from samples 10060, 14305 (2g), 12021, 79035 is closer to zero than the 50˚C fraction (or equal to the 50˚C fraction), within error. This presumably reflects the removal of some water containing non-mass-dependently fractionated oxygen that was incompletely liberated by heating at 50˚C whose isotopic signature is diluted by the presence of a small amount of terrestrial, atmospheric water vapor introduced when the sample was transferred to the vacuum system or during storage. In the case of samples 10057, 14305

(1g), 12021, 12039, the $\Delta^{17}O$ of water extracted at 150˚C is intermediate to that extracted at 50˚C and 1000˚C, which suggests heating these samples at 150˚C releases some water sampled in both the 50˚C and 1000˚C steps.

Heating samples at 1000˚C released water with a large range in $\Delta^{17}O$ values: -0.34‰ for 10060 to 1.0‰ for 12039. As the mostly tightly bound and least readily exchanged water in a sample, the water liberated by heating at 1000˚C most likely reflects the oxygen isotopic composition of primordial lunar water, whether endogenetic or delivered by cometary and/or asteroidal impacts. The amount of water evolved in the 1000˚C heat step (wt% OH/H_2O) is proportional to the amount of glass (measured or inferred from mesostasis abundance) in each sample for which glass abundance is known.

The presence of 1000˚C water having a $\Delta^{17}O > 0$‰ in 10057, 12021, 12039, 14163, and 14305 (1g) could be explained by significant contributions to the lunar water reservoir by CI chondrites or H, L, and LL ordinary chondrites, which make up ~70%, by mass, of the Antarctic Meteorite Collection and, by extension, of the total flux of asteroidal material to the Earth-Moon. In light of the hydrogen and nitrogen isotopic arguments proposed by Alexander et al. 2012, CI chondrites are the most likely source of this positive $\Delta^{17}O$ (> 0‰) water [168].

The presence of 1000˚C water having a $\Delta^{17}O < 0$‰ in 10049, 10060, 14305 (2g), and 79035 could be explained by significant contributions to the lunar water reservoir by a number of asteroidal impacts, but the relatively large flux of carbonaceous chondrites make them a likely candidate.

The abundance of cometary material delivered to the lunar surface by impacts could have greatly contributed to the lunar water reservoir. The range in $\delta^{18}O$ of lunar water is very large and is possibly a secondary effect from photochemistry.

5.5 Conclusions

Most significantly, water extracted from lunar samples in all the heat steps possesses both positive and negative $\Delta^{17}O$ values, reflecting positive and negative deviations from mass dependent fractionation. This requires a multiplicity of non-terrestrial oxygen-bearing components as sources and processes that fractionate oxygen isotopes mass independently to differing degrees.

5.6 Acknowledgements

Chapter 5, in part, is currently being prepared for submission for publication of the material. Morgan H. Nunn and Mark H. Thiemens. The dissertation author conducted the experiments described and is the author of this material.

Chapter 6. Formation of Isotopically Anomalous Ozone by Photolysis of Solid Molecular Oxygen

6.1 Abstract

In cold, dense molecular clouds, the birthplace of stars and their associated planetary systems, ozone (O_3) is thought to be a principal precursor to water. Hence, characterization of the isotopic fractionation effect on O_3 production may shed light on the observed isotopic heterogeneity in oxygen-bearing reservoirs, especially water, in the solar system. To determine the isotopic fractionation that would result from nebular processes, we built a system to carry out surface photolysis experiments under conditions analogous to those believed to have existed in the nascent solar system. Experiments photolyzing cold (T≈ 8, 77K) molecular oxygen (O_2[s] and O_2[g]) by ultraviolet (UV) radiation to produce O_3 have been performed, and the product O_3 is anomalous in terms of its oxygen isotopic composition.

6.2 Methods

To characterize the oxygen isotopic composition of an important precursor to water, O_3, was produced by photolysis of O_2. Photolysis experiments were conducted on a surface comprised of a polished Al_2O_3 section to simulate

nascent interstellar dust grains (Fig. 6.1). The surface sits at the center of the reaction chamber and is connected to a liquid He-cooled cryostat (ColdEdge Technologies). Three walls of the reaction chamber contain optical windows to visually monitor the reaction. The forth window contains a 3mm thick, UV-transparent, MgF_2 window to allow for photolysis. The entire system is connected to a turbo pump to obtain $P \leq 10^{-5}$ Torr.

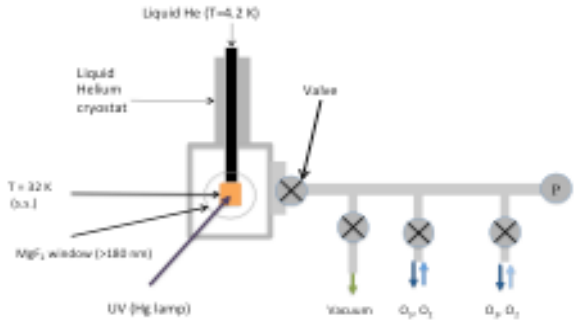

Figure 6.1 Schematic of experimental setup for production of ozone (O_3) by photolysis of O_2. Figure taken from Dominguez *et al.* 2012 [181]

In each experiment, an aliquot of ultra high purity oxygen (UHPO, O_2) of known isotopic composition ($\delta^{18}O = 12.639$, $\delta^{17}O = 6.524‰$) is introduced to the reaction chamber via a nozzle positioned ~1cm from the center of the surface. Using the cryostat, the reaction surface is held at 8 or 77K, at which temperatures, the O_2 will either freeze onto the reaction surface or remain in the gas phase within the reaction chamber. The surface and walls of the reaction

chamber are not in thermal equilibrium so, at T < 54K, O_2(s) is deposited exclusively on the reaction surface. The reaction chamber is isolated during an experiment, and the surface is exposed to UV photons of wavelength, λ, 184.5 nm (flux ~10^{16} cm^{-2}) produced by a microwave generator powered Hg lamp (Opthos Inc.) for 1-2 hours.

Separation of reactant O_2 and product O_3 is accomplished cryogenically, taking advantage of the higher vapor pressure of O_2, relative to O_3. The reaction chamber is opened to the vacuum pump while slowly increasing the surface temperature from 8K to 55K, where O_3 is frozen on the surface but O_2 is in the gas phase. When P ≤ 10^{-2} Torr, indicating most O_2 has been pumped away, the surface is brought to room temperature and the reaction chamber is then opened to zeolitic molecular sieve in a borosilicate sample tube at liquid N_2 temperature (77K) to collect liberated O_3. Exposed to the large surface area molecular sieve, unstable O_3 decomposes to form O_2, and the relative amounts of oxygen isotopes ($^{18}O/^{16}O$ and $^{17}O/^{16}O$) in this O_2 is measured on a MAT 253 (Thermo Finnigan) dual inlet isotope ratio mass spectrometer (IRMS) relative to an UHPO standard of known isotopic composition with respect to Standard Mean Ocean Water (SMOW).

This experimental setup is additionally valuable because of its adaptability. The composition of reactants to be photolyzed, surface composition, temperature, and photon flux can be varied depending on the species and physical conditions of interest.

6.3 Results and Discussion

The isotopic composition of O_3 formed by photolysis of O_2 at 8 and 77K is presented in Figure 6.2 as $\delta^{17}O$ versus $\delta^{18}O$. Perfectly mass-dependent and -independent fractionation are represented by lines in $\delta^{17}O$ versus $\delta^{18}O$ space of slope 0.52 and 1.0, respectively. The line of best fit to the 8K data (shown in green) possesses a slope of 0.58, which, at first glance, seems to suggest the O_3 formation process fractionates oxygen isotopes mass-dependently. In reality, this range of oxygen isotopic compositions reflects the incomplete separation of the mass-independently fractionated product O_3 from the mass-dependently fractionated reactant O_2, and this is revealed by the intersection of the line of best fit with the UHPO composition.

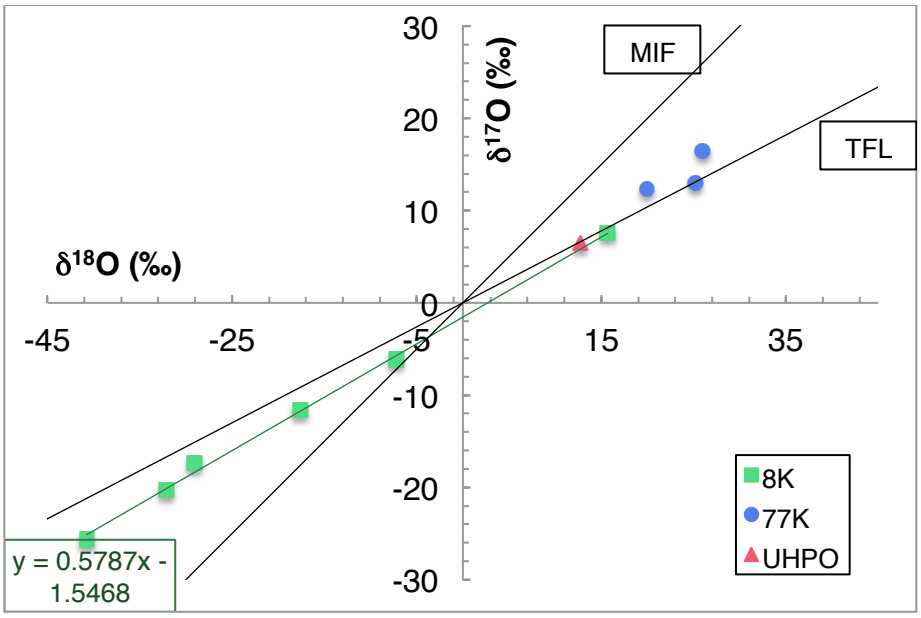

Figure 6.2 Isotopic composition ($\delta^{17}O$ versus $\delta^{18}O$, ‰) of ozone (O_3) formed at 8K and 77K. The composition of the molecular oxygen (O_2) from which the O_3 was formed, ultra high purity oxygen (UHPO), is also shown. All $\delta^{17}O$ and $\delta^{18}O$ values are with respect to Standard Mean Ocean Water (SMOW). Lines representing mass-dependent and -independent fractionation possessing slopes of 0.52 (the terrestrial fractionation line, TFL) and 1.0 (MIF), respectively, are shown for reference. Error bars (smaller than data point marker) are 1σ.

Separation of O_2 and O_3 is accomplished cryogenically, taking advantage of differences in their vapor pressures. Because this difference is small and the O_2 reservoir is ~4 orders of magnitude larger than that of O_3, complete separation of these species is difficult. Other experimental limitations and unknowns make this still more difficult and include potential temperature variation across the reaction surface not reflected in the temperature measurement.

The formation of O_3 by photolysis of solid phase O_2 is believed to be a mass-independent fractionation (MIF) process. At 77K, O_2 is in the gas phase so

these data show the effects of fractionation induced by the $O_2(g) \rightarrow O_3$ reaction, which is also mass-independent. The $\Delta^{17}O$ value of O_3 formed from $O_2(g)$ (2.9, 2.0, -0.13‰, average = 1.6‰) reflects the MIF of this reaction, as well as a contribution from the incompletely separated, reactant $O_2(g)$ (Fig. 6.3).

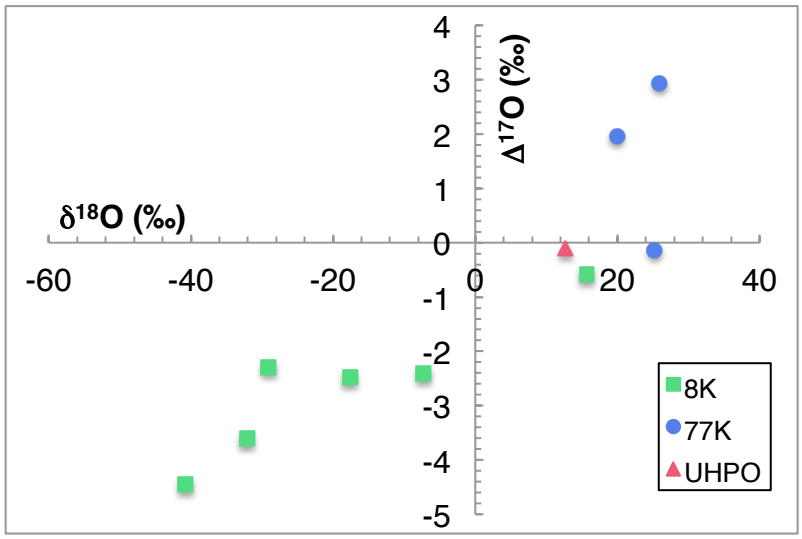

Figure 6.3 The mass-independence of ozone (O_3) formed by photolysis of molecular oxygen (O_2, UHPO) at 8K and 77K is presented as $\Delta^{17}O$ (‰) versus $\delta^{18}O$ (‰). Compositions ($\Delta^{17}O$ and $\delta^{18}O$) are with respect to Standard Mean Ocean Water (SMOW). Error bars (smaller than data point marker) are 1σ.

The mass-independent nature of the $O_2(s) \rightarrow O_3$ reaction is most evident in the relationship between the $\Delta^{17}O$ and $\delta^{18}O$ of the product O_3 (Fig. 6.3). At 8K, O_3 is anomalous in terms of its oxygen isotopic composition, displayed by its average $\Delta^{17}O$ value of -2.6‰. As $\delta^{18}O$ of O_3 decreases away from that of the reactant UHPO (12.7‰), $\Delta^{17}O$ also decreases, reflecting the progressive

fractionation of oxygen.

Based on these results, the $O_2(s) \rightarrow O_3$ reaction appears to induce MIF, but further studies are necessary to confirm and quantify this anomaly.

6.4 Future Work

The ability to study the effects of systematic variations in the experimental conditions of this setup makes it especially useful. More efficient separation of $O_2(g)$ and O_3 would enhance the accuracy of measured O_3 isotopic compositions. Varying the surface composition to mimic other grain types known to exist in the solar nebula would shed light on the expected range of isotopic compositions of nebular O_3. Varying the wavelength of incoming photons would reveal how the isotopic composition of nebular O_3 might change throughout a star's life. The O_3 yield could be increased by using an electron gun to bombard O_2 with a higher flux of electrons than the photon flux used in the aforementioned experiments.

6.5 Conclusions

The non-mass-dependent anomalies in O_3 produced at 8 and 77K are reflected in the negative and positive $\Delta^{17}O$ values, respectively. These $\Delta^{17}O$ values indicate non-mass-dependently fractionated O_3 and UHPO reservoirs contributed to the oxygen sample analyzed.

6.6 Acknowledgements

Chapter 6 describes experiments designed and carried out by Morgan H. Nunn and Gerardo Dominguez. The work was funded by the NASA Cosmochemistry grant. The dissertation author was a co-investigator and is the author of this material.

Chapter 7. Oxygen Isotopic Effects of Ion-Molecule Reactions and Implications on Interstellar Molecular Cloud Chemistry

7.1 Abstract

Ion-molecule reactions dominate the production of new molecules in some regions of interstellar molecular clouds, which eventually collapse to form stars and associated planetary systems. A novel approach has been employed to better understand the isotopic effects of ion-molecule reactions where a mass spectrometer (MS) is used to both carry out the reactions and analyze product species. The oxygen isotopic compositions of O_2^+ produced in ion molecule reactions involving O_2 and varying amounts of Ar, He, or N_2 were measured. The results reveal ion molecule reactions between O_2 and Ar, O_2 and He, or O_2 and N_2 induce mass independent fractionation of oxygen isotopes to varying degrees, which could have contributed to the diversity in mass independent oxygen isotopic compositions observed in our solar system.

7.2 Introduction

Ion-molecule reactions in cold regions of both diffuse and dense interstellar molecular clouds dominate the production of new molecules in these regions, which will eventually collapse to form stars and their associated

planetary systems. Despite the significance of these reactions in understanding the formation and evolution of the solar system, there is a paucity of data on the isotopic fractionation factors associated with these ion molecule reactions because measurement with sufficiently high precision to yield elucidative results is difficult. In mass spectrometric analyses, the presence of rare gases in oxygen (O_2) gas samples shifts measured oxygen isotopic compositions to inaccurate values, and we hypothesize this shift is induced by ion-molecule reactions occurring in the ionization source of the mass spectrometer. We present here a rigorous examination of this effect where the amount of Ar, He, and N_2 in O_2 is varied to reveal ion molecule reactions occurring in the ionization source of an isotope ratio mass spectrometer (IRMS). Oxygen isotopic composition measurements are performed in situ using the mass analyzer and collectors of the MS. These results can be used not only to obtain more accurate oxygen isotopic compositions of gases measured using an IRMS but also to improve our understanding of the chemistry occurring in the ionization source of a MS and isotopic fractionation factors associated with ion-molecule reactions.

When the analyte identity is molecular oxygen, as in this study, electron ionization (EI) succeeds in ionizing O_2 molecules to form O_2^+, and it is the relative amounts of O_2^+ isotopologues ($^{16}O_2^+$, $^{17}O^{16}O^+$, and $^{18}O^{16}O^+$) that are determined during mass spectrometric analyses. MS analyses suggest this is not the case for O_2 samples containing an added, rare gas [182].

Oxygen isotopic compositions are measured in terms of the relative amounts of rarer isotopes (^{17}O and ^{18}O) to the most abundant isotope, ^{16}O, and are presented as $\delta^{17}O$ and $\delta^{18}O$. The mass dependence or independence of a process can elucidate changes in reaction rates and equilibrium concentrations as well as differential occupancy of energy states under varying conditions and is presented as $\Delta^{17}O$:

$$\Delta^{17}O = \delta^{17}O - (0.52 * \delta^{18}O)$$

[10], [11] In theory, perfectly mass dependent fractionation is represented by the relationship $\delta^{17}O = 0.5 * \delta^{18}O$, but a slope of 0.52 is used in defining the $\Delta^{17}O$ value because it more accurately reflects the equilibrium fractionation that controls the $\Delta^{17}O$ of terrestrial water reservoirs [183].

7.3 Methods

Sample gases were prepared by quantitatively mixing ultra-high purity oxygen (UHPO) gas having a known isotopic composition ($\delta^{17}O$ = 6.8‰, $\delta^{18}O$ = 13.4‰) with varying amounts (8-75% of total sample, by volume) of a rare gas (Rg), which is either Ar, He, or ultra-high purity nitrogen (N_2) gas. Nitrogen was chosen for this study because ion molecule reactions in the Earth's upper atmosphere between oxygen and nitrogen, the most abundant gaseous species in the Earth's atmosphere, have significant effects on the isotopic composition of atmospheric oxygen.

Gas mixtures were also prepared by introducing varying amounts of the noble gasses, Ar or He, to UHPO gas. Each gas mixture has a distinct O_2/N_2, O_2/Ar, and O_2/He ratio. The ion molecule reactions were carried out in the ionization chamber of a Thermo Finnigan MAT 253 dual inlet stable isotope ratio mass spectrometer and the oxygen isotopic composition of each gas mixture was measured in situ relative to an UHPO standard gas ($\delta^{17}O$ = 11‰, $\delta^{18}O$ = 22‰). Oxygen isotopic compositions are reported in terms of isotopic abundance ratios, $\delta^{17}O$ and $\delta^{18}O$, with respect to Standard Mean Ocean Water (SMOW). Each sample was analyzed over a range of sample inlet voltages (0.1-3V) and electron energies (80-95V).

The analytical utility of mass spectrometry (MS) depends upon the exploitation of differences in mass to charge ratios (m/z) of ionized analyte species. After a sample is introduced into the MS, it must first be ionized before being accelerated through an electromagnetic field, where separation based on m/z occurs, and collected by mass analyzers. A common form of ionization used in MS and the technique employed by the MAT 253 used in our analyses is electron ionization (EI) (Figure 7.1). In EI, electrons are generated from the surface of a filament (most often tungsten) by applying a current across it. A voltage difference is applied across the ionization chamber and ensures ionizing electrons move through the chamber in a trajectory perpendicular to the path of analyte atoms/molecules, maximizing the probability of collision and ionization.

The magnitude of the voltage difference is set as an operational parameter of the MS called the electron energy (eE) and can be varied between 70 and 124eV.

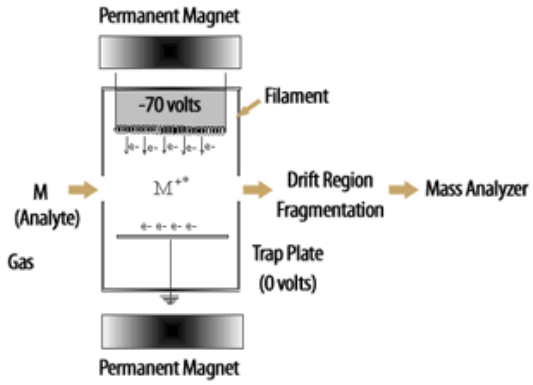

Figure 7.1 Schematic showing how analyte atoms and molecules (M) are ionized during electron impact (EI). In the MAT 253, electrons are generated by a heated tungsten filament and subsequently induce ionization via EI. (http://www.noble.org/plantbio/sumner/ionization-technique/)

7.4 Results and Discussion

Ion molecule reactions involving O_2 and Ar, He, or N_2 produce O_2 that is isotopically distinct from UHPO in the pressure/voltage range used for analysis (0.3-75.9mb/0.1-3.0V). The shift in the oxygen isotopic composition ($\delta^{18}O$ and $\Delta^{17}O$) of this product O_2 from UHPO is largest and smallest in the Ar and He samples, respectively, and increases with the amount of Rg (Fig. 7.2). The relative magnitude of the shift at different pressures/voltages for a given O_2 to Rg ratio is the same for all sample mixtures, except O_2 and 75% Ar.

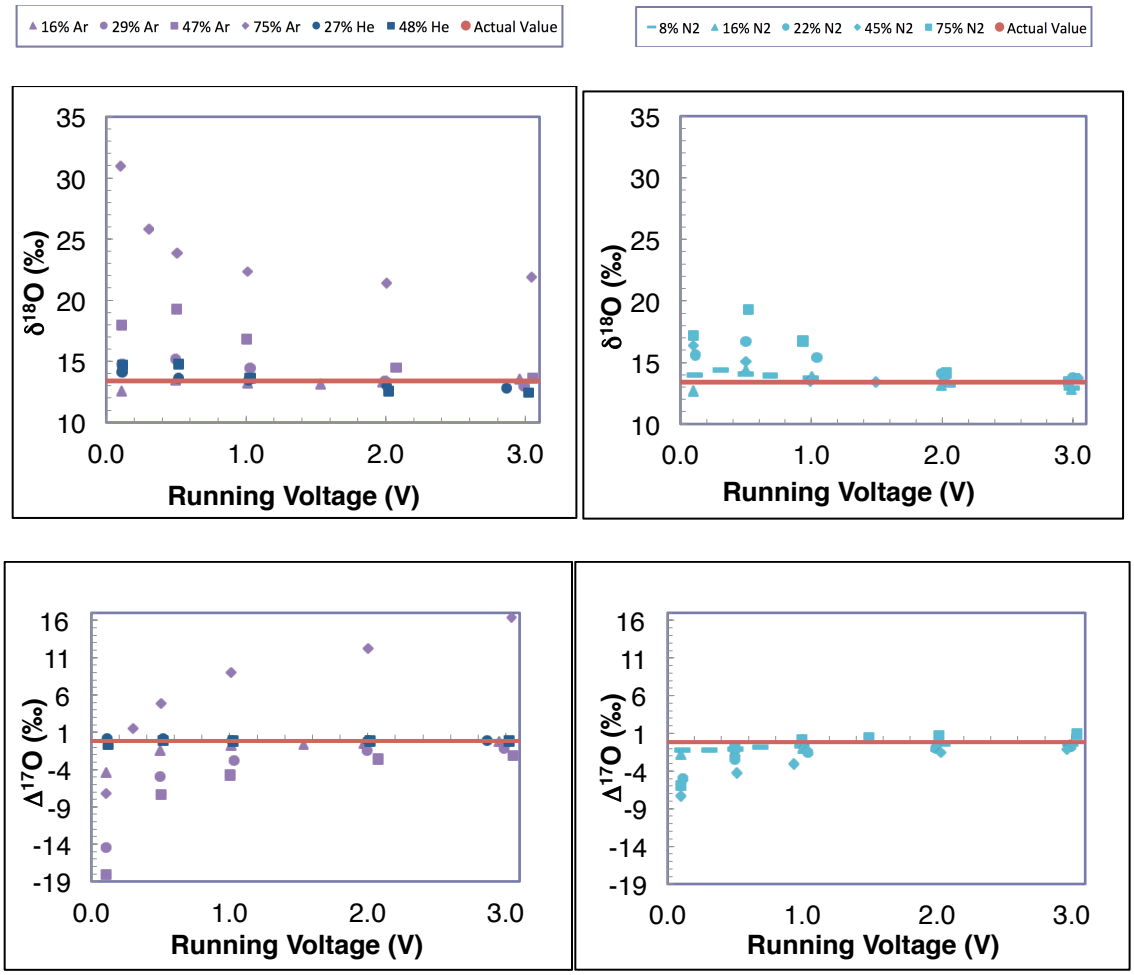

Figure 7.2 Oxygen isotopic composition ($\delta^{18}O$ and $\Delta^{17}O$, ‰) of oxygen produced in ion molecule reactions involving Ar, He, and N_2. Ultra High Purity Oxygen (UHPO) gas has $\delta^{18}O$ = 13.4‰ and $\Delta^{17}O$ = -0.168‰. Results reflect analyses conducted at voltages varying from 0.1 to 3V.

As shown in Figure 7.2, the magnitude of the deviation in $\delta^{18}O$ increases with increasing aberration in voltage from 2.5V and peaks at ~500mV for all UHPO and rare gas samples except 8% N_2, which shows maximum $\delta^{18}O$ deviation at ~300mV. Because 8% N_2 is the only mixture run at a voltage between 100 and 500mV, the real maximum deviation in $\delta^{18}O$ might actually occur in this range for the other gas mixtures and not at ~500mV, as our data

reflect. The minimum deviation in $\delta^{18}O$ for all samples was measured at a voltage of 3V. The magnitude of the deviation in the $\Delta^{17}O$ value from that of the pure UHPO gas increases with increasing aberration in voltage from 2.5V and asymptotically approaches a $\Delta^{17}O$ value < -20‰ at voltage approaching 0V for all UHPO and rare gas mixtures.

Increasing the amount of Ar, He, or N_2 in every UHPO and rare gas mixture at every voltage increases the shift in $\delta^{18}O$ from that of pure UHPO. The presence of Ar in an O_2 sample induces a larger shift in $\delta^{18}O$ than does N_2, which in turn induces a greater shift in $\delta^{18}O$ than He. The $\delta^{18}O$ value of most gas mixtures is greater than 0‰, and the few, negative $\delta^{18}O$ values are measured for the He mixtures and low %Ar or N_2, mostly at the highest and lowest voltages used. The $\delta^{18}O$ of the 16% and 22% N_2 samples is higher than that of the 16% and 29% Ar samples, respectively. The difference in the $\delta^{18}O$ of O_2 samples containing Ar or N_2 and the most similar %Rg mixture of the other gas at all voltages increases with increasing %Rg 16% to 29/22% but the $\delta^{18}O$ of the ~45% Ar and N_2 mixtures are approximately equal. The large effect seen in Ar and small effect seen in He suggests reactivity or valence electron occupancy of the Rg is unimportant or much less important, at least, than other factors in determining the oxygen isotopic effect of an ion-molecule reaction involving O_2 and the Rg.

Ion molecule reactions involving O_2 and Ar, He, or N_2 differentially affect the relative amounts of ^{17}O and ^{18}O, compared to ^{16}O, of product oxygen,

reflected in the varying $\Delta^{17}O$ value with pressure/voltage. The exponential decrease in the $\Delta^{17}O$ value toward -18‰ at pressure/voltage approaching zero reflects the increasingly disproportionate effect on the $\delta^{18}O$, compared to $\delta^{17}O$, value at low pressure/voltage. For every UHPO and rare gas mixture at every voltage, increasing the amount of Ar, He, or N_2 increases the shift in $\Delta^{17}O$ from that of pure UHPO. The presence of Ar induces a larger shift in $\Delta^{17}O$ than does N_2, which in turn induces a larger shift than He. The most negative $\Delta^{17}O$ values measured (down to $\Delta^{17}O$ = -18‰) were obtained for the O_2 sample containing 47% Ar. The $\Delta^{17}O$ of O_2 samples containing 29% Ar and 45% N_2 are very close at all voltages. The magnitude of the deviation in $\Delta^{17}O$ from 0‰ of the other UHPO and rare gas mixtures decreases in changing the identity of the rare gas from N_2 to He and with decreasing percent of each rare gas (N_2 or He).

The observed trends in non-mass-dependently fractionated oxygen produced in ion molecule reactions involving Ar and He are most consistently explained by varying contributions from several reactions that affect the relative amounts of product O_2^+ and transition state O_4^+ isotopomers in qualitatively known ways.

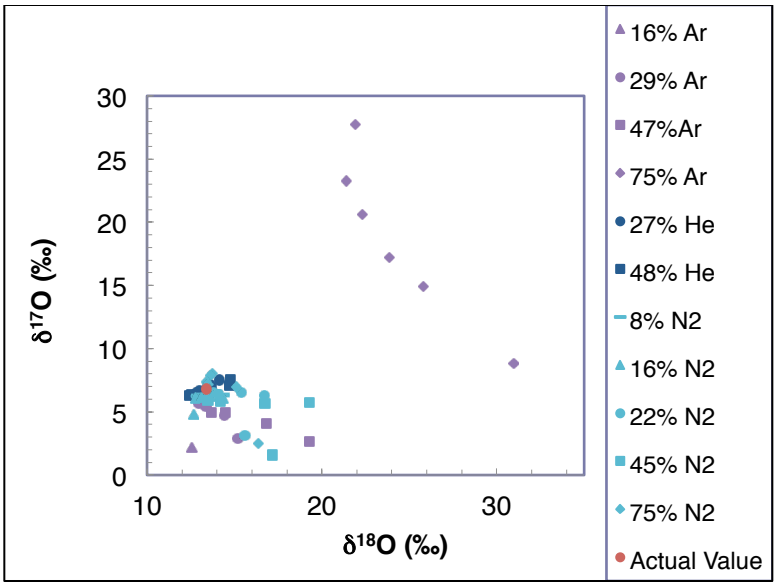

Figure 7.3 Oxygen isotopic composition ($\delta^{17}O$ versus $\delta^{18}O$, ‰) of oxygen produced in ion molecule reactions involving Ar, He, and N_2. Analyses were conducted with varying sample pressure from 0.3 to 75.0mb. The actual composition of Ultra High Purity Oxygen (UHPO) is $\delta^{17}O$ = 6.8‰ and $\delta^{18}O$ = 13.4‰, with respect to Standard Mean Ocean Water (SMOW).

For each mixture, decreasing the voltage used for analysis resulted in a decrease in $\delta^{17}O$ and increases in $\delta^{18}O$ and $|\Delta^{17}O|$. For each mixture, the data point with the lowest $\delta^{17}O$ corresponds to an analysis carried out at a voltage of 100mV. For the UHPO samples containing 29 and 47% Ar; 16, 22, and 45% N_2 sample gases (i.e., all sample gases except 27 and 48% He and 8% N_2), the measured oxygen isotopic composition ($\delta^{17}O$ and $\delta^{18}O$) of the sample run at 100mV is outside the trend set by the other data points.

Trend lines associated with the Ar gas mixture data points in $\delta^{17}O$ versus $\delta^{18}O$ space have a more negative slope than those associated with the N_2 data. The trend lines associated with the He gas mixtures are positive and reveal

nearly perfect mass-dependent fractionation during ionization and analysis in the mass spectrometer. None of these trend lines converges on the actual value of UHPO ($\delta^{17}O$ = 6.8‰ and $\delta^{18}O$ = 13.4‰), indicating multiple processes were involved in the formation of the measured O_2^+.

In the ionization source of the MS, newly formed O_2^+ ions encountering relatively abundant O_2 molecules can react to form O_4^+. A non-mass-dependent isotope effect has been shown to exist in the two-step, termolecular reaction that leads to the formation of O_4^+:

$$O_2 + e^- \rightarrow O_2^+ + 2e^-$$

$$O_2^+ + 2O_2 \rightarrow O_4^+ + O_2$$

[182]. The presence of a third body in the form of a rare gas affects the relative rates and isotopic effects of the O_4^+ formation reactions by isotopic exchange, clustering, quenching of the a^4P_u state of O_2^+ by the rare gas, and charge transfer from the rare gas to O_2. All of the rare gases studied by Griffith and Gellene (Ar, He, and Kr) had a different effect on the isotopic composition of O_4^+ ($O_4^+ = {}^{16}O_4^+$, ${}^{17}O{}^{16}O_3^+/{}^{16}O_4^+$, ${}^{18}O{}^{16}O_3^+/{}^{16}O_4^+$). This result is consistent with the identity and concentration of the rare gas being deterministic of the extent and direction of change of each of the aforementioned four processes.

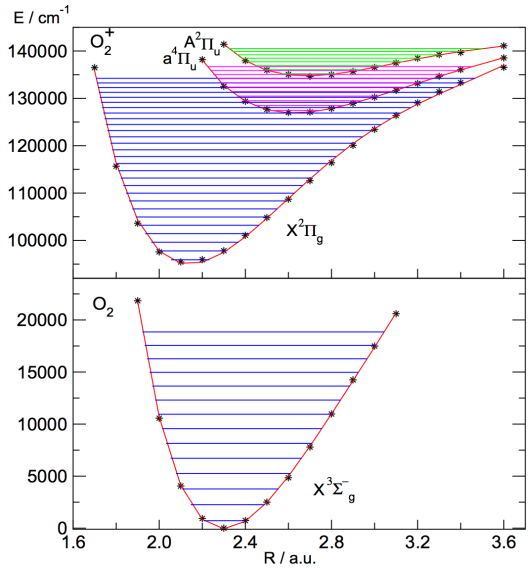

Figure 7.4 Potential energy (cm^{-1}) of ground and excited electronic states of O_2 and O_2^+ with respect to internuclear separation (a.u.).

The relative efficiency in collisionally quenching the O_2^+ (a^4P_u) state of Ar, compared to He, means the following reaction increases the ^{18}O-enrichment of O_4^+ more at higher Ar pressures:

$$O_2^+ (a^4P_u) + Rg \rightarrow O_2 (^3S_g^-) + Rg^+$$

[182]. Introducing He to an O_2 gas sample effectively lowers the partial pressure of O_2. This affects the oxygen isotopic composition of O_2 by shifting the equilibrium of the following reaction to the left:

$$^{66}O_4^+ + {}^{32}O_2 \rightarrow {}^{64}O_4^+ + {}^{34}O_2$$

[182].

In contrast to Ar and He, the introduction of N_2 to an O_2 sample enables the formation of metastable ionic species that act as a sink for oxygen atoms in the reaction chamber. This isotope selective sequestration of oxygen results in

markedly different measured oxygen isotopic compositions of O_2 in gas mixtures where Ar or N_2 are present in the same relative amount. This is shown most clearly by comparing the $\Delta^{17}O$ values and signals of NO^+ ion for O_2 samples containing 75% Ar or 75% N_2 analyzed at a range of O_2^+ voltages (Fig. 7.4). The drastically different isotopic compositions measured for the 75% Ar and 75% N_2 mixtures suggest chemical processes are more deterministic of the final oxygen isotopic composition than the isotopic exchange, clustering, quenching, and charge transfer processes.

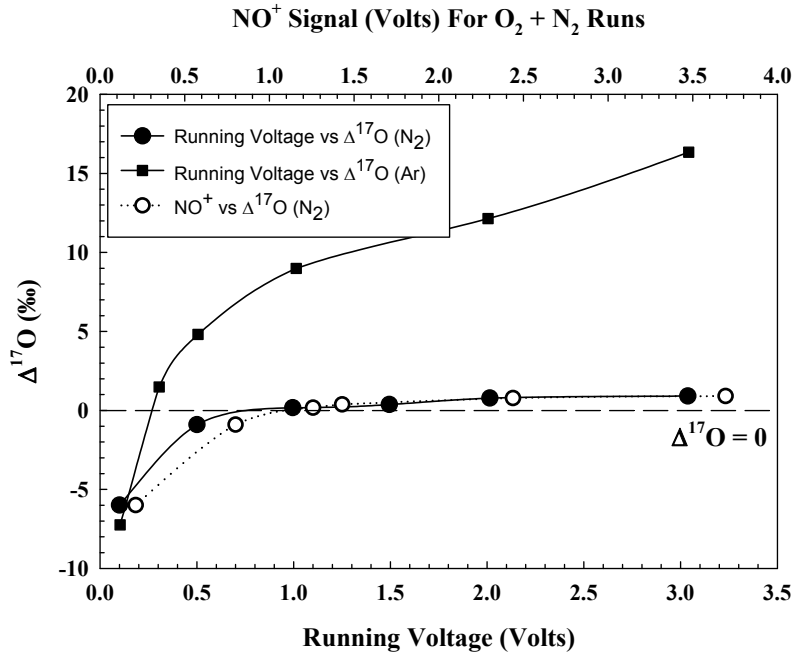

Figure 7.5 Oxygen isotopic composition ($\Delta^{17}O$, ‰) of oxygen gas mixtures containing 75% Ar and 75% N_2 versus running voltage and $\Delta^{17}O$ (‰) versus NO^+ signal for the 75% N_2 gas mixture. Analyses were carried out at varying running voltage from 0.1 to 3.0V.

7.5 Future Work

Determination of the nitrogen isotopic composition ($\delta^{15}N$) of ultra high purity nitrogen gas ($UHPN_2$) in the presence of varying amounts of UHPO gas would elucidate the nitrogen isotopic effect of ion molecule reactions involving these species. This study could also provide valuable insight on the mechanism of this ion-molecule reaction and the isotopic selection steps of the mechanism.

7.6 Conclusions

Ion-molecule reactions involving O_2 and either He, N_2, or Ar, in order of increasing ability, can induce highly anomalous oxygen isotopic fractionation. The results of the studies of these reactions are consistent with the Rg affecting, to varying degrees depending on its concentration and identity, the rate and isotopic effect of formation of the O_4^+ species. These results could aid in the prediction and interpretation of oxygen isotopic compositions in interstellar molecular clouds and components of the planetary systems they produce.

7.7 Acknowledgements

Chapter 7, in part, is currently being prepared for submission for publication of the material. Morgan H. Nunn, Subrata Chakraborty, Mark H.

Thiemens. The dissertation author conducted the experiments described and is the primary author of this material.

References

[1] M. Berglund and M. E. Wieser, “Isotopic compositions of the elements 2009 (IUPAC Technical Report),” *Pure Appl. Chem.*, vol. 83, no. 2, Jan. 2011.

[2] B. S. Meyer, L. R. Nittler, A. N. Nguyen, and S. Messenger, “Nucleosynthesis and Chemical Evolution of Oxygen,” *Rev. Mineral. Geochem.*, vol. 68, no. 1, pp. 31–53, Jan. 2008.

[3] B. M. Tinsley, “Evolution of the stars and gas in galaxies,” *Fundam. Cosm. Phys.*, vol. 5, pp. 287–388, 1980.

[4] C. Patterson, G. Tilton, and M. Inghram, “Age of the Earth,” *Science*, vol. 121, no. 3134, pp. 69–75, Jan. 1955.

[5] G. Oddo, “Die Molekularstruktur der radioaktiven Atome,” *Z. Fr Anorg. Chem.*, vol. 87, no. 1, pp. 253–268, May 1914.

[6] W. D. Harkins, “THE EVOLUTION OF THE ELEMENTS AND THE STABILITY OF COMPLEX ATOMS. I. A NEW PERIODIC SYSTEM WHICH SHOWS A RELATION BETWEEN THE ABUNDANCE OF THE ELEMENTS AND THE STRUCTURE OF THE NUCLEI OF ATOMS.,” *J. Am. Chem. Soc.*, vol. 39, no. 5, pp. 856–879, May 1917.

[7] R. N. Clayton, “Oxygen isotopes in meteorites,” *Annu. Rev. Earth Planet. Sci.*, vol. 21, pp. 115–149, 1993.

[8] H. Yurimoto, K. Kuramoto, A. N. Krot, E. R. Scott, J. N. Cuzzi, M. H. Thiemens, and J. R. Lyons, “Origin and evolution of oxygen isotopic compositions of the solar system,” *Protostars Planets V*, vol. 1, pp. 849–862, 2007.

[9] R. N. Clayton, L. Grossman, and T. K. Mayeda, “A component of primitive nuclear composition in carbonaceous meteorites,” *Science*, vol. 182, no. 4111, pp. 485–488, 1973.

[10] R. Clayton, R. Hinton, and A. Davis, “Isotopic variations in the rock-forming elements in meteorites,” *Philos. Trans. R. Soc. Lond. Math. Phys. Eng. Sci.*, vol. 325, no. 1587, pp. 483–501, 1988.

[11] Y. Matsuhisa, J. R. Goldsmith, and R. N. Clayton, “Mechanisms of hydrothermal crystallization of quartz at 250 C and 15 kbar,” *Geochim. Cosmochim. Acta*, vol. 42, no. 2, pp. 173–182, 1978.

[12] H. C. Urey, “The thermodynamic properties of isotopic substances,” *J. Chem. Soc. Resumed*, pp. 562–581, 1947.

[13] J. Bigeleisen and M. G. Mayer, “Calculation of Equilibrium Constants for Isotopic Exchange Reactions,” *J. Chem. Phys.*, vol. 15, no. 5, p. 261, 1947.

[14] E. D. Young, A. Galy, and H. Nagahara, “Kinetic and equilibrium mass-dependent isotope fractionation laws in nature and their geochemical and cosmochemical significance,” *Geochim. Cosmochim. Acta*, vol. 66, no. 6, pp. 1095–1104, 2002.

[15] M. H. Thiemens, “HISTORY AND APPLICATIONS OF MASS-INDEPENDENT ISOTOPE EFFECTS,” *Annu. Rev. Earth Planet. Sci.*, vol. 34, no. 1, pp. 217–262, May 2006.

[16] J. Hulston and H. Thode, “Variations in the S33, S34, and S36 contents of meteorites and their relation to chemical and nuclear effects,” *J. Geophys. Res.*, vol. 70, no. 14, pp. 3475–3484, 1965.

[17] M. H. Thiemens and J. E. Heidenreich, “The mass-independent fractionation of oxygen: A novel isotope effect and its possible cosmochemical implications,” *Science*, vol. 219, no. 4588, pp. 1073–1075, 1983.

[18] S. Chakraborty, B. Muskatel, T. L. Jackson, M. Ahmed, R. Levine, and M. H. Thiemens, “Massive isotopic effect in vacuum UV photodissociation of N2 and implications for meteorite data,” *Proc. Natl. Acad. Sci.*, vol. 111, no. 41, pp. 14704–14709, 2014.

[19] J. Morton, J. Barnes, B. Schueler, and K. Mauersberger, “Laboratory studies of heavy ozone,” *J. Geophys. Res. Atmospheres 1984–2012*, vol. 95, no. D1, pp. 901–907, 1990.

[20] R. A. Marcus, “Mass-independent isotope effect in the earliest processed solids in the solar system: A possible chemical mechanism,” *J. Chem. Phys.*, vol. 121, no. 17, p. 8201, 2004.

[21] B. Hathorn and R. Marcus, “An intramolecular theory of the mass-independent isotope effect for ozone. I,” *J. Chem. Phys.*, vol. 111, no. 9, pp. 4087–4100, 1999.

[22] D. Babikov, B. K. Kendrick, R. B. Walker, R. Schinke, and R. . Pack, “Quantum origin of an anomalous isotope effect in ozone formation,” *Chem. Phys. Lett.*, vol. 372, no. 5–6, pp. 686–691, May 2003.

[23] C. Janssen, J. Guenther, K. Mauersberger, and D. Krankowsky, “Kinetic origin of the ozone isotope effect: a critical analysis of enrichments and rate coefficients,” *Phys. Chem. Chem. Phys.*, vol. 3, no. 21, pp. 4718–4721, 2001.

[24] J. Aleon, A. N. Krot, K. D. McKeegan, G. J. MacPherson, and A. A. Ulyanov, “Fine-grained, spinel-rich inclusions from the reduced CV chondrite Efremovka: II. Oxygen isotopic compositions,” *Meteorit. Planet. Sci.*, vol. 40, no. 7, pp. 1043–1058, 2005.

[25] A. N. Krot, K. D. McKeegan, L. A. Leshin, G. J. MacPherson, and E. R. Scott, “Existence of an 16O-rich gaseous reservoir in the solar nebula,” *Science*, vol. 295, no. 5557, pp. 1051–1054, 2002.

[26] E. R. Scott and A. N. Krot, “Oxygen isotopic compositions and origins of calcium-aluminum-rich inclusions and chondrules,” *Meteorit. Planet. Sci.*, vol. 36, pp. 1307–1319, 2001.

[27] B.-G. Choi, K. D. McKeegan, A. N. Krot, and J. T. Wasson, “Extreme oxygen-isotope compositions in magnetite from unequilibrated ordinary chondrites,” *Nature*, vol. 392, no. 6676, pp. 577–579, 1998.

[28] A. N. Krot, G. Libourel, and M. Chaussidon, “Oxygen isotope compositions of chondrules in CR chondrites,” *Geochim. Cosmochim. Acta*, vol. 70, no. 3, pp. 767–779, 2006.

[29] S. Maruyama, H. Yurimoto, and S. Sueno, “Oxygen isotope evidence regarding the formation of spinel-bearing chondrules,” *Earth Planet. Sci. Lett.*, vol. 169, no. 1, pp. 165–171, 1999.

[30] Y. Yu, R. H. Hewins, R. N. Clayton, and T. K. Mayeda, “Experimental study of high temperature oxygen isotope exchange during chondrule formation,” *Geochim. Cosmochim. Acta*, vol. 59, no. 10, pp. 2095–2104, 1995.

[31] S. Weidenschilling, “MNRAS, 180, 57 Weidenschilling, SJ, 1980,” *Icarus*, vol. 44, p. 172, 1977.

[32] J. Cuzzi, F. Ciesla, M. Petaev, A. Krot, E. Scott, and S. Weidenschilling, “Nebula evolution of thermally processed solids: Reconciling models and meteorites,” in *Chondrites and the Protoplanetary Disk*, 2005, vol. 341, p. 732.

[33] J. N. Cuzzi, S. S. Davis, and A. R. Dobrovolskis, “Blowing in the wind. II. Creation and redistribution of refractory inclusions in a turbulent protoplanetary nebula,” *Icarus*, vol. 166, no. 2, pp. 385–402, 2003.

[34] J. N. Cuzzi and K. J. Zahnle, “Material enhancement in protoplanetary nebulae by particle drift through evaporation fronts,” *Astrophys. J.*, vol. 614, no. 1, p. 490, 2004.

[35] H. Yurimoto and K. Kuramoto, “Molecular cloud origin for the oxygen isotope heterogeneity in the solar system,” *Science*, vol. 305, no. 5691, pp. 1763–1766, 2004.

[36] M. F. Miller, I. A. Franchi, A. S. Sexton, and C. T. Pillinger, “High precision δ17O isotope measurements of oxygen from silicates and other oxides: method and applications,” *Rapid Commun. Mass Spectrom.*, vol. 13, no. 13, pp. 1211–1217, Jul. 1999.

[37] S. Chakraborty, P. Yanchulova, and M. H. Thiemens, “Mass-Independent Oxygen Isotopic Partitioning During Gas-Phase SiO2 Formation,” *Science*, vol. 342, no. 6157, pp. 463–466, Oct. 2013.

[38] T. E. Cerling, “The stable isotopic composition of modern soil carbonate and its relationship to climate,” *Earth Planet. Sci. Lett.*, vol. 71, no. 2, pp. 229–240, Dec. 1984.

[39] R. N. Clayton and T. K. Mayeda, “The oxygen isotope record in Murchison and other carbonaceous chondrites,” *Earth Planet. Sci. Lett.*, vol. 67, no. 2, pp. 151–161, 1984.

[40] J. Farquhar and M. H. Thiemens, “Oxygen cycle of the Martian atmosphere-regolith system: Δ17O of secondary phases in Nakhla and Lafayette,” *J. Geophys. Res. Planets 1991–2012*, vol. 105, no. E5, pp. 11991–11997, 2000.

[41] M. Thiemens and R. Shaheen, “Mass independent isotopic composition of terrestrial and extraterrestrial materials,” *Treatise Geochem. Atmosphere*, 2013.

[42] K. McKeegan, A. Kallio, V. Heber, G. Jarzebinski, P. Mao, C. Coath, T. Kunihiro, R. Wiens, J. Nordholt, R. Moses, and others, “The oxygen isotopic composition of the Sun inferred from captured solar wind,” *Science*, vol. 332, no. 6037, pp. 1528–1532, 2011.

[43] L. V. Starukhina and Y. G. Shkuratov, “The lunar poles: water ice or chemically trapped hydrogen?,” *Icarus*, vol. 147, no. 2, pp. 585–587, 2000.

[44] R. N. Clark, “Detection of adsorbed water and hydroxyl on the Moon,” *Science*, vol. 326, no. 5952, pp. 562–564, 2009.

[45] C. M. Pieters, J. N. Goswami, R. N. Clark, M. Annadurai, J. Boardman, B. Buratti, J.-P. Combe, M. D. Dyar, R. Green, J. W. Head, C. Hibbitts, M. Hicks, P. Isaacson, R. Klima, G. Kramer, S. Kumar, E. Livo, S. Lundeen, E. Malaret, T. McCord, J. Mustard, J. Nettles, N. Petro, C. Runyon, M. Staid, J. Sunshine, L. A. Taylor, S. Tompkins, and P. Varanasi, "Character and Spatial Distribution of OH/H2O on the Surface of the Moon Seen by M3 on Chandrayaan-1," *Science*, vol. 326, no. 5952, pp. 568–572, Oct. 2009.

[46] J. M. Sunshine, T. L. Farnham, L. M. Feaga, O. Groussin, F. Merlin, R. E. Milliken, and M. F. A'Hearn, "Temporal and Spatial Variability of Lunar Hydration As Observed by the Deep Impact Spacecraft," *Science*, vol. 326, no. 5952, pp. 565–568, Oct. 2009.

[47] W. Boynton, G. Taylor, L. Evans, R. Reedy, R. Starr, D. Janes, K. Kerry, D. Drake, K. Kim, R. Williams, and others, "Concentration of H, Si, Cl, K, Fe, and Th in the low-and mid-latitude regions of Mars," *J. Geophys. Res. Planets 1991–2012*, vol. 112, no. E12, 2007.

[48] R. Gellert, R. Rieder, J. Brückner, B. Clark, G. Dreibus, G. Klingelhöfer, G. Lugmair, D. Ming, H. Wänke, A. Yen, and others, "Alpha particle X-ray spectrometer (APXS): Results from Gusev crater and calibration report," *J. Geophys. Res. Planets 1991–2012*, vol. 111, no. E2, 2006.

[49] D. W. Ming, R. Gellert, R. V. Morris, R. E. Arvidson, J. Brueckner, B. C. Clark, B. A. Cohen, C. d'Uston, T. Economou, I. Fleischer, and others, "Geochemical properties of rocks and soils in Gusev crater, Mars: Results of the Alpha Particle X-ray Spectrometer from Cumberland Ridge to Home Plate," *J. Geophys. Res. Planets 1991–2012*, vol. 113, no. E12, 2008.

[50] A. Nier and M. B. McElroy, "Composition and structure of Mars' upper atmosphere: Results from the neutral mass spectrometers on Viking 1 and 2," *J. Geophys. Res.*, vol. 82, no. 28, pp. 4341–4349, 1977.

[51] R. N. Clayton and T. K. Mayeda, "Oxygen isotopes in eucrites, shergottites, nakhlites, and chassignites," *Earth Planet. Sci. Lett.*, vol. 62, no. 1, pp. 1–6, 1983.

[52] C. B. Agee, N. V. Wilson, F. M. McCubbin, K. Ziegler, V. J. Polyak, Z. D. Sharp, Y. Asmerom, M. H. Nunn, R. Shaheen, M. H. Thiemens, A. Steele, M. L. Fogel, R. Bowden, M. Glamoclija, Z. Zhang, and S. M. Elardo, "Unique Meteorite from Early Amazonian Mars: Water-Rich Basaltic Breccia Northwest Africa 7034," *Science*, vol. 339, no. 6121, pp. 780–785, Feb. 2013.

[53] I. Franchi, I. Wright, A. Sexton, and C. Pillinger, “The oxygen-isotopic composition of Earth and Mars,” *Meteorit. Planet. Sci.*, vol. 34, no. 4, pp. 657–661, 1999.

[54] R. N. Clayton and T. K. Mayeda, “Oxygen isotope studies of achondrites,” *Geochim. Cosmochim. Acta*, vol. 60, no. 11, pp. 1999–2017, 1996.

[55] H. R. Karlsson, R. N. Clayton, E. Gibson, and T. K. Mayeda, “Water in SNC meteorites: Evidence for a martian hydrosphere,” *Science*, vol. 255, no. 5050, pp. 1409–1411, 1992.

[56] R. N. Clayton, T. K. Mayeda, J. Goswami, and E. J. Olsen, “Oxygen isotope studies of ordinary chondrites,” *Geochim. Cosmochim. Acta*, vol. 55, no. 8, pp. 2317–2337, 1991.

[57] T. B. McCord, J. B. Adams, and T. V. Johnson, “Asteroid Vesta: Spectral reflectivity and compositional implications,” *Science*, vol. 168, no. 3938, pp. 1445–1447, 1970.

[58] G. J. Consolmagno and M. J. Drake, “Composition and evolution of the eucrite parent body: Evidence from rare earth elements,” *Geochim. Cosmochim. Acta*, vol. 41, no. 9, pp. 1271–1282, 1977.

[59] H. Takeda, “Mineralogical records of early planetary processes on the howardite, eucrite, diogenite parent body with reference to Vesta,” *Meteorit. Planet. Sci.*, vol. 32, no. 6, pp. 841–853, Nov. 1997.

[60] R. Hewins and H. Newsom, “Igneous activity in the early solar system,” *Meteor. Early Sol. Syst.*, vol. 1, pp. 73–101, 1988.

[61] E. R. Scott, R. C. Greenwood, I. A. Franchi, and I. S. Sanders, “Oxygen isotopic constraints on the origin and parent bodies of eucrites, diogenites, and howardites,” *Geochim. Cosmochim. Acta*, vol. 73, no. 19, pp. 5835–5853, 2009.

[62] L. I. Cleeves, E. A. Bergin, C. M. Alexander, F. Du, D. Graninger, K. I. Öberg, and T. J. Harries, “The ancient heritage of water ice in the solar system,” *Science*, vol. 345, no. 6204, pp. 1590–1593, 2014.

[63] N. Sakamoto, Y. Seto, S. Itoh, K. Kuramoto, K. Fujino, K. Nagashima, A. N. Krot, and H. Yurimoto, “Remnants of the Early Solar System Water Enriched in Heavy Oxygen Isotopes,” *Science*, vol. 317, no. 5835, pp. 231–233, Jul. 2007.

[64] G. Dominguez, “A HETEROGENEOUS CHEMICAL ORIGIN FOR THE ^{16} O-ENRICHED AND ^{16} O-DEPLETED RESERVOIRS OF THE EARLY SOLAR SYSTEM,” *Astrophys. J.*, vol. 713, no. 1, pp. L59–L63, Apr. 2010.

[65] E. A. Bergin and M. Tafalla, “Cold Dark Clouds: The Initial Conditions for Star Formation,” *Annu. Rev. Astron. Astrophys.*, vol. 45, no. 1, pp. 339–396, Sep. 2007.

[66] H. Cuppen and E. Herbst, “Simulation of the formation and morphology of ice mantles on interstellar grains,” *Astrophys. J.*, vol. 668, no. 1, p. 294, 2007.

[67] T. I. Hasegawa, E. Herbst, and C. M. Leung, “Models of gas-grain chemistry in dense interstellar clouds with complex organic molecules,” *Astrophys. J. Suppl. Ser.*, vol. 82, pp. 167–195, 1992.

[68] A. Tielens and W. Hagen, “Model calculations of the molecular composition of interstellar grain mantles,” *Astron. Astrophys.*, vol. 114, pp. 245–260, 1982.

[69] S. M. Anderson, D. Hülsebusch, and K. Mauersberger, “Surprising rate coefficients for four isotopic variants of O+O[sub 2]+M,” *J. Chem. Phys.*, vol. 107, no. 14, p. 5385, 1997.

[70] J. Guenther, D. Krankowsky, and K. Mauersberger, “Third-body dependence of rate coefficients for ozone formation in 16O–18O mixtures,” *Chem. Phys. Lett.*, vol. 324, no. 1, pp. 31–36, 2000.

[71] J. Sehested, O. J. Nielsen, H. Egsgaard, N. W. Larsen, T. S. Andersen, and T. Pedersen, “Kinetic study of the formation of isotopically substituted ozone in argon,” *J. Geophys. Res. Atmospheres 1984–2012*, vol. 103, no. D3, pp. 3545–3552, 1998.

[72] P. J. Flory, “Predissociation of the Oxygen Molecule,” *J. Chem. Phys.*, vol. 4, no. 1, p. 23, 1936.

[73] J. Savarino and M. H. Thiemens, “Mass-Independent Oxygen Isotope (16O, 17O, 18O) Fractionation Found in H x, O x Reactions,” *J. Phys. Chem. A*, vol. 103, no. 46, pp. 9221–9229, 1999.

[74] R. M. Canup and E. Asphaug, “Origin of the Moon in a giant impact near the end of the Earth’s formation,” *Nature*, vol. 412, no. 6848, pp. 708–712, Aug. 2001.

[75] A. G. W. Cameron and W. Benz, “The origin of the moon and the single impact hypothesis IV,” *Icarus*, vol. 92, no. 2, pp. 204–216, Aug. 1991.

[76] R. C. Ogliore, K. Nagashima, G. R. Huss, A. J. Westphal, Z. Gainsforth, and A. L. Butterworth, “Oxygen isotopic composition of coarse- and fine-grained material from comet 81P/Wild 2,” *Geochim. Cosmochim. Acta*, vol. 166, pp. 74–91, Oct. 2015.

[77] E. D. Young, “Oxygen Reservoirs in the Early Solar Nebula Inferred from an Allende CAI,” *Science*, vol. 282, no. 5388, pp. 452–455, Oct. 1998.

[78] R. N. Clayton, N. Onuma, L. Grossman, and T. K. Mayeda, “Distribution of the pre-solar component in Allende and other carbonaceous chondrites,” *Earth Planet. Sci. Lett.*, vol. 34, no. 2, pp. 209–224, 1977.

[79] M. Fries and J. Fries, “Doppler weather radar as a meteorite recovery tool: Doppler weather radar as a meteorite recovery tool,” *Meteorit. Planet. Sci.*, vol. 45, no. 9, pp. 1476–1487, Sep. 2010.

[80] E. A. Silber, A. Le Pichon, and P. G. Brown, “Infrasonic detection of a near-Earth object impact over Indonesia on 8 October 2009: THE INDONESIAN BOLIDE,” *Geophys. Res. Lett.*, vol. 38, no. 12, p. n/a–n/a, Jun. 2011.

[81] M. H. Shaddad, P. Jenniskens, D. Numan, A. M. Kudoda, S. Elsir, I. F. Riyad, A. E. Ali, M. Alameen, N. M. Alameen, O. Eid, A. T. Osman, M. I. AbuBAKER, M. Yousif, S. R. Chesley, P. W. Chodas, J. Albers, W. N. Edwards, P. G. Brown, J. Kuiper, and J. M. Friedrich, “The recovery of asteroid 2008 TC3: The recovery of asteroid 2008 TC3,” *Meteorit. Planet. Sci.*, vol. 45, no. 10–11, pp. 1557–1589, Oct. 2010.

[82] K. D. Smith, “Evidence for Deep Magma Injection Beneath Lake Tahoe, Nevada-California,” *Science*, vol. 305, no. 5688, pp. 1277–1280, Aug. 2004.

[83] H. Haack, T. Grau, A. Bischoff, M. Horstmann, J. Wasson, A. SøRensen, M. Laubenstein, U. Ott, H. Palme, M. Gellissen, R. C. Greenwood, V. K. Pearson, I. A. Franchi, Z. Gabelica, and P. Schmitt-Kopplin, “Maribo-A new CM fall from Denmark: Maribo-A new CM fall from Denmark,” *Meteorit. Planet. Sci.*, vol. 47, no. 1, pp. 30–50, Jan. 2012.

[84] H. Haack, R. Michelsen, G. Stober, D. Keuer, W. Singer, and I. Williams, “CM Chondrites from Comets?—New Constraints from the Orbit of the Maribo CM Chondrite Fall,” *LPI Contrib.*, vol. 1639, p. 9100, 2011.

[85] K. Nishiizumi and M. Caffee, “Exposure Histories of Cm2 Carbonaceous Chondrites-an Update,” 2009.

[86] V. S. Heber, R. Wieler, H. Baur, C. Olinger, T. A. Friedmann, and D. S. Burnett, “Noble gas composition of the solar wind as collected by the Genesis mission,” *Geochim. Cosmochim. Acta*, vol. 73, no. 24, pp. 7414–7432, Dec. 2009.

[87] I. Leya, H.-J. Lange, S. Neumann, R. Wieler, and R. Michel, “The production of cosmogenic nuclides in stony meteoroids by galactic cosmic-ray particles,” *Meteorit. Planet. Sci.*, vol. 35, no. 2, pp. 259–286, Mar. 2000.

[88] M. Gounelle, A. Morbidelli, P. A. Bland, P. Spurny, E. D. Young, and M. Sephton, “Meteorites from the outer solar system,” *Sol. Syst. Neptune*, vol. 1, pp. 525–541, 2008.

[89] D. Nesvornỳ, P. Jenniskens, H. F. Levison, W. F. Bottke, D. Vokrouhlickỳ, and M. Gounelle, “Cometary origin of the zodiacal cloud and carbonaceous micrometeorites. Implications for hot debris disks,” *Astrophys. J.*, vol. 713, no. 2, p. 816, 2010.

[90] K. J. Walsh, M. Delbo, and W. Bottke, “New Findings on Primitive Asteroid Families in the Inner Asteroid Belt: An Important Source of Primitive NEOs,” in *AAS/Division for Planetary Sciences Meeting Abstracts*, 2012, vol. 44.

[91] A. Tsuchiyama, E. Mashio, Y. Imai, T. Noguchi, Y. Miura, H. Yano, and T. Nakamura, “Strength measurement of carbonaceous chondrites and micrometeorites using micro compression testing machine,” *Meteorit. Planet. Sci. Suppl.*, vol. 72, p. 5189, 2009.

[92] O. Popova, J. BorovičKa, W. K. Hartmann, P. Spurný, E. Gnos, I. Nemtchinov, and J. M. Trigo-RodríGuez, “Very low strengths of interplanetary meteoroids and small asteroids: Very low strengths of interplanetary meteoroids and small asteroids,” *Meteorit. Planet. Sci.*, vol. 46, no. 10, pp. 1525–1550, Oct. 2011.

[93] D. S. Ebel and M. L. Rivers, “Meteorite 3-D synchrotron microtomography: Methods and applications,” *Meteorit. Planet. Sci.*, vol. 42, no. 9, pp. 1627–1646, Sep. 2007.

[94] R. J. Macke, D. T. Britt, and G. J. Consolmagno, “Density, porosity, and magnetic susceptibility of achondritic meteorites: Achondrite density, porosity, and magnetic susceptibility,” *Meteorit. Planet. Sci.*, vol. 46, no. 2, pp. 311–326, Feb. 2011.

[95] M. S. Spergel, R. C. Reedy, O. W. Lazareth, P. W. Levy, and L. A. Slatest, “Cosmogenic neutron-capture-produced nuclides in stony meteorites,” *J. Geophys. Res.*, vol. 91, no. B4, p. 483, 1986.

[96] P. Rochette, J. Gattacceca, L. Bonal, M. Bourot-Denise, V. Chevrier, J.-P. Clerc, G. Consolmagno, L. Folco, M. Gounelle, T. Kohout, L. Pesonen, E. Quirico, L. Sagnotti, and A. Skripnik, “Magnetic classification of stony meteorites: 2. Non-ordinary chondrites,” *Meteorit. Planet. Sci.*, vol. 43, no. 5, pp. 959–980, May 2008.

[97] J. Gattacceca and P. Rochette, “Toward a robust normalized magnetic paleointensity method applied to meteorites,” *Earth Planet. Sci. Lett.*, vol. 227, no. 3–4, pp. 377–393, Nov. 2004.

[98] A. Bischoff, E. Scott, K. Metzler, and C. Goodrich, “Meteorites and the Early Solar System II, ed,” *Lauretta HY McSween Jr*, pp. 679–712, 2006.

[99] R. . Walker, M. . Horan, J. . Morgan, H. Becker, J. . Grossman, and A. . Rubin, “Comparative 187Re-187Os systematics of chondrites,” *Geochim. Cosmochim. Acta*, vol. 66, no. 23, pp. 4187–4201, Dec. 2002.

[100] Q.-Z. Yin, K. Yamashita, A. Yamakawa, R. Tanaka, B. Jacobsen, D. Ebel, I. Hutcheon, and E. Nakamura, “53Mn-53Cr Systematics of Allende Chondrules and epsilon 54Cr–Cap Delta17O Correlation in Bulk Carbonaceous Chondrites,” in *Lunar and Planetary Science Conference*, 2009, vol. 40, p. 2006.

[101] K. Lodders, “Solar System Abundances and Condensation Temperatures of the Elements,” *Astrophys. J.*, vol. 591, no. 2, pp. 1220–1247, Jul. 2003.

[102] E. Jarosewich, R. S. Clarke, and J. N. Barrows, “The Allende meteorite reference sample,” *Smithson. Contrib. Earth Sci.*, vol. 27, p. 49, 1987.

[103] P. G. Brown, “The Fall, Recovery, Orbit, and Composition of the Tagish Lake Meteorite: A New Type of Carbonaceous Chondrite,” *Science*, vol. 290, no. 5490, pp. 320–325, Oct. 2000.

[104] R. N. Clayton and T. K. Mayeda, “Oxygen isotope studies of carbonaceous chondrites,” *Geochim. Cosmochim. Acta*, vol. 63, no. 13–14, pp. 2089–2104, Jul. 1999.

[105] G. J. MacPherson, D. W. Mittlefehldt, M. E. Lipschutz, R. N. Clayton, E. S. Bullock, A. V. Ivanov, T. K. Mayeda, and M.-S. Wang, “The Kaidun chondrite breccia: Petrology, oxygen isotopes, and trace element

abundances," *Geochim. Cosmochim. Acta*, vol. 73, no. 18, pp. 5493–5511, Sep. 2009.

[106] J. M. Friedrich, M.-S. Wang, and M. E. Lipschutz, "Comparison of the trace element composition of Tagish Lake with other primitive carbonaceous chondrites," *Meteorit. Planet. Sci.*, vol. 37, no. 5, pp. 677–686, May 2002.

[107] E. Tonui, M. Zolensky, and M. Lipschutz, "Petrography, mineralogy and trace element chemistry of Yamato-86029 Yamato-793321 and Lewis Cliff 85332: Aqueous alteration and heating events," *Antarct. Meteor. Res.*, vol. 15, p. 38, 2002.

[108] M. Haq, F. A. Hasan, D. W. G. Sears, C. B. Moore, and C. F. Lewis, "Thermoluminescence and the origin of the dark matrix of Fayetteville and similar meteorites," *Geochim. Cosmochim. Acta*, vol. 53, no. 6, pp. 1435–1440, Jun. 1989.

[109] G. D. Cody, C. M. O. Alexander, H. Yabuta, A. L. D. Kilcoyne, T. Araki, H. Ade, P. Dera, M. Fogel, B. Militzer, and B. O. Mysen, "Organic thermometry for chondritic parent bodies," *Earth Planet. Sci. Lett.*, vol. 272, no. 1–2, pp. 446–455, Jul. 2008.

[110] E. D. Young, "Fluid Flow in Chondritic Parent Bodies: Deciphering the Compositions of Planetesimals," *Science*, vol. 286, no. 5443, pp. 1331–1335, Nov. 1999.

[111] G. . Benedix, L. . Leshin, J. Farquhar, T. Jackson, and M. . Thiemens, "Carbonates in CM2 chondrites: constraints on alteration conditions from oxygen isotopic compositions and petrographic observations," *Geochim. Cosmochim. Acta*, vol. 67, no. 8, pp. 1577–1588, Apr. 2003.

[112] M. M. Grady, "Astronomy by microscope," *Astron. Geophys.*, vol. 50, no. 4, pp. 4–21, 2009.

[113] P. Schmitt-Kopplin, Z. Gabelica, R. D. Gougeon, A. Fekete, B. Kanawati, M. Harir, I. Gebefuegi, G. Eckel, and N. Hertkorn, "High molecular diversity of extraterrestrial organic matter in Murchison meteorite revealed 40 years after its fall," *Proc. Natl. Acad. Sci.*, vol. 107, no. 7, pp. 2763–2768, Feb. 2010.

[114] G. W. Cooper, W. M. Onwo, and J. R. Cronin, "Alkyl phosphonic acids and sulfonic acids in the Murchison meteorite," *Geochim. Cosmochim. Acta*, vol. 56, no. 11, pp. 4109–4115, Nov. 1992.

[115] A. A. Monroe and S. Pizzarello, “The soluble organic compounds of the Bells meteorite: Not a unique or unusual composition,” *Geochim. Cosmochim. Acta*, vol. 75, no. 23, pp. 7585–7595, Dec. 2011.

[116] D. P. Glavin, M. P. Callahan, J. P. Dworkin, and J. E. Elsila, “The effects of parent body processes on amino acids in carbonaceous chondrites: Amino acids in carbonaceous chondrites,” *Meteorit. Planet. Sci.*, vol. 45, no. 12, pp. 1948–1972, Dec. 2010.

[117] J. R. Cronin and S. Pizzarello, “Aliphatic hydrocarbons of the Murchison meteorite,” *Geochim. Cosmochim. Acta*, vol. 54, no. 10, pp. 2859–2868, Oct. 1990.

[118] G. A. Brennecka and M. Wadhwa, “Uranium isotope compositions of the basaltic angrite meteorites and the chronological implications for the early Solar System,” *Proc. Natl. Acad. Sci.*, vol. 109, no. 24, pp. 9299–9303, 2012.

[119] B. Jacobsen, Q. Yin, F. Moynier, Y. Amelin, A. N. Krot, K. Nagashima, I. D. Hutcheon, and H. Palme, “26Al–26Mg and 207Pb–206Pb systematics of Allende CAIs: Canonical solar initial 26Al/27Al ratio reinstated,” *Earth Planet. Sci. Lett.*, vol. 272, no. 1–2, pp. 353–364, Jul. 2008.

[120] F. Moynier, Q. Yin, and B. Jacobsen, “Dating the First Stage of Planet Formation,” *Astrophys. J.*, vol. 671, no. 2, pp. L181–L183, Dec. 2007.

[121] P. H. Warren, “Stable-isotopic anomalies and the accretionary assemblage of the Earth and Mars: A subordinate role for carbonaceous chondrites,” *Earth Planet. Sci. Lett.*, vol. 311, no. 1–2, pp. 93–100, Nov. 2011.

[122] M. F. Miller, “Isotopic fractionation and the quantification of 17 O anomalies in the oxygen three-isotope system: an appraisal and geochemical significance,” *Geochim. Cosmochim. Acta*, vol. 66, no. 11, pp. 1881–1889, 2002.

[123] A. H. Treiman, J. D. Gleason, and D. D. Bogard, “The SNC meteorites are from Mars,” *Planet. Space Sci.*, vol. 48, no. 12–14, pp. 1213–1230, Oct. 2000.

[124] H. Y. McSween, “Constraints on the composition and petrogenesis of the Martian crust,” *J. Geophys. Res.*, vol. 108, no. E12, 2003.

[125] L. Nyquist, D. Bogard, C.-Y. Shih, A. Greshake, D. Stöffler, and O. Eugster, “Ages and geologic histories of Martian meteorites,” in *Chronology and evolution of Mars*, Springer, 2001, pp. 105–164.

[126] H. Y. McSween, G. J. Taylor, and M. B. Wyatt, “Elemental Composition of the Martian Crust,” *Science*, vol. 324, no. 5928, pp. 736–739, May 2009.

[127] S. P. Wright, P. R. Christensen, and T. G. Sharp, “Laboratory thermal emission spectroscopy of shocked basalt from Lonar Crater, India, and implications for Mars orbital and sample data,” *J. Geophys. Res.*, vol. 116, no. E9, Sep. 2011.

[128] J. J. Papike, J. M. Karner, C. K. Shearer, and P. V. Burger, “Silicate mineralogy of martian meteorites,” *Geochim. Cosmochim. Acta*, vol. 73, no. 24, pp. 7443–7485, Dec. 2009.

[129] F. M. McCubbin and H. Nekvasil, “Maskelynite-hosted apatite in the Chassigny meteorite: Insights into late-stage magmatic volatile evolution in martian magmas,” *Am. Mineral.*, vol. 93, no. 4, pp. 676–684, Apr. 2008.

[130] J. Filiberto, “Experimental constraints on the parental liquid of the Chassigny meteorite: A possible link between the Chassigny meteorite and a Martian Gusev basalt,” *Geochim. Cosmochim. Acta*, vol. 72, no. 2, pp. 690–701, Jan. 2008.

[131] H. Nekvasil, F. M. McCUBBIN, A. Harrington, S. Elardo, and D. H. Lindsley, “Linking the Chassigny meteorite and the Martian surface rock Backstay: Insights into igneous crustal differentiation processes on Mars,” *Meteorit. Planet. Sci.*, vol. 44, no. 6, pp. 853–869, Jun. 2009.

[132] F. M. McCubbin, H. Nekvasil, A. D. Harrington, S. M. Elardo, and D. H. Lindsley, “Compositional diversity and stratification of the Martian crust: Inferences from crystallization experiments on the picrobasalt Humphrey from Gusev Crater, Mars,” *J. Geophys. Res.*, vol. 113, no. E11, Nov. 2008.

[133] J. Zipfel, C. Schroeder, B. L. Jolliff, R. Gellert, K. E. Herkenhoff, R. Rieder, R. Anderson, J. F. BELL III, J. Brueckner, J. A. Crisp, and others, “Bounce Rock—A shergottite-like basalt encountered at Meridiani Planum, Mars,” *Meteorit. Planet. Sci.*, vol. 46, no. 1, pp. 1–20, 2011.

[134] H. C. Aoudjehane, G. Avice, J.-A. Barrat, O. Boudouma, G. Chen, M. J. M. Duke, I. A. Franchi, J. Gattacceca, M. M. Grady, R. C. Greenwood, C. D. K. Herd, R. Hewins, A. Jambon, B. Marty, P. Rochette, C. L. Smith, V. Sautter, A. Verchovsky, P. Weber, and B. Zanda, “Tissint Martian Meteorite: A Fresh Look at the Interior, Surface, and Atmosphere of Mars,” *Science*, vol. 338, no. 6108, pp. 785–788, Nov. 2012.

[135] M. Wadhwa, G. Crozaz, and J.-A. Barrat, “Trace element distributions in the Yamato 000593/000749, NWA 817 and NWA 998 nakhlites:

Implications for their petrogenesis and mantle source on Mars," *Antarct. Meteor. Res.*, vol. 17, p. 97, 2004.

[136] J. M. D. Day, L. A. Taylor, C. Floss, and H. Y. Mcsween, "Petrology and chemistry of MIL 03346 and its significance in understanding the petrogenesis of nakhlites on Mars," *Meteorit. Planet. Sci.*, vol. 41, no. 4, pp. 581–606, Apr. 2006.

[137] W. K. Hartmann and G. Neukum, "Cratering chronology and the evolution of Mars," in *Chronology and evolution of Mars*, Springer, 2001, pp. 165–194.

[138] L. E. Borg and D. S. Draper, "A petrogenetic model for the origin and compositional variation of the martian basaltic meteorites," *Meteorit. Planet. Sci.*, vol. 38, no. 12, pp. 1713–1731, Dec. 2003.

[139] L. E. Borg, L. E. Nyquist, L. A. Taylor, H. Wiesmann, and C.-Y. Shih, "Constraints on Martian differentiation processes from Rb/Sr and Sm/Nd isotopic analyses of the basaltic shergottite QUE 94201," *Geochim. Cosmochim. Acta*, vol. 61, no. 22, pp. 4915–4931, Nov. 1997.

[140] L. E. Borg, L. E. Nyquist, H. Wiesmann, and Y. Reese, "Constraints on the petrogenesis of Martian meteorites from the Rb-Sr and Sm-Nd isotopic systematics of the lherzolitic shergottites ALH77005 and LEW88516," *Geochim. Cosmochim. Acta*, vol. 66, no. 11, pp. 2037–2053, Jun. 2002.

[141] C. K. Shearer, J. J. Papike, P. V. Burger, S. R. Sutton, F. M. McCubbin, and M. Newville, "Direct determination of europium valence state by XANES in extraterrestrial merrillite: Implications for REE crystal chemistry and martian magmatism," *Am. Mineral.*, vol. 96, no. 8–9, pp. 1418–1421, Aug. 2011.

[142] C. B. Till, T. L. Grove, and M. J. Krawczynski, "A melting model for variably depleted and enriched lherzolite in the plagioclase and spinel stability fields," *J. Geophys. Res.*, vol. 117, no. B6, Jun. 2012.

[143] M. D. Norman, "The composition and thickness of the crust of Mars estimated from rare earth elements and neodymium-isotopic compositions of Martian meteorites," *Meteorit. Planet. Sci.*, vol. 34, no. 3, pp. 439–449, May 1999.

[144] C. D. K. Herd, "The oxygen fugacity of olivine-phyric martian basalts and the components within the mantle and crust of Mars," *Meteorit. Planet. Sci.*, vol. 38, no. 12, pp. 1793–1805, Dec. 2003.

[145] A. Basu Sarbadhikari, J. M. D. Day, Y. Liu, D. Rumble, and L. A. Taylor, “Petrogenesis of olivine-phyric shergottite Larkman Nunatak 06319: Implications for enriched components in martian basalts,” *Geochim. Cosmochim. Acta*, vol. 73, no. 7, pp. 2190–2214, Apr. 2009.

[146] A. Basu Sarbadhikari, C. A. Goodrich, Y. Liu, J. M. D. Day, and L. A. Taylor, “Evidence for heterogeneous enriched shergottite mantle sources in Mars from olivine-hosted melt inclusions in Larkman Nunatak 06319,” *Geochim. Cosmochim. Acta*, vol. 75, no. 22, pp. 6803–6820, Nov. 2011.

[147] A. Steele, F. M. McCubbin, M. Fries, L. Kater, N. Z. Boctor, M. L. Fogel, P. G. Conrad, M. Glamoclija, M. Spencer, A. L. Morrow, M. R. Hammond, R. N. Zare, E. P. Vicenzi, S. Siljestrom, R. Bowden, C. D. K. Herd, B. O. Mysen, S. B. Shirey, H. E. F. Amundsen, A. H. Treiman, E. S. Bullock, and A. J. T. Jull, “A Reduced Organic Carbon Component in Martian Basalts,” *Science*, vol. 337, no. 6091, pp. 212–215, Jul. 2012.

[148] M. M. Grady, A. B. Verchovsky, and I. P. Wright, “Magmatic carbon in Martian meteorites: attempts to constrain the carbon cycle on Mars,” *Int. J. Astrobiol.*, vol. 3, no. 2, pp. 117–124, Apr. 2004.

[149] D. W. Mittlefehldt, R. N. Clayton, M. J. Drake, and K. Righter, “Oxygen Isotopic Composition and Chemical Correlations in Meteorites and the Terrestrial Planets,” *Rev. Mineral. Geochem.*, vol. 68, no. 1, pp. 399–428, Jan. 2008.

[150] D. Rumble and A. Irving, “Dispersion of oxygen isotopic compositions among 42 Martian meteorites determined by laser fluorination: evidence for assimilation of (ancient) altered crust,” in *Lunar and Planetary Science Conference*, 2009, vol. 40, p. 2293.

[151] F. M. McCubbin, M. A. Riner, K. E. Vander Kaaden, and L. K. Burkemper, “Is Mercury a volatile-rich planet?: VOLATILES ON MERCURY,” *Geophys. Res. Lett.*, vol. 39, no. 9, p. n/a–n/a, May 2012.

[152] M. A. Riner, F. M. McCubbin, P. G. Lucey, G. Jeffrey Talyor, and J. J. Gillis-Davis, “Mercury surface composition: Integrating petrologic modeling and remote sensing data to place constraints on FeO abundance,” *Icarus*, vol. 209, no. 2, pp. 301–313, Oct. 2010.

[153] L. R. Nittler, R. D. Starr, S. Z. Weider, T. J. McCoy, W. V. Boynton, D. S. Ebel, C. M. Ernst, L. G. Evans, J. O. Goldsten, D. K. Hamara, D. J. Lawrence, R. L. McNutt, C. E. Schlemm, S. C. Solomon, and A. L. Sprague, “The Major-Element Composition of Mercury’s Surface from

MESSENGER X-ray Spectrometry," *Science*, vol. 333, no. 6051, pp. 1847–1850, Sep. 2011.

[154] K. Lodders and B. Fegley, *The planetary scientist's companion*. Oxford University Press, 1998.

[155] J. Farquhar, "Atmosphere-Surface Interactions on Mars: 17O Measurements of Carbonate from ALH 84001 ," *Science*, vol. 280, no. 5369, pp. 1580–1582, Jun. 1998.

[156] L. E. Borg, L. E. Nyquist, H. Wiesmann, C.-Y. Shih, and Y. Reese, "The age of Dar al Gani 476 and the differentiation history of the martian meteorites inferred from their radiogenic isotopic systematics," *Geochim. Cosmochim. Acta*, vol. 67, no. 18, pp. 3519–3536, Sep. 2003.

[157] C. S. Romanek, E. C. Perry, A. H. Treiman, R. A. Socki, J. H. Jones, and E. K. Gibson, "Oxygen isotopic record of silicate alteration in the Shergotty-Nakhla-Chassigny meteorite Lafayette," *Meteorit. Planet. Sci.*, vol. 33, no. 4, pp. 775–784, Jul. 1998.

[158] Y. L. Yung and W. B. DeMore, "Photochemistry of planetary atmospheres," in *Photochemistry of planetary atmospheres/Yuk L. Yung, William B. DeMore. New York: Oxford University Press, 1999. QB603. A85 Y86 1999*, 1999, vol. 1.

[159] F. Nimmo, S. D. Hart, D. G. Korycansky, and C. B. Agnor, "Implications of an impact origin for the martian hemispheric dichotomy," *Nature*, vol. 453, no. 7199, pp. 1220–1223, Jun. 2008.

[160] G. A. Snyder, D.-C. Lee, L. A. Taylor, A. N. Halliday, and E. A. Jerde, "Evolution of the upper mantle of the Earth's Moon: Neodymium and strontium isotopic constraints from high-Ti mare basalts," *Geochim. Cosmochim. Acta*, vol. 58, no. 21, pp. 4795–4808, Nov. 1994.

[161] G. A. Snyder, L. A. Taylor, and C. R. Neal, "A chemical model for generating the sources of mare basalts: Combined equilibrium and fractional crystallization of the lunar magmasphere," *Geochim. Cosmochim. Acta*, vol. 56, no. 10, pp. 3809–3823, Oct. 1992.

[162] P. H. Warren and J. T. Wasson, "The origin of KREEP," *Rev. Geophys.*, vol. 17, no. 1, p. 73, 1979.

[163] Z. . Sharp, V. Atudorei, and T. Durakiewicz, "A rapid method for determination of hydrogen and oxygen isotope ratios from water and

hydrous minerals," *Chem. Geol.*, vol. 178, no. 1–4, pp. 197–210, Aug. 2001.

[164] L. A. Leshin, S. Epstein, and E. M. Stolper, "Hydrogen isotope geochemistry of SNC meteorites," *Geochim. Cosmochim. Acta*, vol. 60, no. 14, pp. 2635–2650, Jul. 1996.

[165] L. Borg, "A review of meteorite evidence for the timing of magmatism and of surface or near-surface liquid water on Mars," *J. Geophys. Res.*, vol. 110, no. E12, 2005.

[166] B. L. Ehlmann, J. F. Mustard, S. L. Murchie, J.-P. Bibring, A. Meunier, A. A. Fraeman, and Y. Langevin, "Subsurface water and clay mineral formation during the early history of Mars," *Nature*, vol. 479, no. 7371, pp. 53–60, Nov. 2011.

[167] F. M. McCubbin, A. Steele, E. H. Hauri, H. Nekvasil, S. Yamashita, and R. J. Hemley, "Nominally hydrous magmatism on the Moon," *Proc. Natl. Acad. Sci.*, vol. 107, no. 25, pp. 11223–11228, 2010.

[168] C. M. O. Alexander, R. Bowden, M. L. Fogel, K. T. Howard, C. D. K. Herd, and L. R. Nittler, "The Provenances of Asteroids, and Their Contributions to the Volatile Inventories of the Terrestrial Planets," *Science*, vol. 337, no. 6095, pp. 721–723, Aug. 2012.

[169] J. P. Greenwood, S. Itoh, N. Sakamoto, P. Warren, L. Taylor, and H. Yurimoto, "Hydrogen isotope ratios in lunar rocks indicate delivery of cometary water to the Moon," *Nat. Geosci.*, vol. 4, no. 2, pp. 79–82, Feb. 2011.

[170] P. Hartogh, D. C. Lis, D. Bockelée-Morvan, M. de Val-Borro, N. Biver, M. Küppers, M. Emprechtinger, E. A. Bergin, J. Crovisier, M. Rengel, R. Moreno, S. Szutowicz, and G. A. Blake, "Ocean-like water in the Jupiter-family comet 103P/Hartley 2," *Nature*, vol. 478, no. 7368, pp. 218–220, Oct. 2011.

[171] A. E. Saal, E. H. Hauri, M. L. Cascio, J. A. Van Orman, M. C. Rutherford, and R. F. Cooper, "Volatile content of lunar volcanic glasses and the presence of water in the Moon's interior," *Nature*, vol. 454, no. 7201, pp. 192–195, Jul. 2008.

[172] A. Cameron and W. Benz, "The origin of the Moon and the single impact hypothesis IV," *Icarus*, vol. 92, no. 2, pp. 204–216, 1991.

[173] E. H. Hauri, T. Weinreich, A. E. Saal, M. C. Rutherford, and J. A. Van Orman, “High pre-eruptive water contents preserved in lunar melt inclusions,” *Science*, vol. 333, no. 6039, pp. 213–215, 2011.

[174] S. Epstein and H. Taylor Jr, “The isotopic composition and concentration of water, hydrogen, and carbon in some Apollo 15 and 16 soils and in the Apollo 17 orange soil,” in *Lunar and Planetary Science Conference Proceedings*, 1973, vol. 4, p. 1559.

[175] S. Epstein and H. Taylor Jr, “D/H and O-18/O-16 ratios of H2O in the’rusty’breccia 66095 and the origin of’lunar water’,” in *Lunar and Planetary Science Conference Proceedings*, 1974, vol. 5, pp. 1839–1854.

[176] L. A. Taylor, H. Mao, and P. Bell, “Identification of the hydrated iron oxide mineral akaganéite in Apollo 16 lunar rocks,” *Geology*, vol. 2, no. 9, pp. 429–432, 1974.

[177] J. Papike, L. Taylor, and S. Simon, “Lunar minerals,” *Lunar Sourceb.*, pp. 121–181, 1991.

[178] A. Colaprete, P. Schultz, J. Heldmann, D. Wooden, M. Shirley, K. Ennico, B. Hermalyn, W. Marshall, A. Ricco, R. C. Elphic, and others, “Detection of water in the LCROSS ejecta plume,” *science*, vol. 330, no. 6003, pp. 463–468, 2010.

[179] J. W. Boyce, Y. Liu, G. R. Rossman, Y. Guan, J. M. Eiler, E. M. Stolper, and L. A. Taylor, “Lunar apatite with terrestrial volatile abundances,” *Nature*, vol. 466, no. 7305, pp. 466–469, 2010.

[180] E. M. Shoemaker, “Asteroid and comet bombardment of the Earth,” *Annu. Rev. Earth Planet. Sci.*, vol. 11, pp. 461–494, 1983.

[181] G. Dominguez, T. Jackson, M. Nunn, D. Basov, and M. Thiemens, “Low Temperature Mass-Independent Ozone Formation on Cold Surfaces,” in *Lunar and Planetary Science Conference*, 2012, vol. 43, p. 2403.

[182] K. S. Griffith and G. I. Gellene, “Symmetry restrictions in diatom/diatom reactions. II. Nonmass-dependent isotope effects in the formation of O+4,” *J. Chem. Phys.*, vol. 96, no. 6, p. 4403, 1992.

[183] A. Angert, C. D. Cappa, and D. J. DePaolo, “Kinetic 17O effects in the hydrologic cycle: Indirect evidence and implications,” *Geochim. Cosmochim. Acta*, vol. 68, no. 17, pp. 3487–3495, Sep. 2004.